Antibacterial Mg-Ag Biodegradable Alloys

Vom Promotionsausschuss der

Technischen Universität Hamburg-Harburg

zur Erlangung des akademischen Grades

Doktor-Ingenieur (Dr.-Ing.)

genehmigte Dissertation

von

Tie Di

aus

Shenyang / China

2013

1. Gutachter:	Prof. Dr.-Ing. habil Karl Ulrich Kainer
2. Gutachter:	Prof. Dr. habil Michael M. Morlock Ph. D.
Vorsitzender:	Prof. Dr.-Ing. Wolfgang Hintze

Tag der mündlichen Prüfung: 13.05.2013

Declaration (Eidesstattliche Erklärung)

No portion of the work in this thesis has been submitted in support of an application for another degree or qualification of this or any other university or institute of learning. Except where reference has been made to the literature of other investigators, the work presented in this thesis is entirely due to the author.

Abstract

The use of magnesium alloys as degradable metals for biomedical applications is topic of ongoing research. As a further aspect, the demand for multifunctional materials is increasing. Hence, binary Mg-Ag alloys were designed to combine the favourable properties of magnesium with the well-known antibacterial property of silver. In this study, three Mg-Ag alloys, Mg2Ag, Mg4Ag and Mg6Ag which contain 1.87%, 3.82% and 6.00% silver by weight respectively were casted and processed with solution and aging heat treatment. Afterwards, the samples were investigated *in vitro* for metallographic, mechanical, corrosive, cytocompatible and antibacterial properties.

The metallurgical analysis and phase identification showed that all alloys contained Mg_4Ag as the dominant second phase. The mechanical properties of the Mg-Ag alloys were dramatically improved in several parameters especially after heat treatment. Corrosion tests revealed that after heat treatment, content of silver reduced the corrosion rate and exhibited less susceptibility to pitting corrosion than pure magnesium. $Mg(OH)_2$ and MgO presented as main magnesium corrosion products while AgCl was found as the primary silver corrosion product. Immersion tests demonstrated that content of silver did not significantly shift the pH, osmolality and magnesium ion release in the environment. Cultivation and cytotoxicity tests with both primary cells and cell lines revealed that Mg-Ag alloys induce no negative effect on cells and show minor cytotoxicity. Antibacterial testing in a dynamic bioreactor system proved the alloys to reduce the viability of two common pathogenic bacteria, *Staphylococcus aureus* and *Staphylococcus epidermidis*. In summary, biodegradable Mg-Ag alloys are cytocompatible biomaterials with adjustable mechanical and corrosion properties while having sound antibacterial ability.

Acknowledgements

First of all, I would like to sincerely thank my academic supervisors, Professor Regine Willumeit and Professor Karl Urlich Kainer, and my academic directors, Dr. Frank Feyerabend and Dr. Norbert Hort, for their fine guidance and support during this project.

I am grateful to Professor Wolf Dieter Mueller in Berlin ‘Charite’ University for his warm help with the electrochemical tests and his guidance to my thesis and paper writing, and Professor Frank Witte in Hannover Medical School for his academic guidance and help with my thesis writing. I also wish to thank Dr. Ronald Schade and his colleagues in ‘iba’ institute for providing experimental instruments.

Gabriele Salamon, Daniela Lange, Berengere Luthringer, Lili Wu and every group member in WPS are acknowledged for your warm help in the laboratory all the time and your efforts to maintain the good atmosphere while working. At the MAGIC center, thanks are due to Willi Punessen, Hajo Dieringa, Zhi Wang, Lei Yang, Sabine Schubert and Qiuming Peng for their helps during the alloy production, treatment and analysis. Thanks also go to all the scientists and workshop staff in the MAGIC center, in particular, Lennart Stutz, Daniel Höche and Daniel Laipple for their caring for the mechanical tests and instrumental analysis.

The financial support from CSC council and the Helmholtz Association are acknowledged for providing me the opportunity to do this project.

Finally, sincere thanks go to my family and friends in China and Germany. I really could not get through my Ph.D. study without your supports especially when I was badly ill last year. I will be more careful and earnest with my health and work in the future.

Contents

1. Introduction

Magnesium based biodegradable alloys are experiencing a renaissance as choice for implant materials suitable for bone and cardiovascular surgery [1-7]. Implants made of magnesium alloys provided initially stable materials that could be fully degraded *in vivo*, eliminating the need for a second operation for implant removal. Biodegradable magnesium alloys became popular also due to their outstanding biodegradability [7], biocompatibility [8-9], and similar mechanical properties compared to bone [2]. However, although lots of effort has been paid for optimizing the performance of these materials [10-12], their comparably high corrosion rate (especially localized corrosion rate) is still one of the main obstacles on the way to medical application [13]. Some attempts such as LAE (lithium/aluminium/rare earth elements) and WE (yttrium/rare earth elements) magnesium alloys systems improved their corrosion properties as well as the mechanical properties [14-16], but rare earth elements may also induce negative effects on cytocompatibility and even cytotoxicity problems [17]. On the other hand, the demand for multifunctional biodegradable materials is urgent, while approaches to this area are still not sufficient yet [18]. As a result, the idea to introduce the well-known antibacterial and cytocompatible properties of silver into magnesium alloy was generated to solve the infection problem during implant surgery [19] and afterwards, while enhance the alloy's corrosion and mechanical performance.

Magnesium has been already used as an biodegradable implant material for more than 100 years [1, 20], but compared to the history of silver applied as an antibacterial material it is still a "young" material. Over 2300 years ago, Alexander the Great used silver vessels to store drinking water for his troops to treat tropical diseases during the war in India [21]. It revealed silver's strong antimicrobial properties had been well-known by human even before thousands of years. The applied formulation of silver kept updated with technology improvement, from bulk silver, to ionic silver supplemented as silver salts (like $AgNO_3$) or adsorbed on carrier materials [21-22] and now to nanosized [23] as well as alloyed silver [24]. Silver keeps high antibacterial reactivity in a wide range of chemical states. Moreover, recent studies found that silver was even effective to treat some extreme microbes, such as Methicillin-resistant *Staphylococcus aureus* (MRSA) and Methicillin-resistant *Staphylococcus epidermidis* (MRSE) which are famous as 'superbugs' and could not be treated by most antibiotics [25-26]. Latest progresses on silver coating and alloys for antibacterial application showed satisfactory results as well [27-29]. Apart from antibacterial capability, small amount of silver content in alloys or coating were also reported to improve cytocompatibility and cell viability evidently [30-31]. Silver in any

form is not thought to be toxic to the immune, cardiovascular, nervous, or reproductive systems [32] and is not considered to be carcinogenic [33]. This feature ensures its safety when applied for medical purpose.

The first reported research of manufacturing Mg-Ag alloys could be traced back to the year 1906 [34], and in the following decades quite a number of studies focused on this system for electronic and hydrogen storage uses [35-36]. For the past few years, some attempts of combining elementary silver to magnesium surface by nanocoating technology also made progress [37]. Different from previous studies, the present work is the first time to use this binary alloy system in the form of magnesium rich alloy for medical applications.

In this thesis, the metallurgical microstructure and heat treatment effects of these three Mg-Ag alloys were analyzed and their mechanical properties were measured under human body temperature (37.0 °C) in order to compare to pure magnesium. Corrosion properties of the alloys were evaluated under cell culture conditions by the mini-cell-system (MCS) [38] and multiple analysis method were employed to reveal the corrosion product component as well as the ion release. The cytocompatibility and cytotoxicity was determined via both microscopy and improved cell viability assay [39]. Antibacterial testing was carried out using an innovative dynamic bioreactor with mixed bacteria flow and *in situ* microscopy [40] to ensure credible results. Based on these results, the feasibility of these originally designed alloys as antibacterial biodegradable materials was evaluated all sidedly.

2. State of the art

2.1. Infections induced by implant materials

2.1.1. Medical and economic consequences

Medical and economic consequences are always induced by infections associated with a variety of surgical implants. Ca. 2 million nosocomial infections cost nearly $ 11 billion in the USA every year [41]. Exposure to invasive medical devices was reported one of the most risky factors [42]. Devices predispose to infection by damaging or invading epithelial or mucosal barriers, or by supporting growth of microorganisms therefore serving as reservoirs. Implant medical devices may even disturb host defense mechanisms, and directly infect patients when contaminated. Resistant infection, chronic inflammations or tissue necrosis thus are the result of these deficiencies, which are the major obstacle inhibiting the extended use of implant devices [43].

Peri-implant infection was defined to describe an inflammatory process impacting the tissues around an osseointegrated implant in function, resulting in loss of supporting bone, while peri-implant mucositis was defined as reversible inflammatory changes of the peri-implant soft tissues without any bone loss [44]. The prevalence rate of peri-implant infections has been reported in the range of 8% to 44% [45-47], while frequency of mucositis has been reported between the range of 1% - 19% [46, 48]. Differences in defining the two entities are thought to be the reason why the wide ranges for the frequencies were found. The frequency of peri-implantitis (peri-implant infection by dental implants) is most likely related to how long implants have been worn. As dental implant treatment was introduced comparatively recently, the numbers will probably increase over the years.

Huge clinical and economic consequences are induced by peri-implant infections (Table 1). [49] Mortality attributable to peri-implant infections is highest among patients with cardiovascular implants, particularly prosthetic heart valves and aortic grafts. Besides, infections associated with orthopedic devices and ventricular shunts often result in serious disabilities. Although infections of mammary and penile implants are seldom life-threatening, they can still cause major disfigurement and psychological trauma. The nature and the number of stages of surgical intervention depend on the type of implant. In most of cases, the cost of an implant itself usually constitutes only a small fraction of the overall cost of treating implant-associated infections.

2.1.2. General principles of treatment

The surgical implant might be affected by some postoperative wound infections [50]. However, bacterial colonization brought by surgical implants does not necessarily indicate infection all the time. Actually, most colonized implants do not become infected. The solid proof of implant associated infection requires the presence of clinical manifestations, intraoperative signs of infection adjacent to the implant, and the growth of pathogens in cultures of surgical specimens. To get rid of the need to operate on a patient who may not suffer an implant-associated infection, one can perform certain microbiologic and imaging studies which are implant-specific. Although bacteria is the sign of prosthetic valve endocarditis and some infections associated with vascular grafts, blood cultures do give positive results in most cases of infection associated with pacemaker–defibrillator systems (unless endocarditis is present), ventricular assist devices, mammary implants, ventricular shunts, orthopedic devices, and penile implants [49].

The core factor in the evolution and persistence of infection is the generation of biofilm around implanted devices [51]. Short after insertion, a conditioning layer composed of host-derived adhesins (including fibrinogen, fibronectin, and collagen) covers the surface of the implant and invites the adherence of free-floating (planktonic) organisms. After this process, bacterial cell division, recruitment of additional planktonic organisms, and secretion of bacterial products (such as the glycocalyx) occur [44].

A structure model of biofilm finally evolves that contains complex communities of tightly attached (sessile) bacteria [52]. The bacteria in that study displayed cell-to-cell signaling and exist within a polymer matrix containing fluid channels that allow for the flow of nutrients and waste. Possible explanations for the restrained susceptibility of biofilm-embedded organisms to antibiotic agents, as compared with their free-floating counterparts, include a lower bacterial growth rate within the biofilm, inhibition of antimicrobial activity by biofilm substances, and poor penetration of the biofilm by antibiotics.

There are several important clinical objectives in treating infections caused by surgical implants. These are to cure the infection, prevent its recurrence, protect body function, and reduce the risk of death. Commonly, these objectives can be achieved with both antibiotic therapy and surgical intervention. At least two thirds of infections are caused by either *Staphylococcus aureus* or coagulase-negative staphylococci. Methicillin-resistant staphylococci are variably susceptible to older antibiotics (doxycycline, trimethoprim - sulfamethoxazole, quinolones, and clindamycin), and they are almost universally sensitive to the newer agent linezolid, but the clinical efficacy of these drugs for the treatment of peri-implant infections has not been prospectively compared with the efficacy of vancomycin.

Table 1. Clinical and Economic Consequences of Infections Associated with Surgical Implants. * [49]

Implant	Implants Inserted in the U.S. Annually	Projected Infections of Implants Annually	Average Rate of Infection (%)	Preferred Practice of Surgical Replacement	Average Cost of Combined Medical and Surgical Treatment (US$)
Cardiovascular					
Mechanical heart valve	85,000	3,400	4	1	50,000
Vascular graft	450,000	16,000	4	1 or 2	40,000
Pacemaker – defibrillator	300,000	12,000	4	2	35,000
Ventricular assist device	700	280	40	1	50,000
Orthopedic					
Joint prosthesis	600,000	12,000	2	2	30,000
Fracture-fixation device	2,000,000	100,000	5	1 or 2	15,000
Neurosurgical - ventricular shunt	40,000	2,400	6	2	50,000
Plastic - mammary implant (pair)	130,000	2,600	2	2	20,000
Urologic - inflatable penile implant	15,000	450	3	2	35,000

* The information is from published studies [53-57], market reports, and data provided by medical and surgical organizations, physicians, and device-manufacturing companies. The average costs reflect the usual charges by private institutions (taking into consideration that portions of the antibiotic courses, particularly prolonged courses, are sometimes administered in an outpatient setting) and exclude loss of income because of infection.

Surgical removal is the primary treatment to most implants which are infected by *S. aureus* or candid. Patients with an established response to medical therapy for a

peri-implant infection caused by the less virulent coagulase-negative staphylococci may not require surgery to remove the implant. If a treatment plan is made to remove the infected implant, complete extraction of all components is essential, if surgically feasible, regardless of the type of infecting organism. Although surgical removal of the infected implant is generally associated with a better outcome than is retention of the infected implant, medical treatment alone may be still more warranted in patients who are at high risk for intraoperative or postoperative complications [49].

2.1.3. Current approaches

Increased tolerance to the normal antibiotic therapies was observed for bacteria sequestered in biofilms. Although the mechanism of this resistance is ongoing studied, current hypotheses on the subject include the heterogeneity of biofilm-encased bacteria and the decreased diffusion of antibiotics due to interactions with the exopolysaccharide matrix [51, 58-59]. Currently, the only proved treatment for biofilm infections is removing the implant, fighting the infection with antibiotics, and replacing the implant, a costly and stressful procedure.

2.1.3.1. Animal studies

During the 1990s, interest in methods for the improved treatment of peri-implant infections emerged. An increasing number of animal studies and reports on clinical outcomes in patients have been published [44]. Although some studies were restrained to measurements of the amount of new bone at a surgical re-entry [60], biopsy with histological examination was most often applied to determine the amount of new bone and the degree of re-osseointegration. The methods for these determinations varied among the studies. What seems to be the most adequate method, measurement of the height of new bone adjacent to the implant was utilized in some of the studies (not separated by a connective tissue capsule) [61]. Other studies measured the growth rate of new bone to the most coronal bone crest (including bone separated from implant by a connective tissue capsule) [62].

Some studies showed mechanical cleaning using abrasive air-powder appeared to offer adequate detoxification to allow for new bone formation in direct contact with the implant surface. On the other hand, more recent results by Persson et al. [61] suggest that cotton pellets and saline may be adequate for the treatment of rough implant surfaces. They speculated that re-osseointegration may not only be a matter of detoxification of the implant material surface but also a matter of capability of the treated surface to provide adhesion and stability of the coagulum during the initial stage of healing process. Some other studies make use of systemic antibiotics to treat infections, among which postoperative systemic antibiotics were used in the majority of the available studies, and metronidazole or amoxicillin + metronidazole was the most common choice. The value of systemic antibiotics is difficult to be assessed, since there are few studies comparing results versus their nonuse.

Different surgical techniques were also evaluated, and the majority of these attempts made use of primary flap closure and postoperative submerging of the treated defect and implant. However, few of these studies successfully showed convincing evidence that the submerged technique is superior. Findings by Machado et al.[63], and Nociti et al. [60] indicate some adjunctive side effects. Application of bioactive glass supplementing the surgical debridement was reported created a number of three-wall defects, while adjunctive effects were observed [64]. PTFE barrier membranes to supplement the surgical curettage was utilized with submerged closure by Machado and Nociti [60]. Most of these studies found the use of PTFE membranes gave improved treating effects, in spite of the fact that postoperative exposure of the membranes seems to be a frequent complication. Moreover, biodegradable collagen membranes provided comparable bone fill to PTFE membranes as assessed at surgical re-entry [60].

2.1.3.2. Human studies

Compared to animal studies, treatment of peri-implant infections using open debridement was widely applied method for human studies. Osteoplasty and apical flap positioning were used and soft tissue healing effect was observed. Behneke et al. [65] reported a couple of cases treated with autogenous bone grafts and with observation intervals extending up to 3 years. Notable reductions of probing depths coupled with significant radiographic bone fill were reported as well [65]. The use of grafts of demineralized freeze-dried allogenic bone, bovine anorganic bone or hydroxyapatite may also lead to improved clinical conditions. However, only a limited number of cases for each of the different graft materials were reported. Methods for implant debridement / detoxification varied among the human studies, as did the use of systemic antibiotics. Based on the case reports available, it can be drawn that treatment of peri-implant infections with autogenous bone grafts / bone graft substitutes may lead to fill of the defects and improved soft tissue conditions. Apart from the presented cases, some failures have been also reported. Furthermore, one comparative study evaluating the use of autogenous bone grafts with and without the application of barrier membranes was reported [66].

Similar to animal studies, another choice for human studies is treatment of peri-implant infections using barrier membranes. PTFE membranes were used the most common whilst a few groups used submerged approaches such as primary closure of the surgical flaps. Methods for implant debridement / detoxification varied among the studies, but systemic antibiotics were used in most cases. Early membrane exposure was a common complication and may lead to treatment failure. Aughtun et al. [67] reported the treatment outcome of 15 lesions in 12 patients. Some radiographic bone loss was observed using orthopantomograms averagely, while only minor improvements of soft tissue conditions were certified. Membrane exposures happened after 4 - 6 weeks in 13 of the 15 treated sites in this study. It

can be concluded that treatment of peri-implant infections with PTFE membranes may lead to bone fill of the defects and achieve better soft tissue conditions.

2.1.4. Summary

The majority of current studies was based on the short-term peri-implant treatment and included a few cases only, so the case reports can just be useful to indicate the potential of different therapies. Thus, the available studies demonstrate that efforts to reduce the submucosal infection may result in improvements of peri-implant lesions, at least on a short-term basis. These case reports also reveal that regenerative procedures in intrabony peri-implant defects may lead to the formation of new bone. A 3-year follow-up case of 10 out of 25 implants treated with autogenous bone suggests that the stability of these initial improvements can be maintained [65]. Khoury & Buchmann reported the stability of average treatment results over 3 years following autogenous bone grafting with or without placement of barrier membranes treating a total of 41 implants., and also proved the lasting improvement [66].

Many studies provided suggestive strategies for the treatment of peri-implant infections. However, due to the lack of controlled or comparative long-term research, these recommendations have to be recognized as empirical. Several uncertainties remain about the treatment plans of peri-implant infections: the relative importance of mechanical debridement, use of topical antimicrobials and systemic antibiotics during closed debridement has not revealed yet; the benefits of open pocket reduction and debridement are uncertain; methods for effective detoxification of various types of implant surfaces need to be standardized. However, the most efficient regenerative procedure has not been identified. There seems to be no report in human studies in which histologic examination addresses the issue of the confirmed potential for re-osseointegration to a previously contaminated implant surface. Limited knowledge was obtained as to what extent initial improvements are sustained over the long-term treatment and if further loss of implant-supporting bone could be prevented.

It might not be realistic to expect increasing number of comparative studies on methods for the treatment of peri-implant infections in the near future. In lieu of this, the long-term monitoring of consecutively treated cases based on a given approach should be therefore encouraged, since this may assist in constructing the predictability, magnitude and stability of improvements that can be obtained relying on current studies [44].

2.2. Silver’s medical application and its effects on health

Silver naturally occurred in most of areas of the earth while it is a rare element. It is quite ductile and malleable, and slightly harder than gold. Pure silver has the highest electrical and thermal conductivity among all metals whilst has the lowest contact

resistance [68]. Due to these properties, silver has been used in a wide variety of applications in human history. Ancient civilizations were already aware of silver's bactericidal properties [69]. Metallic silver was commonly used for surgical prosthesis and splints, fungicides, and coinage, while soluble silver compounds, like silver salts, have been used in treating mental illness, epilepsy, nicotine addiction, gastroenteritis, and infectious diseases, including syphilis and gonorrhea for hundreds of years [70-71].

Table 2 lists some of the current important uses of silver metal and silver compounds [32, 68, 72-73]. The photosensitive properties of silver halides is widely utilized the photographic industry [32]. Moreover, the widest and most well-known application of silver in medical area is in combination with sulfadiazine, where it becomes a popular topical antibacterial drug for the treatment of burns [74]. Colloidal silver proteins were commonly used to treat colds [75] and are after a couple of years gaining interest as a dietary supplement to deal with many diseases [70].

There are several facets impacting the capability of a metal's toxic effects on the body: the solubility of the metal or alloy; the ability of the agent to bind to biological targets; and the level to which the agent complexes generated are sequestered or metabolized and excreted [76]. Toxic effects are defined as an undesirable or adverse health effect [77]. Existing researches seem to show that some forms of silver have higher toxic effects than others [69, 78-79]. Viewed from the apparently different toxicities that soluble and insoluble kinds of silver compound have on the body, the following contents will focus on occurrence of adverse health outcomes related with silver, in which cases of occupational exposure is mainly discussed [71].

2.2.1. Toxicity of silver

Silver may get into the body via various routes of entry because of its wide variety of applications. Direct ingestion is one of the dominant routes of entry for colloidal silver proteins and silver compounds. In occupational settings, inhalation of dusts or fumes mixed with silver compounds is the main exposure way [32]. Skin contact primarily happened in occupational settings [32], from the medical application of burn creams and from direct contact with silver containing jewelry. Silver can also acquire entry into human body through the utilization of acupuncture needles (in Chinese medical treatment), catheters, dental fixture equipment, and accidental puncture wounds [80].

Soluble silver compounds are far more easily absorbed than metallic or insoluble silver chemicals [73] and therefore have the highest potential to generate adverse effects on human health [76, 81]. Some acute symptoms caused by over-exposure to silver nitrate can decrease blood pressure, diarrhea, stomach functions and respiration. Chronic symptoms induced by prolonged treatment with small doses of silver salts are fatty degeneration in the liver and kidneys and changes in plasma and blood cells [82]. Compared with common treatment, long-term inhalation or ingestion

with soluble silver compounds or colloidal silver products may therefore cause argyrosis and / or argyria [68, 70, 75]. Soluble silver chemicals are also capable for accumulating in small amounts especially in the brain and in muscle [75]. However, silver in any form is not thought to be cytotoxic to the immune, cardiovascular, nervous, or reproductive systems [32] and is not considered to be carcinogenic neither [33].

Table 2. Current industrial applications of silver metal and silver compounds. [71]

Silver compounds	Silver and silver alloys
Photography	Jewelry
Batteries	Silverware
Bactericide	Electronic components
Catalysts	Heat sink
Medicinals	Solders
Lubrication	Brazing alloys
Cloud seeding	Superconductors
Window coatings	Bactericide
Mirrors	Dental amalgams
Flower preservative	Bearings
Electroplating	Coinage/medals
Sanitation of:	
Swimming pools	
Hot tubs/spas	
Drinking water	
Cosmetics	

The development of a characteristic and irreversible pigmentation of the skin (argyria) and / or the eyes (argyrosis) seems to be the most common health effects related with long-term exposure to silver according to current studies. The affected area usually turns bluish-gray or ash gray and the situation could be more severe in areas of the body exposed to sunlight [32, 70]. Argyria and argyrosis have been observed after implantation of silver-containing solid materials into the skin or body [83]. Argyria and argyrosis are also common in inhalation in occupational settings [81], the application of colloidal silver and silver-containing drugs [70, 75], smoking deterrents [84], some dental materials [85], and silver solder [86].

According to the method of entry, argyria and argyrosis could be classified as either localized or generalized [87]. Localized argyria is primarily caused by direct external contact with silver chemicals. Very small-sized silver particles could enter the human body through the exocrine sweat glands or through punctures [88]. These deposits of silver which remain in the skin indefinitely [89] are light brown to dark blue in color and look like small round or oval patches [80]. The most commonly affected tissues are hands, eyes, and mucous membranes [79]. Localized argyrosis may develop over time if fine particles of silver are rubbed into the eyes (i.e. in occupational settings) [79]. Localized argyria can also occur following the application of silver compounds to wounds especially in burn treatment [90].

Generalized argyria may occur when silver compounds are applied to mucosal surfaces, inhaled, ingested, or injected into the body, and is recognized by a widespread pigmentation of the skin, eyes, and nails [91]. After the entry to the body, it is absorbed and carried by the bloodstream and deposited in various tissues throughout the body. Tissue or organs of the body most likely to suffer pigmenting include eyes, internal organs, and sun-exposed areas such as the face, ears, forearms, hands, and nails [92]. Generalized argyria was most often reported occurring after the ingestion or application of silver-containing drugs, and it has also been reported following occupational exposure among silver nitrate makers [81].

Both upper (nose and throat) and lower (chest) respiratory tract irritation have been reported by inhalation of soluble silver compounds [81], although irritation is most likely induced by the corrosive effect of nitrate in some silver compounds rather than by silver element itself [81]. Staining of alveoli and bronchial tissue may occur after inhaling silver dust or fumes, but this is proved not harmful to health [93]. However, emphysema, bronchitis and a reduction in pulmonary volume was reported in the operator of silver polishers when exposed to metallic silver, as well as to other metals [81].

2.2.2. Accumulation and metabolism

Natural concentrations of silver in human tissues are only trace amount, and If there is overexposure, silver can primarily accumulate in the skin, liver, kidneys, corneas, gingiva, mucous membranes, nails and spleen [81, 94]. Silver ions possess a high affinity to the thiol groups in the liver [95] and have been shown to bind to reduced concentration of glutathione and to be transported into the bile, thus exhausting the amount of reduced glutathione awaiting for biochemical pathways. The reduced glutathione should play an important role in maintaining proper structure and function of red blood cells, as well as eliminating organic peroxides [95]. Although silver is found to accumulate in some organs and tissues, there are limited data available that indicate its possible toxic effects. Venugopal and Luckey [82] reported that argyria can be considered a mechanism for detoxifying silver by storing it in the tissues by the means of harmless chemicals, such as silver-protein complexes and silver sulfide.

Ingested elemental silver by human are estimated to be intaked by the body at a level of at 10% to the maximum, whilst with only 2 - 4% being retained in tissues [96-97]. Silver concentration can be measured in urine, blood, and feces. Even though the body eliminates most of silver by feces [96], it can be accurately measured in whole blood [98] and is, therefore, many biological medium of choice due to collection convenience. Urine alysis is useful only for a high degree of silver exposure because there is little silver excreted via the urine [92].

Many researchers attribute the pigmentation process associated with generalized argyria solely to soluble silver compounds [69, 78-79, 93] because metallic silver and insoluble silver compounds are not readily taken up by the body [79, 99]. It is thought that when the body absorbs silver compounds, they form complexes primarily with proteins, but also with RNA and DNA, by binding to sulfhydryl, amino, carboxyl, phosphate and imidazole groups [32, 75].

Triggering process of the photo-reduction of these compounds to form metallic silver commonly catalyzed by light, similar to the process involved when developing a negative in photography [70]. Metallic silver is subsequently oxidized by tissue and is bound as silver sulfide [70]. Black silver sulfide and silver selenide complexes bound to tissue were identified as comprising the silver particles deposited in many individuals with argyria [80]. These compounds may then stimulate increased melanin production, especially in sun-exposed areas, which leads to pigmentation [75, 87-88]. The pigmentation resulting from silver deposition is irreversible. Some studies showed chelation therapy and dermabrasion are ineffective in removing silver deposits out of the body [75, 89].

2.2.3. Exposure limit to human

The Mine Safety and Health Administration (MSHA) and the Occupational Safety and Health Administration (OSHA) currently enforce a Permissible Exposure Limit (PEL) of 0.01 mg • m^{-3} for metallic and soluble silver compounds [100-101]. NIOSH (The National Institute for Occupational Safety and Health) established a Recommended Exposure Limit (REL) of 0.01 mg • m^{-3} for both soluble silver compounds and silver metal dust, which does not differ from the OSHA PEL [102].

The American Conference of Governmental Industrial Hygienists (ACGIH) established a Threshold Limit Value (TLV) of 0.01 mg • m^{-3} for all chemical status of silver [103] in 1966, largely based on Hill and Pillsbury's publication [69]. However, in response to findings from studies undertaken since Hill and Pillsbury's work, ACGIH set a new TLV of mg • m^{-3} for metallic silver in 1980. ACGIH recognized the different

outcomes from exposure to soluble and/or insoluble silver, rationalizing that 'the available data on soluble compounds of silver demonstrate that silver salts have a greater propensity to cause argyria than does the dust or fume of metallic silver and that the respective exposure levels of 0.01 mg • m^{-3}, for soluble silver, and 0.1 mg • m^{-3}, for metallic silver, are adequate to prevent argyria in workers exposed to airborne silver [103].

Argentina, Bulgaria, Columbia, Jordan, Korea, New Zealand, Singapore and Vietnam recognize the ACGIH TLV of 0.1 mg • m^{-3} for silver metal, while Austria, Denmark, Germany, Japan, The Netherlands, Norway, and Switzerland recognize 0.01 mg • m^{-3} as the occupational exposure limit for all forms [101].

2.2.4. Summary

A number of arguments may raise for the need to differentiate occupational exposure limits based on the different forms of silver. Some studies indicated insoluble silver levels have been tolerated without any health effects at levels 10-100 times higher than OSHA's current PEL of 0.01 mg • m^{-3}, as well as ACGIH's TLV of 0.1 mg • m^{-3} [78-79]. Many of these studies have recommended that occupational exposure levels to insoluble and metallic silver be reconsidered and that the standards for metallic and insoluble silver be established without any consideration of the toxicity of soluble silver compounds [73, 76, 79].

More emphasis on safety and health, and better engineering controls, future cases of occupational argyria or argyrosis will be extremely rare because of improved technology,. Actually, the number of argyria cases due to overexposure to silver by direct contact is quite few, since silver has been in use for thousands of years as a natural antibiotic. The low toxicity and good compatibility assures silver's safety when utilized under controllable dose in biomaterials. These standards of exposure limits to silver also give suggestive dose for the following *in-vitro* research.

2.3. Silver containing antibacterial materials

The ionized silver(Ag^+) is bioactive and readily kills bacteria *in vitro* in sufficient concentration. Silver also kills bacteria in external wounds in living tissue, so physicians use wound dressings containing silver sulfadiazine (Ag-SD) or silver nanomaterials to treat external infections [19, 104]. Wound dressings containing

silver are increasing in importance due to the recent increase of antibiotic-resistant bacteria, such as MRSA [105]. The disinfectant properties of silver are used in medical applications, such as urinary catheters and endotracheal breathing tubes [106]. Silver is also used in bone prostheses, reconstructive orthopaedic surgery and cardiac devices, as well as on surfaces and fabrics to reduce the spread of infection [107-108].

2.3.1. History of silver's medical application

In 327 B.C. Alexander the great was on his way to conquer India. Suddenly the great army was struck by an outbreak if a mysterious gastrointestinal diseases. Alexander was forced to retreat. Commanders suffered less frequently compared to the soldiers. Commanders used silver cups whereas soldiers used tin cups which were evidence of the fact that it was healthier to store as well as drink water in silver vessels. It was then that people began to realize the use of the noble metal – 'Silver' [21].

Since the 1990s, "colloidal silver", a liquid suspension of microscopic silver particles, has been marketed as an alternative medicine, often claiming impressive "cure-all" qualities. The effectiveness of these products has never been scientifically proven, and in some jurisdictions, it is currently illegal to include such claims in product advertisements. Medical authorities and publications advise against the ingestion of colloidal silver preparations, because of their lack of proven effectiveness and because of the risk of adverse side effects, such as argyria [109]. Historically, colloidal silver was also used as an internal medication to treat a variety of diseases.

2.3.2. Principles of silver's antibacterial action

Silver ions are highly bio-active and can penetrate bacterial membranes rapidly. They interact with enzymes and other proteins in bacteria, causing cellular distortion and loss of viability. Furthermore silver ions interact with the bacterial cell wall and bind to bacterial DNA and RNA causing an inhibition of bacterial replication (Fig. 1). Clinical studies clearly demonstrate that silver provides a significant inhibition of a wide range of germs.

Metallic silver is relatively unreactive however, when exposed to aqueous environments some ionic silver (Ag^+) is released. Certain salts (*eg* silver nitrate) are readily soluble in water and have been exploited as antiseptic agents for many decades [110]. The generation of silver ions can also be achieved through ion exchange using complexes of silver with other inorganic materials (*eg* silver - zeolite complexes; [111]). Silver ions interact with a number of components of bacterial,

protozoal and fungal cells. Toxicity to microbial cells is exhibited at very low concentrations with masses being associated with bactericidal activity [112]. The kinetics vary depending on the source of silver ions with silver derived from ion exchange processes demonstrating delayed activity compared with that derived from soluble salts [113]. Activity appears to increase with temperature and pH [113]. Studies have demonstrated that silver ions interact with sulfydryl (-SH) groups of proteins as well as the bases of DNA leading either to the inhibition of respiratory processes or DNA unwinding [114]. Inhibition of cell division and damage to bacterial cell envelopes is also recorded [115] and interaction with hydrogen bonding processes has been demonstrated to occur [116].

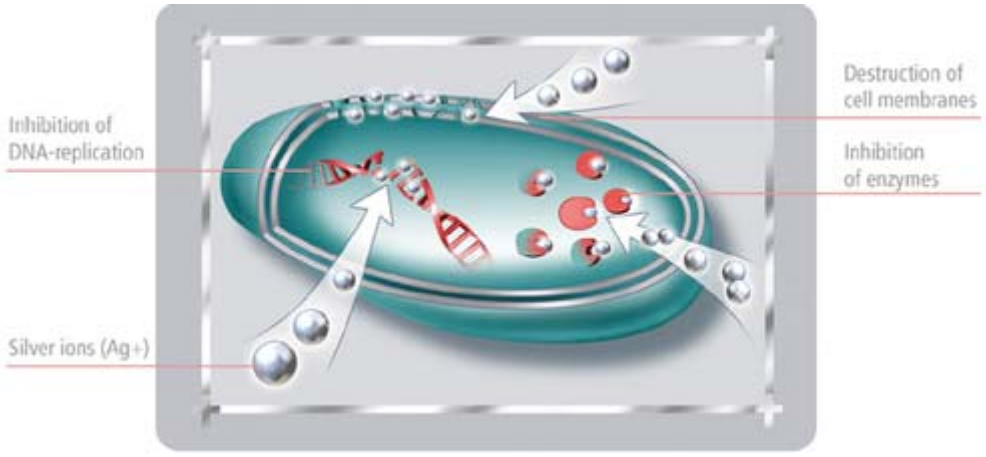

Fig. 1. Principles of silver ion's antibacterial action. [117]

Silver ions clearly do not possess a single mode of action. They interact with a wide range of molecular processes within microorganisms resulting in a range of effects from inhibition of growth, loss of infectivity to cell death. The mechanism depends on both the concentration of silver ions present and the sensitivity of the microbial species to silver. Contact time, temperature, pH and the presence of free water all impact on both the rate and extent of antimicrobial activity. However, the spectrum of activity is very wide and the development of resistance relatively low, especially in clinical situations [118].

2.3.3. Silver containing antimicrobial agents

2.3.3.1. Metallic and ionized silver

The use of metallic silver as an antimicrobial agent has long been recognized [119]. Dilute solutions of silver nitrate had been used since the 19th century to treat

infections and burns before the introduction of silver sulphadiazine cream [120]. Of the commonly used forms of topical silver applications, silver-coated dressings have been demonstrated to be effective at killing a broader range of bacteria than the cream base, were less irritating than the silver nitrate solution and were better tolerated [121]. Silver-coated dressings are used extensively for wound management, particularly in burn wounds [122], chronic leg ulcers [123], diabetic wounds [124] and traumatic injuries. These dressings vary in containing compounds of silver nitrate or sulphadiazine, to sustained silver-ion release preparation [125] and silver-based crystalline nanoparticles [126]. The dressing component also varies, as nylon, mesh, hydrocolloid or methylcellulose. A range of silver-impregnated dressings are now commercially available for use. However, there has been little comparative analysis as to the 'antimicrobial' effect of each of the dressings and the spectrum of bacterial killing that each dressing provides.

Silver has the advantage of having broad antimicrobial activities against Gram-negative and Gram-positive bacteria and there is also minimal development of bacterial resistance. The use of these compounds and the mechanisms of silver resistance have been reviewed [127]. One major advantage of its use is the limited side effects of topical silver therapy; silver toxicity or argyrosis can be resolved with cessation of therapy [110]. The incorporation of silver for topical dressings or as coating on medical products may therefore play an important role in the era of antibiotic resistance.

Although silver containing antibacterial agents like colloidal silver products are legally available at health food stores in the United States and Australia and are marketed over the Internet as a dietary supplement, it is illegal in the U.S. and Australia for marketers to make claims of medical effectiveness for colloidal silver. Ingestion of colloidal silver may result in argyria. [128-129]

Apart from its antibacterial reactivity, silver was also found to increase material biocompatibility as well according to Jendrik Hardes' [30] and M. Bosetti's [31] studies. Bosetti studied *in vitro* biocompatibility of silver-coated stainless steel external fixation pins. Silver coated steel presented better cellular compatibility than naked steel, which was widely applied in implant surgery Fig. 2. Jendrik Hardes's study also confirm the fact that silver at low concentrations is not cytotoxic for osteoblast cells *in vitro* [30] Both cells' survival rate and rate of extension were significantly higher on silver coated material than uncoated alloys.

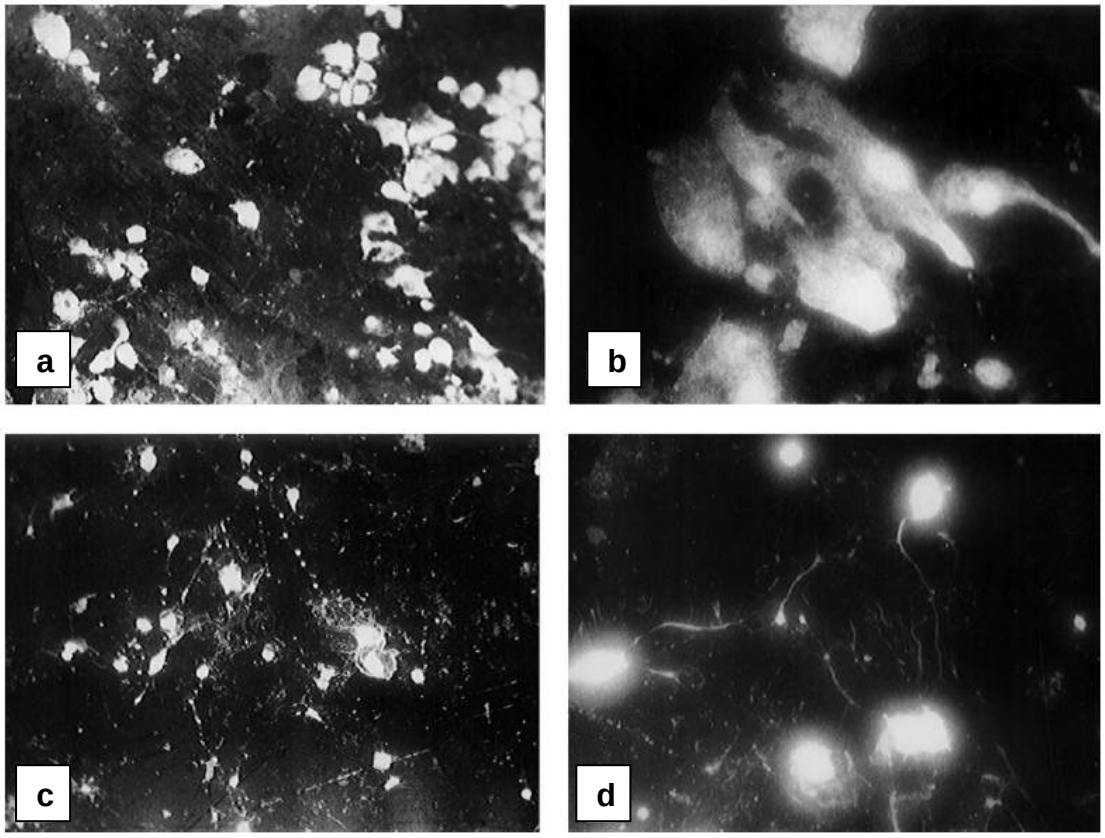

Fig. 2. Acridine orange staining of human trabecular osteoblast-like cells cultured on the surface of coated and uncoated materials at 4 days proliferation. Fluorescence micrographs of (cells are in white color while dark background is material): (a) cells on silver coated material at 100× magnification; (b) cells on silver coated material at 400× magnification; (c) cells on uncoated stainless steel at 100× magnification; (d) cells on uncoated stainless steel at 400× magnification. [31]

2.3.3.2. Nano-silver

Nano-silver has biological properties which are significant for consumer products, food technology (e.g., food processing equipment, packaging materials, food storage), textiles/fabrics (e.g., antimicrobial clothing), and medical applications (e.g., wound care products, implantable medical devices). In addition, nano-silver has unique optical and physical properties that are not present in bulk silver, and which are claimed to have great potential for medical applications (e.g., diagnostics, drug delivery, and imaging).

Nano-silver is an effective killing agent against a broad spectrum of Gramnegative and Gram-positive bacteria [130], including antibiotic-resistant strains [121, 131]. Gram-negative bacteria include genera such as Acinetobacter, Escherichia,

Pseudomonas, Salmonella, and Vibrio. Acinetobacter species are associated with nosocomial infections, i.e., infections which are the result of treatment in a hospital or a healthcare service unit, but secondary to the patient's original condition. Gram-positive bacteria include many well-known genera such as Bacillus, Clostridium, Enterococcus, Listeria, Staphylococcus, and Streptococcus. Antibiotic-resistant bacteria include strains such as methicillin-resistant and vancomycin-resistant Staphylococcus aureus, and Enterococcus faecium. Recently, it has been shown that silver nanoparticles (diameter 5 - 32 nm, average diameter 22.5 nm) enhance the antibacterial activity of various antibiotics [132]. The antibacterial activities of penicillin G, amoxicillin, erythromycin, clindamycin, and vancomycin against Staphylococcus aureus and Escherichia coli were increased in the presence of silver nanoparticles.

2.4. Mg based biodegradable alloys

2.4.1. History

Compare with the long history of application of silver as antibiotics, the history of biodegradable magnesium implants only started shortly after the discovery of elemental magnesium by Sir Humphrey Davy in 1808 [133]. His assistant, Michael Faraday, enabled the production of Mg metal by electrolysis of fused anhydrous MgCl2 in 1833 [133]. The commercial production of Mg by electrolysis was realized by Robert Bunsen, who created a small laboratory cell for the electrolysis of fused MgCl2 in 1852 [133]. These initial Mg products were presented at the world exhibition in London in 1862 [133]. It is most likely that the physician Edward C. Huse used some of those Mg wires as ligatures to stop bleeding vessels of three human patients in 1878 [134]. He already observed that the corrosion of Mg was slower *in vivo* and that the time period until complete degradation was dependent on the size of the Mg wire used [134]..

The most influential pioneer was the physician Erwin Payr from Graz, Austria whose versatile clinical applications and reports inspired many other clinicians to advance the field of biodegradable magnesium implants to various surgical areas (Fig. 3). He started his first experiments on Mg resorption in 1892 [135], but his main problem at that time was to get filigree fabricated devices made of Mg for his studies [135-136]. Around 1900, Payr already proposed that tissue oxygen and water content, carbon dioxide, the dissolved salts in blood and the chemical processes in cells were mainly

responsible for the corrosion of Mg in vivo [135-136]. Albin Lambotte was also an early clinical investigator of biodegradable Mg and the mentor of his assistant Jean Verbrugge, who continued and extended the animal experiments and clinical studies [137-138].

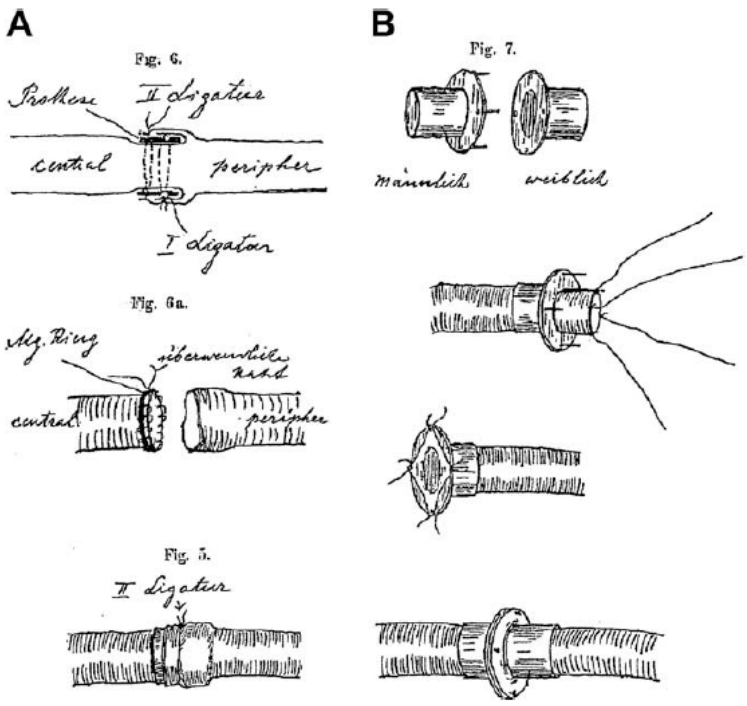

Fig. 3. Tubal magnesium connectors designed by Payr for vessel anastomosis [135]. Method (A) used an extravasal magnesium ring, which ensures an open postoperative anastomosis. Method (B) uses a two-part extravasal connector with a male and female part. In both methods the magnesium connector is extravasal and the anastomosis is achieved by a duplication of the intima. Thus, no foreign material is located intravasal after the anastomosis.

Troitskii and Tsitrin, in 1944, reported on 34 cases where magnesium, alloyed with small levels of cadmium, was fashioned into plates and screws and used to secure various fractures [139]. Of the 34 cases, 9 were unsuccessful; these failures were attributed to infection, or difficulties arising with the mounting of a plaster cast, which presumably did not allow for treatment of gas cysts [139]. In all patients, no increase in serum levels of magnesium was observed. No distinct inflammatory reactions to the implant were observed [139]. The material is reported to have stimulated the development of a hard callous at the fracture site [139]. Hydrogen gas was given off in the corrosion process,

McBride reported on the use of screws, pegs, plates and bands prepared from magnesium – aluminum – manganese alloys to secure 20 fractures and bone grafts [20]. Consistent with other reports, no systemic reactions to the use of magnesium alloys or inflammatory reactions adjacent to the implant are observed [20]. While no effect on the cancellous bone tissues is observed, a positive effect on the periosteal tissue and deposits of the osseous callous are reported [20]. These early examples imply that magnesium-based materials are non-toxic and may actually stimulate bone tissue healing. However, the rate of corrosion of pure magnesium, or these simple alloys, occurs at a rate that is too high to allow a satisfactory time for recovering of tissue as it is desirable to have the implanted fixture can stand for at least 84 days [140].

2.4.2. Current studied magnesium alloys

The most currently investigated magnesium alloys as implant materials are commercial alloys which have been developed for transportation industry [141]. The designation system of magnesium alloys is generally following the nomenclature of the American Society for Testing and Materials (ASTM) [142] and uses a typical letter-figure combination. The magnesium alloys can be divided into three major groups: pure magnesium (Mg) with traces of other elements, aluminium (Al) containing alloys and those alloys which are free of Al [8, 140, 143]. Typical Al containing magnesium alloys are AZ91, AZ31, AE21, calcium (Ca) modified AZ alloys, and LAE442. AZ31 and AZ91 have been used over decades in technical applications [141, 144].

There are several typical Al-free magnesium alloy systems, WE, MZ, WZ, and Mg – Ca alloys. The magnesium alloy WE43 has been developed to improve creep resistance and high temperature stability [141, 144]. This alloy contains yttrium (Y), zirconium (Zr) and RE respectively. Manganese – zinc (MZ) alloys have comparable properties to the alloying system ZM, which is a known system for wrought applications in the transportation industry [141, 144]. However, almost none of the above mentioned alloys have been originally developed to be a biodegradable implant material. Due to the complex alloy composition it is not certain, if the observed *in vivo* degradation can be truly connected to a chemical element, an intermetallic compound or a microstructural effect based on the processing route [2].

2.4.3. Mg alloy's corrosion and research methods

A increasing number of studies have been carried out to investigate the corrosion behaviour of magnesium alloys in artificial physiological fluids and most of them are Al containing Mg alloys [145]. Most alloying elements will dissolve into the human body during the magnesium alloy degradation, for example, when the AZ91D magnesium alloy is used, the Al present in the alloy would get into the human body, which might be hazardous, from the health point of view. The magnesium alloy implants are expected not to degrade until the healing is completed and tissue growth has occurred. However it is unfortunate to observe that magnesium and its alloys corrode too quickly at the physiological pH of 7.2 to 7.4 as well as in physiological media containing high concentrations of aggressive ions, thereby loosing mechanical integrity before the tissues have sufficient time to heal [69][8]. Various methods such as alkali heat treatment [70][146], plasma immersion ion implantation (PIII) [71][147], micro-arc oxidization (MAO) [72][148], and anodic oxidization [73][149] have been proposed to improve the corrosion resistance of Mg alloys.

The major concern over biomedical Mg alloys is their corrosion behaviour, and it is necessary to determine the corrosion rate and acquire knowledge of the corrosion mechanism in order to develop better adapted biomaterials for practical applications. Mg and its alloys in aqueous solutions react and produce hydrogen according to

$$Mg + 2H_2O \rightarrow Mg(OH)_2 + H_2 \uparrow \qquad \text{(Eq. 1)}$$

When the presence of chloride ions the magnesium hydroxide dissolves by reacting into the soluble salt $MgCl_2$ according to Eq. (2)

$$Mg(OH)_2 + 2Cl^- \rightarrow MgCl_2 + 2OH^- \qquad \text{(Eq. 2)}$$

Atrens [150] and Song [151] have shown that the quantity of hydrogen can be measured and used for the interpretation of the results obtained from electrochemical measurements, and they have given an explanation of the negative difference effect (NDE), caused by the different amounts of hydrogen and Mg ions that do not fit with Faraday's law. How and how fast these reactions take place depend on various parameters.

In the case of the corrosion of Mg and Mg alloys, the main problem for biomaterial application is not solely the hydrogen development: 0.01 ml • cm^{-2} per day is a tolerated level in the human body according to Zeng et al. [152]. The major issue

then becomes the prediction of the evolution of corrosion rate, since that mechanical stability and degradation should be balanced so that as long as the recovery process is going on, the mechanical stability by the biomaterial can be assured without premature failure [2].

Fig. 4 illustrates the influence of pH value on the corrosion rate in electrolytes containing different amounts of chloride. The graphic depiction was drawn based on the data taken from Zhao's research [153]. The study used different approaches and methodologies to determine the corrosion rate. It is worthy of paying attention to the fact that between at a pH of 7 and 11, the influence of the different parameters is much lower than would be expected. Furthermore, these differences are much smaller than those at a pH of 3. An exception could be observed is that the corrosion rate estimated according to hydrogen development in higher NaCl concentration, at a pH of 7 and 11.

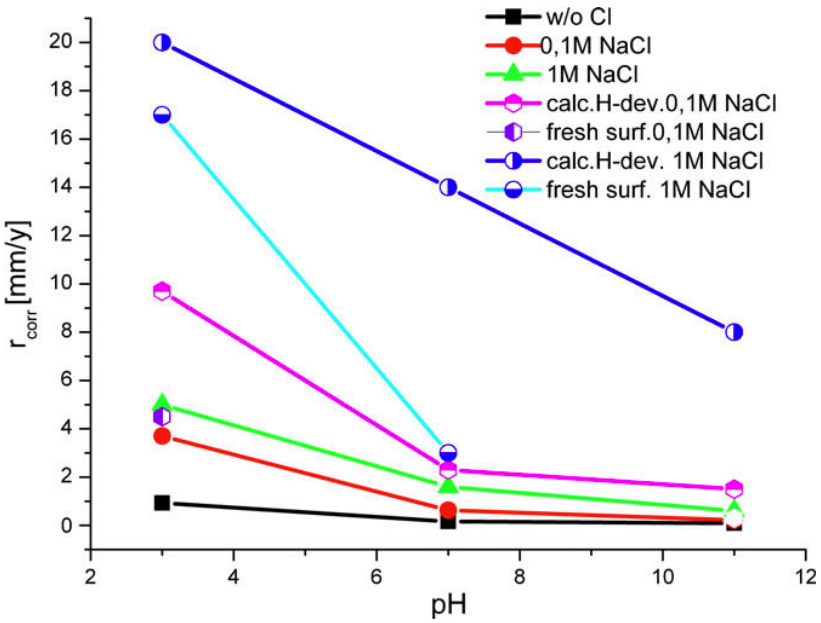

Fig. 4. Dependence of corrosion rate of ZE41 on the Cl-ion concentration; estimate based on different methods. Calc, corrosion rate (rcorr) was calculated from hydrogen development measurements; fresh surf, rcorr was determined by electrochemical measurements on a freshly prepared surface; w/o Cl, without chloride. [154]

As the collection of data presented, the observed inconsistencies between electrochemical and *in vivo* data mostly rely on the employed medium, the alloy composition and surface conditions. Nevertheless, the summarized differences could also be found when comparing different studies using different in vitro methodologies

as well as different studied materials. In the future this should be the crucial object of further and throughout discussions. After better understanding of the effects of connecting processes on the degradation of magnesium alloys, the simulation of transport conditions of the *in vivo* interface could become a focus of research interest [154].

Former studies employed quite different methods, instruments and standards which made the outputs not completely comparable, and therefore a credible *in vitro* study system is urgently wanted to be established for the future researches. The compositions, research strategies, corrosive media and circumstance (temperature, osmolality, pH value and et. al) of materials have to be considered as key parameters to warrantee the data more accurate and comparable. Hence, in this study, *in vitro* corrosion research methods were studied firstly and emphasized as an important part of the thesis.

2.5. Metallurgical Parameters of Mg-Ag Alloy

2.5.1 Phase equilibrium diagram

The Mg-Ag phase diagram shown with solid lines in Fig. 5 is established applying for a thermodynamic assessment by [155]. This diagram also include another diagram drawn by Lim (dashed lines in Fig. 5) [156] based on experimental data. Notable disagreement can be found along the (Ag)+ β' (AgMg) two-phase field boundaries. [157] Several portions are presented in the assessed phase diagram, shown in Fig. 5 and 2: (1) the liquid; (2) the solid solution of Mg with a maximum solid solubility of 3.83 at%, Ag at the eutectic temperature of 472 °C; (3) the solid solution of Ag with a maximum solid solubility of 29.3 a%t. Mg at the eutectic temperature of 759.3 ℃; (4) the intermediate phase Mg_4Ag; (5) the congruently melting Ag-Mg compound with a wide range of homogeneity that narrows at lower temperature (this in intermediate phase is in ordered condition upon the melting point); (6) the intermediate phase Mg_4Ag with a complex structure formed by a peritectic reaction at 492 °C.

Zemczuznyj determined the liquidus curve across the entire phase diagram for the first time by thermal analysis, using Mg and Ag of 99.85 %wt. and 99.74 %wt. purity respectively [34]. The melts were not stirred during the experiment, which can result in lower liquidus temperatures from undercooling. However, the outputs of this early investigation of the Ag-Mg system are in good agreement with those reported studies later.

Afterwards, the thermal analysis by Zemczuznyj revealed four invariant reactions [34]:

eutectic reactions

$$(1)\ L \leftrightarrow Mg_3Ag + (Mg) \qquad \text{(Eq. 3)}$$

$$(2)\ L \leftrightarrow (Ag) + MgAg \qquad \text{(Eq. 4)}$$

peritectic reaction

$$(3)\ L + MgAg \leftrightarrow Mg_3Ag \qquad \text{(Eq. 5)}$$

congruent melting

$$(4)\ L \leftrightarrow AgMg. \qquad \text{(Eq. 6)}$$

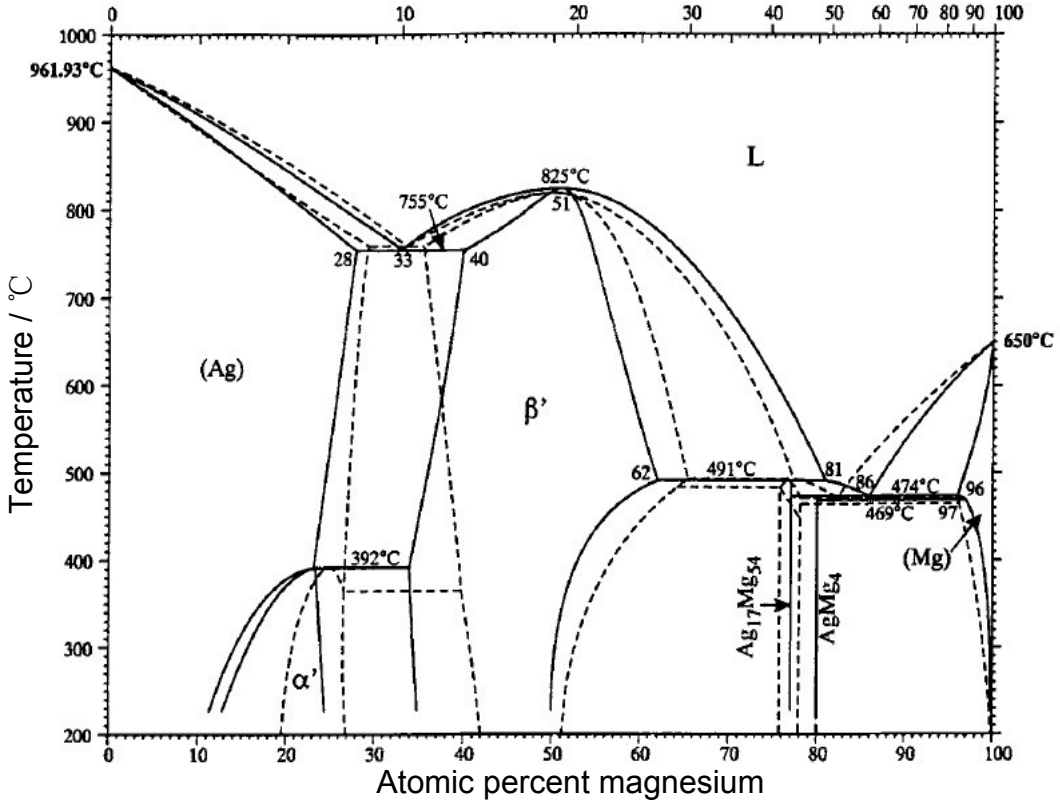

Fig. 5. The Ag-Mg phase diagram. [155]

Zemczuznyj [34] failed to find any solid solubility of Ag in Mg or the homogeneity range of the $AgMg_3$ phase, which was reported later by Smirnow and Kurnakow [158] by resistometry analysis. The liquidus temperatures, reported by Andrews and Hume-Rothery [159] (also see Hume Rothery and Butchers [160]) for the (Ag) phase and by Payne and Haughton [161] for the (Mg) phase, are 0 to 15 ℃ and 0 to 5 ℃ accordingly, above those determined by Zemczuznyj. [34] The difference is mainly due to the higher purity of the metals tested by the latter authors (Payne and Haughton [160]) and also because of their utilizing of stirring during thermal analysis,

which prevents undercooling. (Ag) solid solution extends from 0 to 60 %at. Mg with no Mg-Ag eutectic was reported by Saeftel and Sachs [162]. However, the outputs of the metallography, as well as X-ray analysis, from many investigators showed that Saeftel's study [162] was in error.

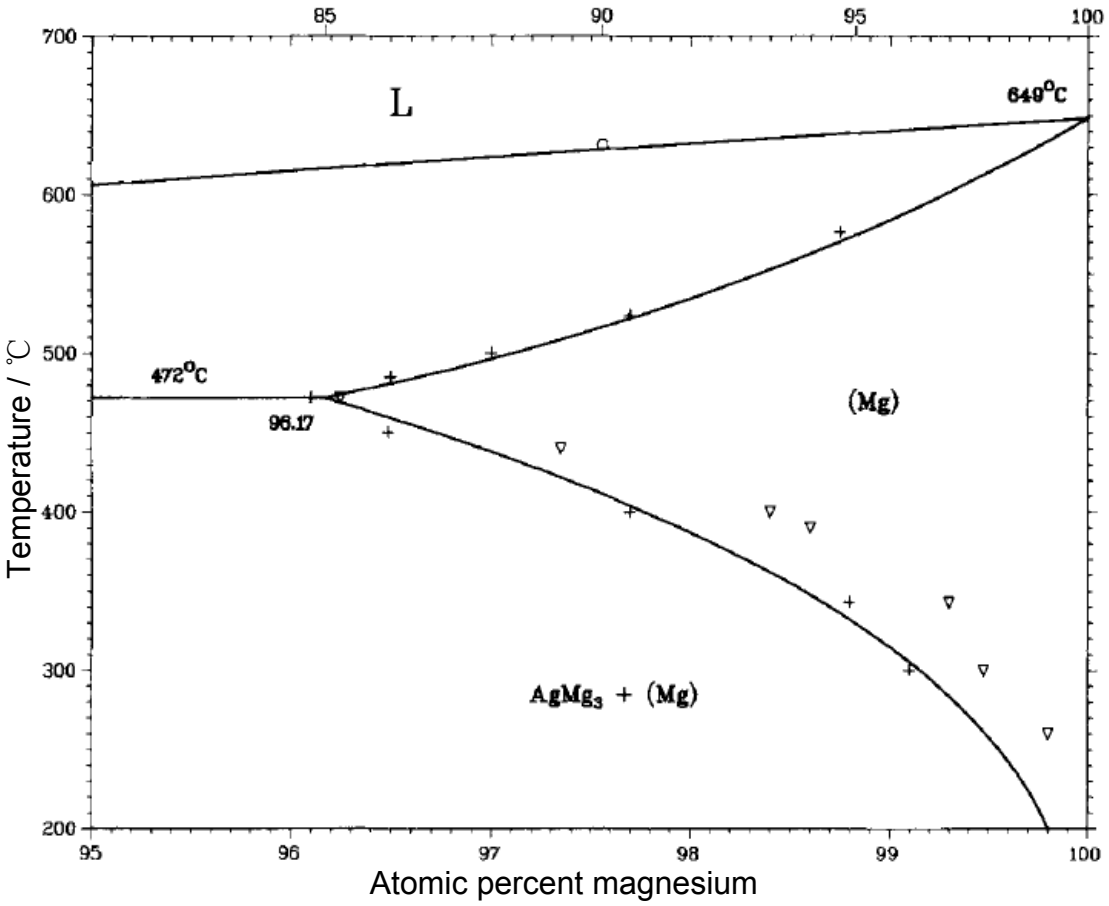

Fig. 6. Enlarged portion of the magnesium-rich region of the assessed Mg-Ag phase diagram with selected data points

Hume-Rothery and Butchers [160] and Payne and Haughton determined the (Mg) solidus curve by metallography [160]. Hume-Rothery and Butchers annealed their samples, first for six days at 420°C or eight days at 440°C and then performed a final anneal at 450 to 460 °C for nine and a half days, before step-heating to the (Mg) + L region. Payne and Haughton [161] annealed their samples at 450°C for six days. Therefore, the small difference between the reported data in these investigations could be introduced by the shorter annealing time used by Payne [161].

2.5.2. Solubility of Ag in Mg

Although the atomic diameter of Ag is within the favorable size factor with respect to Mg, the relative valency factor still restricts the solubility of monovalent Ag in divalent Mg. Zemczuznyj [34] announced that there is no solid solubility of Ag in Mg firstly. Later by electrical resistivity and hardness measurements, Stairnow and Kurnakow

[158] showed that Ag has a limited solubility in Mg, and they gave a maximum solubility of 2.58 at.% Ag (97.42 at.% Mg). Hume-Rothery and Butchers and Payne and Haughton [160] independently determined the solvus curve by metallographic analysis. Butchers annealed their samples for periods more than twice as long as Payne did [163].

Ageew and Kuznezow [164] utilized X-ray analysis to determine the solubility limits of samples annealed for a period of one-third of that applied by Hume- Rothery and Butchers [160]. The solubility limits calculated by Ageew and Kuznezow [164] and Payne and Haughton [160], while in good agreement with each other, yet are less than those presented by Hume- Rothery and Butchers [160].

2.5.3. Intermediate phases

2.5.3.1. MgAg or β' phase

The intermediate phase MgAg is a superlattice over the whole phase field and has a wide range of composition. This highly ordered structure (also designated β') is stable up to the melting temperature and was described by Kogachi for the first time [165]. The boundary of the MgAg field on the Ag-rich side (β' / [(Ag) + β']) was determined metallographically by Andrews and Hume-Rothery [159] and by lattice parameter measurements by Ageew and Kuznezow [164]. The MgAg / [(Ag) + MgAg] boundary in the assessed Mg-Ag phase diagram (Fig. 5), has been fixed by Andrews and Hume-Rothery [159] because the samples were annealed for a long time. Smirnow and Kurnakow [158], according to limited resistometry measurements, predicted that both (Ag) / [(Ag) + MgAg] and MgAg / [(Ag) + MgAg] are straight vertical lines. Metallographic analysis by Andrews and Hume-Rothery [159] and X-ray analysis by Letner and Sidhu [166] and by Ageew and Kuznezow [164] showed that, as the temperature decreases, these boundaries become slightly inclined.

Ageew and Kuznezow determined the Mg-rich boundary of the MgAg phase field over the temperature range of 260 to 390 °C by lattice parameter measurements. [164] The upper end and lower parts of this boundary remain to be fixed. The solid line portion of the MgAg/[MgAg + Mg_3Ag] boundary, shown in Fig. 5, has been derived by the data obtained by Hansen [164].

2.5.3.2. Mg_3Ag (γ' phase) and $MgAg_3$ (a' phase)

Smirnow and Kurnakow [158] found that the intermediate phase Mg_3Ag (or γ') has a narrow range of homogeneity of the Mg-rich side of the stoichiometric Mg_3Ag compound by resistivity measurements. The MgAg / [Mg_3Ag + (Mg)] boundary in the temperature range of 260 to 390 °C was determined relying on lattice parameter measurements by Ageew and Kuznezow [164].

The intermediate phase Ag_3Mg (or α' phase) generated as a result of the ordering process in the (Ag) phase was determined by Clarebrough and Nicholas [167] using

X-ray analysis. The authors also revealed that annealing of quenched Mg with 24.3 %at. alloy at temperatures between 386 and 389 °C causes ordering. Kachi [168] and Gangulee and Bever [169], reported transition temperatures of 400 and 392 ± 2 °C respectively by emf cell, calorimeter, and heat capacity measurements. These studies [170] also demonstrated that the ordering process occurs in alloys of non-stoichiometric composition. However, the two phase region ((Ag) + Mg Ag_3), reported by Gangulee and Bever [169] was not identified by Hamalainen et al. [171]. Grayevskaya et al. [172] found long and short range order coexisting in a Mg with 19 %at. Ag alloy annealed below the ordering temperature, in whose research the sample was first annealed at 600 °C for 2 hours and then quenched, followed by heating to 210 °C with quenching. Grayevskaya et al. [172] attributed this to both the existence of a two-phase range and insufficient soaking time to construct maximum possible long-range order at this temperature.

The temperature hysteresis of ca. 15 °C reported by Buckley et al. [173], however was not confirmed by Hamalainen Buckley et al., who determined the ordering as well as disordering temperatures by electrical resistivity measurements of samples within a rate of temperature change of 0.5 °C. [173] The samples disordered on heating at about 15 °C above the ordering temperature determined [155].

3. Motivation and objectives

This research work was embarked on in order to address the issues as raised in the previous sections. A systematic investigation was designed to critically discuss on the feasibility of Mg-Ag binary alloys applied as biodegradable antibacterial materials. The aims of this present work are therefore:

1. Identification of the factors affecting Mg-Ag alloys' mechanical properties and the effects of heat treatment on mechanical properties.

2. To determine the corrosion properties of Mg-Ag alloys, and establish human body like *in vitro* circumstance to simulate the corrosion process after surgery.

3. Choose properly heat treated alloys to execute the biocompatibility and antibacterial reactivity test, according to their mechanical and corrosive properties.

4. To test biocompatible and antibacterial properties of the heat treated alloys.

5. To draw the suitability of Mg-Ag alloys applied as implant materials. Choose one or two optimized alloy with balanced properties for the future *in-vivo* tests.

4. Experimental

4.1. Material manufacturing

Considering silver's solubility in magnesium (ca. 10%) [155], three magnesium-silver alloys were studied: Mg2Ag, Mg4Ag and Mg6Ag, which were cast by adding 2%, 4% and 6% silver (99.99%, Sigma-Aldrich, Steinheim, Germany) by weight into pure magnesium (>99.98%, Hydro Magnesium, Norway). For comparison, pure magnesium was used. All materials were prepared by permanent mould casting and then treated by a solidification cooling process. Magnesium and silver were melted in a steel crucible under protective atmosphere (Ar + 2% SF_6) at a temperature of 750° C for 1.5 h. Then the melt was stirred for 30 min with 200 rpm prior to casting the material into a preheated mould (550° C) made out of mild steel. To assure cleanness of the cast ingots a filter (Foseco SIVEX FC, Foseco GmbH, Borken, Germany) was used. The filled mould was held at 670 °C for 1 h under the protective atmosphere. Then, the whole steel crucible with the melt was immersed at 10 mm/s into continuous cooling water. As soon as the liquid level of the inside melt was in alignment with the height of outside water, the solidification process was finished.

4.1.2. Heat treatment

Solution treatments (T4) of the materials were carried out at 440 °C for 16 h in argon atmosphere followed by water quench at 25 ℃. Ageing treatment (T6) of the solution-treated samples was performed at 185 ℃ for 8 h followed by water quench at 25 °C. Afterwards, the as-cast and heat-treated ingots were machined to different dimensions for the following measurements.

4.2. Metallurgical analysis

4.2.1. Composition and density

The realistic composition of the alloys was obtained by X-ray fluorescence (XRF) analyzis (Bruker AXS S4 Explorer, Bruker AXS GmbH. Karlsruhe, Germany) with Bruker AXS SPECTRA plus software (version 1.70). The density of the alloys was determined by Archimedean principle.

4.2.2. Microstructure and phase identification

4.2.2.1. Optical microscopy

Optical light polarization microscopy was performed (PM, 020-520-008 DM/LM, Leica GmbH, Wetzlar, Germany) to get an overview of the distribution and sizes of the phases within the material. 5.0 mm × 20.0 mm × 20.0 mm brick samples were machined for all microstructure characterizations. Measured surfaces were ground with water and ethanol (> 99.5%, Sigma-Aldrich, Steinheim, Germany) down to a grinding size of grade 1200, polished with a lubricant containing 3 µm diamond particles (> 99.5%, Sigma-Aldrich, Steinheim, Germany) followed by a lubricant containing 1 µm diamond particles under addition of dish liquid (Struers GmbH, Willich, Germany). Then they were etched for a few seconds in an ultrasound bath with 10% nital (10% nitric acid in ethanol, Sigma Aldrich Chemie, Taufkirchen, Germany) to clean off remains, followed by etching with a solution of 35 mL H_2O, 6.5 g acetic acid (≥ 99.7%, Sigma-Aldrich, Steinheim, Germany) and 5 g picric acid (≥ 98%, Sigma-Aldrich, Steinheim, Germany) in 140 mL ethanol [174]. The etched samples were cleaned by ethanol and then dried by compress hot air.

4.2.2.2. SEM and EDX analysis

Scanning electron microscopy (SEM Auriga, Zeiss, Oberkochen, Germany) equipped with an energy-dispersive X-ray spectrometer (EDX; Sapphire CDU, EDAX Int, Mahwah, USA) was applied to evaluate the composition of the microstructure. Samples for SEM analysis were polished with emery paper of various grades up to 3200 grade followed by a diamond suspension down to 3 µm diamond particles. In the last step of polishing, ethanol was used as lubricant instead of water. The specimen were then degreased and rinsed with pure ethanol. SEM analysis was performed shortly after finishing the sample preparation to characterize the initial conditions. The morphological features were examined by recording secondary electron (SE) images under high vacuum (10^{-6} mbar), at 15 kV accelerating voltage, 90 µA beam current and 200 × magnification.

4.2.2.3. XRD analysis

Samples were polished with emery paper of various grades up to 3200 grade followed by a diamond suspension down to 1 µm diamond particles. Then they were investigated by X-ray diffraction (XRD) in a parallel beam geometry, using Cu-$K_{\alpha 1}$ radiation (wavelength λ=1.5406 Å). The X-ray diffractometer (Siemens D5000 from Siemens AG, Munich, Germany) was operated in transmission mode in the range 2θ = 15–90° with a step length of 0.0153° and 3 s/step. The determination of the lattice parameter has shown a precision of better than 0.01 Å. Diffraction patterns were analysed using the database PDF-2 (Release 2002) from the International Center for Diffraction (ICDD) [175].

4.2.3. Mechanical properties

Vickers hardness (HV5), tension and compression measurements have been carried out for mechanical characterization of the materials. Vickers hardness measurements (HV 5) were done with a standard microhardness tester (Carl Zeiss, Jena, Germany) after mirror polishing following ASTM standard [176]. The tension and compression tests were performed using standard mechanical testing machine (Zwick Z050, Zwick GmbH, Ulm, Germany). The samples were placed in the chamber at the test temperatures for 10 min before measurement in order for the homogenous distribution of temperature before tests. Each mechanical test was carried out under human body temperature (37.0 ºC), which assured the results more credible and closer to realistic implant conditions than many other studies. All measurements were carried out in quintuplicate to assure statistical accuracy according to ASTM standard [177].

4.3. Optimum of *in vitro* corrosion testing methods

4.3.1. Comparison and choosing of Corrosion media

4.3.1.1. Materials

Pure magnesium samples (99.98%, Hydro Magnesium, Norway) were prepared by permanent mould casting. The metal was molten under protective atmosphere (Ar + 2% SF_6) at a temperature of 750 °C. Then the melt was stirred for 30 min with 200 rpm prior to casting the material into preheated moulds (550 °C) made out of mild steel. To assure cleanliness of the cast ingots a filter (Foseco SIVEX FC, Foseco GmbH, Borken, Germany) was used. Cylindrical specimens with a diameter of 5 mm and a height of 1.5 mm were cut from the cast blocks via electrical discharge machining. Specimens were carefully mechanically polished with water and SiC, from 1000 grid to 4000 grid gradually. After polishing, the specimens were immediately put into pure? Ethanol.

Dulbecco's Modified Eagle Medium (DMEM) with 4.5 $g \cdot L^{-1}$ Glucose and Hank's Buffered Salt Solution without calcium and magnesium (HBSS) are commercially available (Life Technologies, Darmstadt, Germany). Simulated Body Fluid (SBF) was produced according to the recommendation of Bohner [178]. The compositions of DMEM, HBSS and SBF are listed in Table 3.

4.3.1.2. Immersion experiments

Immersion media were sorted into 3 groups, namely DMEM, HBSS and SBF. The specimen were immersed in 2 mL of the respective media under sterile conditions and incubated under cell culture conditions (37°C, 21% O_2, 5 % CO_2, 95% relative humidity) for 20 h. After immersion, half of the samples were directly put into the vacuum dryer, whereas the other half were rinsed with deionized water for 1 min and

then vacuum dried. After drying for 12 hrs, all the samples were stored in argon atmosphere.

Table 3. The compositions of DMEM, HBSS and SBF

Ingredient	DMEM [mM]	HBSS [mM]	SBF [mM]
Calcium Chloride ($CaCl_2$)	1.80		1.84
Ferric Nitrate ($Fe(NO_3)_3$)	0.000248		
Hydrochloric acid (HCl)			
Magnesium Sulfate ($MgSO_4$)	0.813		25.62
Potassium Chloride (KCl)	5.33	5.33	
Potassium Phosphate monobasic (KH_2PO_4)		0.441	
Sodium Bicarbonate ($NaHCO_3$)	44.05	4.17	35.05
Sodium Chloride (NaCl)	110.34	137.93	105.62
Sodium Phosphate monobasic (NaH_2PO_4)	0.916		
Sodium Phosphate dibasic (Na_2HPO_4)		0.338	1.75
D-Glucose (Dextrose)	25.00	5.56	
Glycine	0.4		
L-Alanyl-L-Glutamine	3.97		
L-Arginine hydrochloride	0.398		
L-Cystine·2HCl	0.201		
L-Histidine hydrochloride	0.2		
L-Isoleucine	0.802		
L-Leucine	0.802		
L-Lysine hydrochloride	0.798		
L-Methionine	0.201		
L-Phenylalanine	0.4		
L-Serine	0.40		
L-Tyrosine	0.398		
L-Valine	0.803		
Choline chloride	0.029		
D-Calcium pantothenate	0.008		
i-Inositol	0.04		
Niacinamide	0.033		
Pyridoxine hydrochloride	0.0196		
Riboflavin	0.001		
Thiamine hydrochloride	0.012		
Phenol Red	0.0399		
Sodium Pyruvate	1.000		

4.3.1.3. XPS analysis

X-ray induced photoelectron spectroscopy (XPS) experiments were carried out on a Kratos Axis Ultra DLD (Kratos Analytical Ltd., Manchester, UK) attached with a 15 kV X-ray gun using monochromatic Al K-alpha radiation. The spot size was 700×300 μm

and the pass energy was 40 eV at the regions measurements and 160 eV for survey scans. As a result of nonconductive properties of the corrosion products, a charge neutralizer was used to correct the chemical shifts due to charging. Due to physical limits the information depth is limited to approx. 5 nm.

Additionally, argon ions (4000 eV) have been used to etch the samples in order to prevent surface contamination. The applied sputter rate of approx. 36 nm per minute was used to remove other contamination effects by sputtering for two minutes. The following core levels were analyzed besides survey spectra: Mg 2p, O 1s, C 1s, Ca 2p and P 2p. By determination of the binding energy on these states, the present chemical bonds have been accurately determined. Curve fitting of the spectra was performed with Casa 2.3.15 software (Casa Software Ltd., Teighnmouth, Devon, UK, 2003). The binding energy can be estimated to an accuracy of ±0.3eV.

4.3.2. Protein's effects on corrosion of Mg-Ag alloys

4.3.2.1. Materials

Cylindrical specimens with a diameter of 5 mm and a height of 1.5 mm were cut from the cast blocks via electrical discharge machining. Specimens were carefully mechanically polished with water and SiC, from 1000 grid to 4000 grid gradually. After polishing, the specimens were immediately put into deaerated ethanol for the following measurement. The electrolytes were DMEM Glutamax-I (Life Technologies, Darmstadt, Germany) with and without the addition of 10% (by volume) Fetal Bovine Serum (FBS) (FBS Gold, PAA Laboratories, Linz, Austria). The composition of the corrosion medium is summarised in table 3. A detailed description of the formulation can be found elsewhere [179].

4.3.2.2. Electrochemical measurement

The corrosion resistance of the specimens was evaluated by linear sweep voltammetry, and cyclic voltammetry using a mini cell system setup (MCS). The choice of the MCS was made due to the small dimensions of the samples and the need to test the material without any further preparation, to better simulate the clinical conditions [180]. The electrochemical measurements were performed using MCS connected to a potentiostat (EI 1286 Schlumberger, Braunschweig, Germany) (Fig. 7).

A saturated calomel electrode (SCE, E_0 = 0.241 V vs. SHE - standard hydrogen electrode) was used as reference electrode. The scan rate was set at 10mV/s, and the contact area was 0.008 cm^2. The potential range was between -2.0 V and -0.5 V (vs SHE) for single sweep voltammogram test and between -0.5V and +0.5 V (vs. OCP - open circuit potential) for cyclic voltammeter test. All measurements were performed at room temperature. From the current density-potential curves, the following electrochemical parameters were determined: polarization resistance (R_p), exchange current density (I_0) and corrosion potential (E_{corr}). The data were collected

and analyzed by using the Corrware and Corrview software respectively (Scribner Associates Inc., Southern Pines, NC, USA).

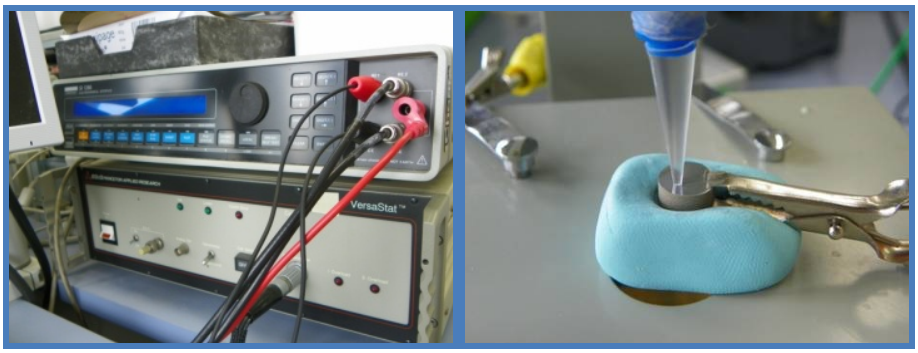

Fig. 7. Mini cell system applied for corrosion tests

4.3.2.3. Microstructure characterization

Microstructural investigations were performed using optical microscopy and scanning electron microscopy (SEM). Optical microscopy has been performed to get an overview of distribution and size of components within the material. The SEM (Quanta 200, FEI, Hillsboro, OR, USA) equipped with an energy-dispersive X-ray spectrometer (Sapphire CDU, EDAX Int, Mahwah, NJ, USA) was applied. The morphological features were examined by recording secondary electron (SE) images under high vacuum (10^{-6} mbar), at 20 kV accelerating voltage, 90 µA beam current and 1000× original magnification on specimen. The sample preparation for optical microstructure investigations is reported briefly: cross and longitudinal sections were ground with water and ethanol down to a grinding size of 1200, polished with a lubricant containing 3 mm diamond particles followed by a lubricant containing 1 mm diamond particles under addition of dish liquid (Struers GmbH, Willich, Germany). They were etched first with 10% nital for a few seconds to clean off remains in the ultrasound bath and then etched with a solution, which contains 35 mL H_2O, 6.5 g acetic acid and 5 g picric acid in 140 mL ethanol [174].Compressed air was utilized for a dry surface.

4.3.2.4. XPS investigation

X-ray induced photoelectron spectroscopy (XPS) experiments were carried out on a Kratos Axis Ultra DLD (Kratos Analytical Ltd., Manchester, UK) attached with a 15 kV X-ray gun using monochromatic Al K-alpha radiation. The spot size was 700 × 300 µm and the pass energy was 40 eV at the regions measurements and 160 eV for survey scans. As a result of nonconductive properties of the corrosion products, a charge neutralizer was used to correct the chemical shifts due to charging. Due to physical limits the information depth is limited to approx. 5 nm. Additionally, argon ions (4000 eV) have been used to etch the samples in order to prevent surface contamination. The applied sputter rate of approx. 36 nm per minute was used to

remove other contamination effects by sputtering for two minutes. Measured areas were at the depth of around 72 nm from the surface, which were still at the surface of the whole corrosion layer of up to 100 µm thickness. The following core levels were analyzed besides survey spectra: Mg 2p, O 1s, Cl 2p and Ag 3d. By determination of the binding energy on these states, the present chemical bonds have been accurately determined. The binding energy can be estimated to an accuracy of ±0.3 eV. Curve fitting of the spectra was performed with Casa 2.3.15 software (Casa Software Ltd., Teighnmouth, Devon, UK, 2003) to each element. The applied element binding energy database is NIST Standard Reference Database 20, Version 3.5.

4.4. Corrosion properties

4.4.1. Electrochemical analysis

The corrosion resistance of the specimen was evaluated by single sweep voltametry, using a mini cell system setup (MCS). The choice of the MCS was made due to the small dimensions of the samples and the need to test the material without any further preparation to better simulate the clinical conditions [180]. The specimens were 10.0 mm in diameter and 1.5 mm in height. As electrolyte the cell culture medium Dulbecco's Modified Eagle Medium (DMEM) Glutamax-I (Life Technologies, Darmstadt, Germany) with the addition of 10% (by volume) Fetal Bovine Serum (FBS, FBS Gold, PAA Laboratories, Linz, Austria) with the total amount of proteins of 30 - 45 g/L was used. The detailed description of the formulation can be found elsewhere [179]. The MCS was connected to a computer controlled potentiostat (EI 1286, Schlumberger, Braunschweig, Germany) driven by the software Corrware@ for Windows (Scribner Associates, Southern Pines, USA). A saturated calomel electrode (SCE, E_0 = 0.241 V vs standard hydrogen electrode, SHE) was used as reference electrode. The scan rate was set at 10 mV/s; the contact area was 0.008 cm^2 and the potential range was varied between -2.0 V and -0.5 V (vs SHE). Measurements were executed at 37.0º C under atmosphere with 5% CO_2 to maintain the data comparable to immersion tests results and cell culture conditions. The data were collected and analyzed by using the Corrware and Corrview software respectively (Scribner Associates Inc., Southern Pines, NC, USA). Treated areas of the samples were also analyzed by SEM microscopy (Quanta 200, FEI, Hillsboro, OR, USA) to identify the corrosion type.

4.4.2. XPS depth profiling

X-ray induced photoelectron spectroscopy (XPS) experiments were carried out on a Kratos Axis Ultra DLD (Kratos Analytical Ltd., Manchester, UK) attached with a 15 kV X-ray gun using monochromatic Al Kα radiation. The spot size was 700 × 300 µm and the pass energy was 40 eV at the regions measurements and 160 eV for survey

scans. As a result of the nonconductive properties of the corrosion products, a charge neutralizer was used to correct the chemical shifts caused by charging. Due to physical limits the information depth is limited to approx. 5 nm. Before starting the measurements argon ions (4000 eV) were used for 2 min (applied sputter rate of approx. 36 nm / min) to etch the samples to prevent surface contamination. The first measured layer therefore was at the depth of around 72 nm from the surface. Depth profiles of the samples were obtained by combining a sequence of 100 min ion gun etching cycles interleaved with XPS measurements. This leads to measured layers which are ca. 3 µm deeper than the former layer. Ion gun etching cycles ran twice per sample resulting in three XPS spectra for each sample.

The following core energy levels were analyzed besides survey spectra: Mg 2p, O 1s, Cl 2p, Ca 2p, P 2p and Ag 3d. By determination of the binding energy of these states, the present chemical bonds were accurately determined. The binding energy (binding energy database NIST Standard Reference Database 20, Version 3.5) can be estimated with an accuracy of ±0.3eV. The curve fitting of the spectra was performed with Casa 2.3.15 software (Casa Software Ltd., Teighnmouth, Devon, UK, 2003). Side view pictures were captured by SEM (Auriga, Zeiss, Oberkochen, Germany) to analyze the vertical distribution of corrosion products.

4.4.3. Immersion tests

After the comparison of the material corrosion properties without and with different heat treatment, T4 treated alloys and pure magnesium as reference were selected for immersion tests to get ion release information. The specimens were 10.0 mm in diameter and 1.5 mm in height, and successively polished with emery paper of various grades up to 3200 grade followed by a diamond suspension down to 1 µm diamond particles. Prior to the corrosion test, the concentration of Mg^{2+} and Ag^{+} ions (ISE electrode WD-35802, Oakton Instruments, Vernon Hills, USA and Ion Selective Electrode HI 4015, Hanna Instrument, Woonsocket, USA) as well as the osmolality (Osmomat 030, Gonotec, Berlin, Germany) and the pH (pH/mV meter PH210, Hanna Instrument, Woonsocket, USA) of the media was measured. Then the samples were immersed in triplicates in 3.0 mL of growth medium DMEM with 10% FBS and incubated under cell culture conditions (37 ºC, 20% O_2, 5% CO_2, 95% relative humidity) for 72 h. Then the Mg^{2+} and Ag^{+} ion concentrations, the osmolality and pH of the extract were determined. The corroded specimens were photographed, rinsed with deionized water and dried. The morphology of the corrosion surface was determined by SEM (Auriga, Zeiss, Oberkochen, Germany) in backscattering mode (Detector BSD, 20 keV, 8.5 mm working distance).

4.5. Cytocompatibility tests

4.5.1. Specimen preparation

Cylindrical specimens with a diameter of 10.0 mm and a height of 1.5 mm were cut from the T4 treated blocks via electrical discharge machining. The average weight of the specimen was 207.1 ± 1.5 mg for pure magnesium and 212.0 - 216.0 ± 1.5 mg for Mg-Ag alloys. For strict sterilization, the samples were sonicated for 20 min in dry isopropanol, dried and gamma-sterilized at the In Core Irradiation (ICI) facility of the Research Reaktor FRG-1 (Geesthacht Neutron Facility GeNF, Germany) with a total dosage of 29 kGy.

4.5.2. Isolation and culture of cells

The MG-63 cell lines, RAW 264.7 cell lines and Human umbilical cord perivascular cells (HUCPV) were chosen to evaluate cytotoxicity of silver ions, while human osteoblast primary cells were isolated and cultured for cell attachment test.

4.5.2.1. MG-63 cells and RAW 264.7 cells

The human osteosarcoma cell line MG-63 was obtained from the European collection of cell cultures (ECACC, Salisbury, UK). The cells were cultured under standard cell culture conditions (37 ºC, 20% O_2, 5% CO_2, 95% rH) in DMEM with 10% FBS. Cells were passaged at subconfluency (70 - 80%) and reseeded in a density of 2×10^4 cells • cm^{-2}. For cell culture experiments cells after the fifth passage were used. The tumor-derived mouse macrophage cell line (RAW 264.7, ECACC, Salisbury, UK) is capable of producing cytokines like nitric oxide (NO) and tumor necrosis factor α (TNF-α) as an *in vitro* inflammatory response. Cells were cultured in DMEM low glucose with 2 mM glutamine and 10% FBS and passaged at 60-70% confluence. Cells starting from the fifth passage were used for experiments.

4.5.2.2. Human umbilical cord perivascular cells (HUCPV)

Mesenchymal stem cells derived from Wharton`s jelly of the umbilical cord were isolated by a modified isolation protocol from Sarugaser et al. [181]. Isolation was approved by the local ethical committee. In brief, umbilical cords from consenting full term caesarean section patients were cut into pieces of about 5 cm. The vessels from the cord pieces were isolated and tied together at the ends with sutures, leading to a vessel loop. These were placed in T-175 cell culture flasks and cultured for 10 days without medium change in α-MEM (Life Technologies, Darmstadt, Germany) with 10% FBS for mesenchymal stem cells (Stem Cell Technologies, Vancouver, Canada). After visible outgrowth from the loops medium was changed every 2-3 days. At about 60% confluency the cells were harvested with a cell scraper and subcultivated in a density of 1000 cells • cm^{-2}. For the experiments cells of the third to fifth passage were used.

4.5.2.3. Human osteoblast cells

Human osteoblast primary cells were cultured from bone chips obtained from patients undergoing total hip arthroplasty. The cancellous bone was cut into 5-mm pieces, and after removal of bone marrow, the bone chips were cultured in DMEM with 10% FBS. The culture was maintained for approximately 10 days without medium change. Thereafter, the medium was changed every three days and cells were passaged after reaching 70-80% confluency.

4.5.3. MTT-assay for silver ion cytotoxicity

1 nM to 100 mM $AgNO_3$ (Sigma Aldrich Chemie, Taufkirchen, Germany) was applied as silver ion provider for the measurement of silver ion cytotoxicity. The MG-63 and RAW 264.7 cells were seeded on 96-well-plates (5000 cells per well) with 100 µL of the cell type specific medium with according concentration of silver ion. The cells were cultivated for 24 h under cell culture conditions and their viability was analyzed by the MTT (methylthiazolyldiphenyl-tetrazolium bromide, Sigma Aldrich Chemie, Taufkirchen, Germany) assay. After incubation, 10 µL of the MTT-solution (5 mg/mL MTT in phosphate buffered saline, PBS) was added. After 5 hours the cells were lysed and the formazan crystals solubilized by adding 100 µL solubilization solution (10% SDS in 0.01M HCl, Merck, Darmstadt, Germany), followed by an incubation overnight under cell culture conditions. The solubilized formazan product was photometrically quantified using an ELISA reader (Tecan Sunrise, TECAN Deutschland GmbH, Crailsheim, Germany) at 570 nm with a reference wavelength of 655 nm. The same experiments were performed without cells to exclude an influence of the salt concentrations on the MTT-assay (negative control). In addition the same tests were executed with $NaNO_3$ (≥ 99.0%, Sigma-Aldrich, Steinheim, Germany) to determine the influence of nitrate and to monitor the change of osmolarity with increasing nitrate. The experiments gave the lethal concentration LC50 where 50% of the cells survive.

4.5.4. Cell adhesion testing

To evaluate the biocompatibility of the Mg-Ag alloys, primary osteoblasts were cultured on the surfaces of pure magnesium and T4 treated alloys. Human osteoblast cells were incubated with a seeding density of ca. 1×10^5 cells per specimen with 10 ml DMEM + 10% FBS. Three triplicates were tested for every material. Cell culture medium was changed every 48 h and the total incubation time was 14 days. The viability of osteoblast cells was then determined using a LIVE/DEAD Viability/Cytotoxicity Kit (Life Technologies, Darmstadt, Germany), which measures the membrane integrity of cells. A fluorescence microscope (Eclipse Ti-S, Nikon, Düsseldorf, Germany) was utilized to observe and calculate the viability of tested cells. Viable cells show a green fluorescence through the reaction of the acetomethoxy derivate of calcein with intracellular esterase, whereas non-viable cells

show red fluorescence due to the diffusion of ethidium homodimer across damaged cell membranes and binding with nucleic acids.

SEM (Auriga, Zeiss, Oberkochen, Germany) was used to view the cell cultured surfaces of pure magnesium and T4 treated alloys. Human osteoblast cells were firstly incubated on the specimen surface for 6 hours, with a seeding density of ca. 1×10^5 cells per specimen. After incubation, cells on specimens were fixed with 1% glutaraldehyde solution (Glutaraldehyde solution, Sigma-Aldrich Chemie GmbH, Taufkirchen, Germany) for cell analyses. The fixed specimens were then dehydrated with five different concentrations of aqueous ethanol solution, 20%, 40%, 60%, 80% and 100% sequentially. The samples were then dried using a critical point dryer (EM CPD030, Leica GmbH, Wetzlar, Germany). The dried samples were immediately visualized by SEM to avoid rehydration and contamination.

4.6. Antibacterial properties

The detection of antibacterial effects of Mg-Ag alloys was done by testing the bacterial adhesion and the change in the vitality of adhering bacteria populations. An dynamic *in vitro* biofilm simulation system (developed by iba Heiligenstadt, Germany) allows the testing of bacteria proliferation and biofilm formation could be performed under reproducible conditions and it was proven with high clinical relevance [182]. The main features of the test system are summarized in Fig. 8.

4.6.1. Specimen preparation

Cylindrical specimens with a diameter of 10.0 mm and a height of 1.5 mm were cut from the T4 treated alloys. Titanium, glass and pure magnesium specimens of the same size were prepared as reference. The specimens were grinded with 1200 and 4000 emery paper, and then polished with 1 μm diamond suspension. For a clean surface and sterilization all the specimens were immersed in 100% ethanol in an ultrasonic bath for 10 min. After cleaning and sterilization, the specimens were stored in 100% ethanol before tests.

4.6.2. Antibacterial testing with bioreactor

The antibacterial properties of the material were determined in a co-culture of two staphylococcus strains: *S. aureus* (DSMZ 20 231) and *S. epidermidis* (DSMZ 3269) at the rate of 1:1, using tryptic Soy Yeast Extract medium (Trypticase Soy Broth 30 g/L, Yeast Extract 3 g/L, pH = 7.2, Sigma Aldrich Chemie, Taufkirchen, Germany). The bacteria concentration was 107 / ml after mixture. The co-culture was first incubated in the bioreactor with 500 mL media (dynamic cultivation of bacteria, 37º C, aerated, sterile conditions, pH = 7.2). As Fig. 8 illustrated, the biofilm formation on the samples was then studied by connecting the bioreactor to the flow chambers which contained one specimen each. Thus specimens were tested in parallel by

flushing the medium containing the bacteria with a flow rate of 0.3 mL / min for 15 hours above the sample. Each material was studied in three separate tests.

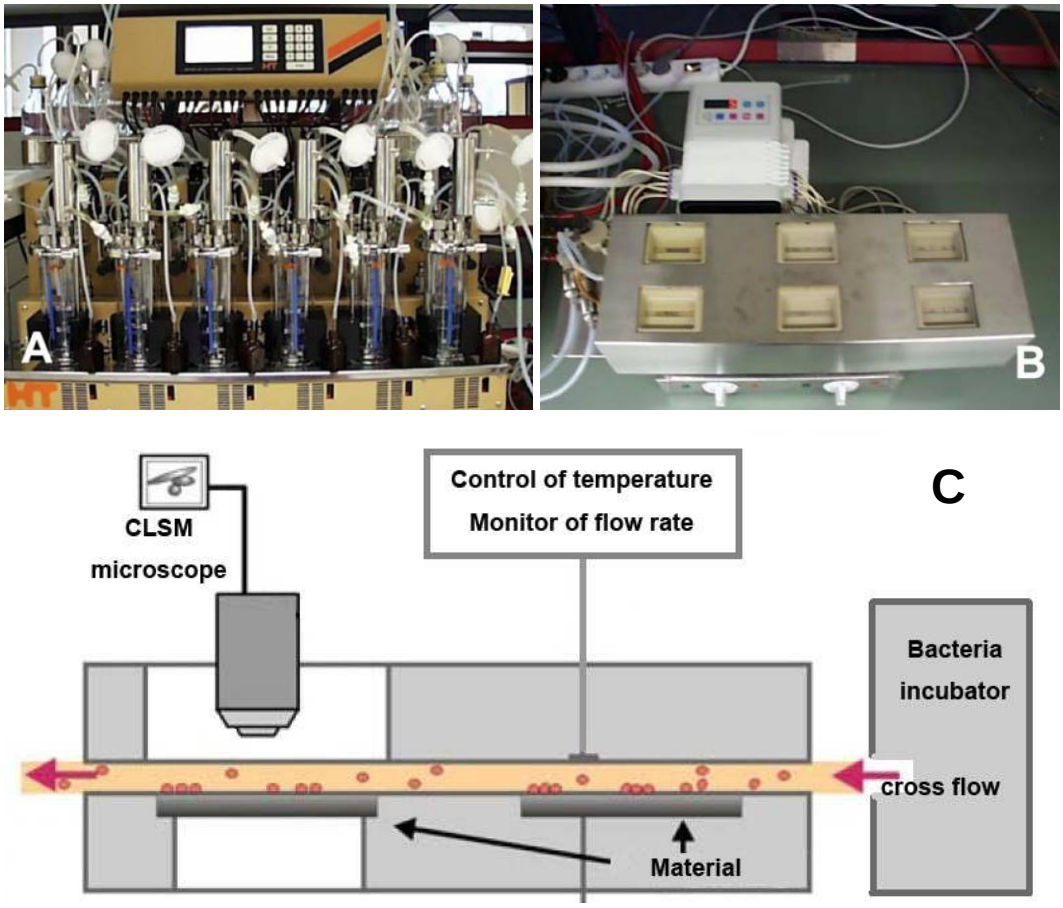

Fig. 8. *In-vitro* bio-film simulation system: A. multi-bioreactor for bacteria mixed culture; B. flow chamber with temperature and flow control; C. scheme of the bioreactor applied for antibacterial testing.

4.6.3. Quantitative determination and in situ imaging

Qualitative assessment of biofilm formation was done by *in situ* imaging of adhering bacteria with live-dead staining using CLSM (Confocal laser scanning microscopy, TCS SP2, Leica GmbH, Wetzlar, Germany) at 488 nm wave length during the run of the bioreactor.

After 15 hours incubation the samples were carefully rinsed with PBS to remove unattached bacteria, and then treated by ultrasonic bath to collect all the adhering bacteria. By checking sample surfaces via microscopy after ultrasonic treatment, it was ensured that all the originally adherent bacteria were removed by ultrasound and available for following quantitative analysis. Quantitative determination of the number of adhering bacteria and their vitality was carried out by counting with a nucleo counter (6 duplicate areas per sample and 3 duplicate samples per material) and live-dead staining (Live / Dead BacLight TM, Molecular Probes).

4.7. Statistical analysis

Statistics were performed using the SigmaStat package (Systat software GmbH, Erkrath, Germany). Standard analysis comparing more than two treatments was done by using the one-way ANOVA with Holm-Sidak versus control group Post-Hoc testing. Statistical significance was defined as $p < 0.05$, and statistical results are indicated at the relevant experiments.

5 Results

5.1. Metallurgical analysis

5.1.1. Composition and density

The realistic compositions of three Mg-Ag alloys obtained from XRF measurements were 1.87% in Mg2Ag, 3.82% in Mg4Ag and 6.00% in Mg6Ag silver content in magnesium by weight respectively. Table 4 shows the composition of the studied materials, their equivalent mass and their average density.

Table 4. Mass composition, atomic ratio and average density for the alloys studied.

Materials	Mass composition (%)	Atomic ratio (%)	Equivalent Mass (g)	Density (g/cm^3)
Mg	100 Mg	100 Mg	12.16	1.74
Mg2Ag	98.13 Mg, 1.87 Ag	99.56 Mg, 0.44 Ag	12.54	1.76
Mg4Ag	96.18 Mg, 3.82 Ag	99.11 Mg, 0.89 Ag	13.02	1.79
Mg6Ag	94.00 Mg, 6.00 Ag	98.54 Mg, 1.46 Ag	13.49	1.83

5.1.2. Metallurgical microstructure and phase identification

The microstructure of the cast samples revealed that inside the grains secondary dendrites drastically increase with higher silver content (Fig. 9).

The average grain size of Mg2Ag, Mg4Ag and Mg6Ag was 600 μm, 480 μm and 350 μm respectively. Due to the relatively slow cooling rate of the casting process, the structure of the sample mainly consisted of coarse equiaxed grains rather than columnar grains. As can be seen in Fig. 9, under the same heat treatment conditions, the grain size of Mg-Ag alloys was obviously reduced by increasing content of silver. Compared to cast materials, heat treatment did not show notable influence on changing grain size. Eutectic phases, formed during the solidification and distributed along the grain boundaries, were erased by T4 treatment. T4 and T6 treatment also wiped out most of secondary dendrite which hinted the solution treatment was successful. There were quite few visible re-precipitated secondary phases in T6 treated samples fewer than 50 × magnifications, which illustrates secondary phases re-precipitated in very small amount.

The refined microstructures provided by SEM patterns showed the effects of silver content addition and heat treatment on phase transformation (Fig. 10). Eutectics could be clearly observed along grain boundaries, whose amount increased dramatically with more silver content. The size of the secondary phases varied from hundreds of nanometers to several micrometers. Eutectic structures appeared continuously along grain boundaries in cast Mg6Ag and formed networks.

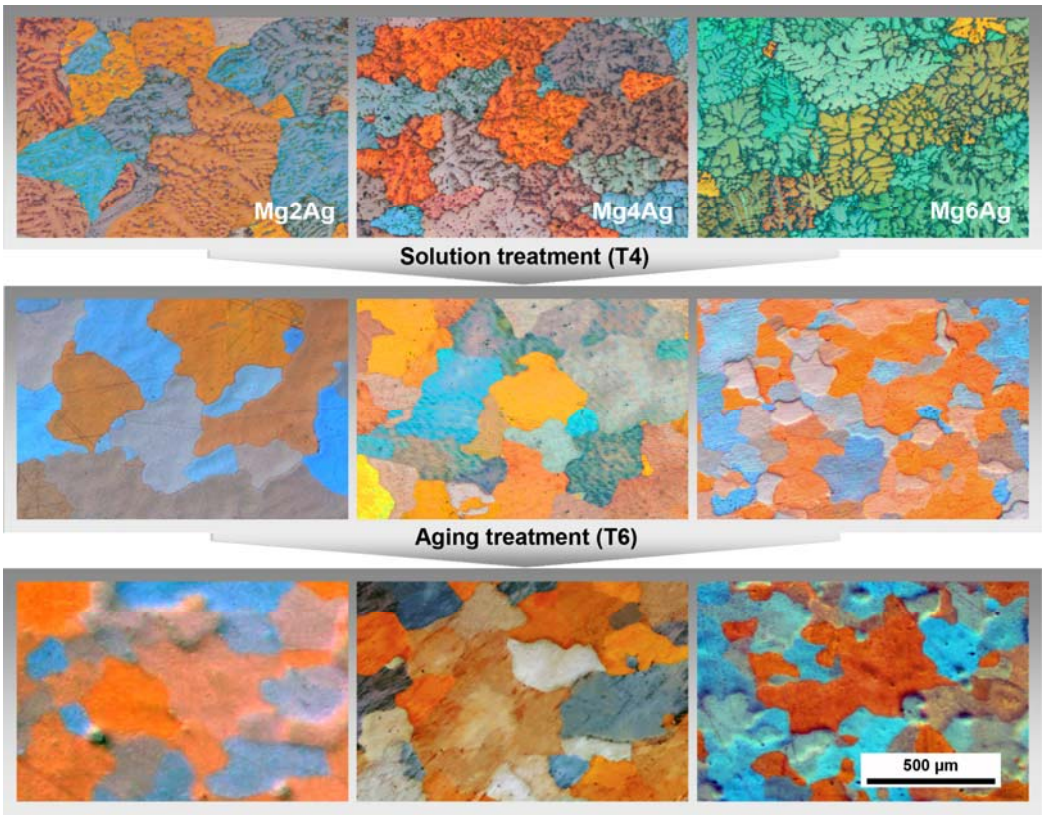

Fig. 9. Microstructures of casted, T4 treated and T6 treated alloys from optical microscopy. Most dendrites and eutectic tissue were eliminated after T4 treatment.

Secondary as well as eutectic phases could be hardly found in all T4 and T6 treated samples, which demonstrated they had vanished during aging process and re-precipitated phases were smaller than 500 nm (Fig. 12). EDX analysis results in Fig. 10 reveals that the dominant secondary phase in all three cast alloys was Mg_4Ag according to element distribution.

The X-ray diffraction pattern of the cast alloys (Fig. 11) exhibited dominant α-Mg reflections. Apart from primary phase, there were notable reflections from the Mg_4Ag phase, which confirmed the phase identification results from EDX analysis. Weak indications of $Mg_{54}Ag_{17}$ could also be observed in XRD patterns especially in Mg6Ag.

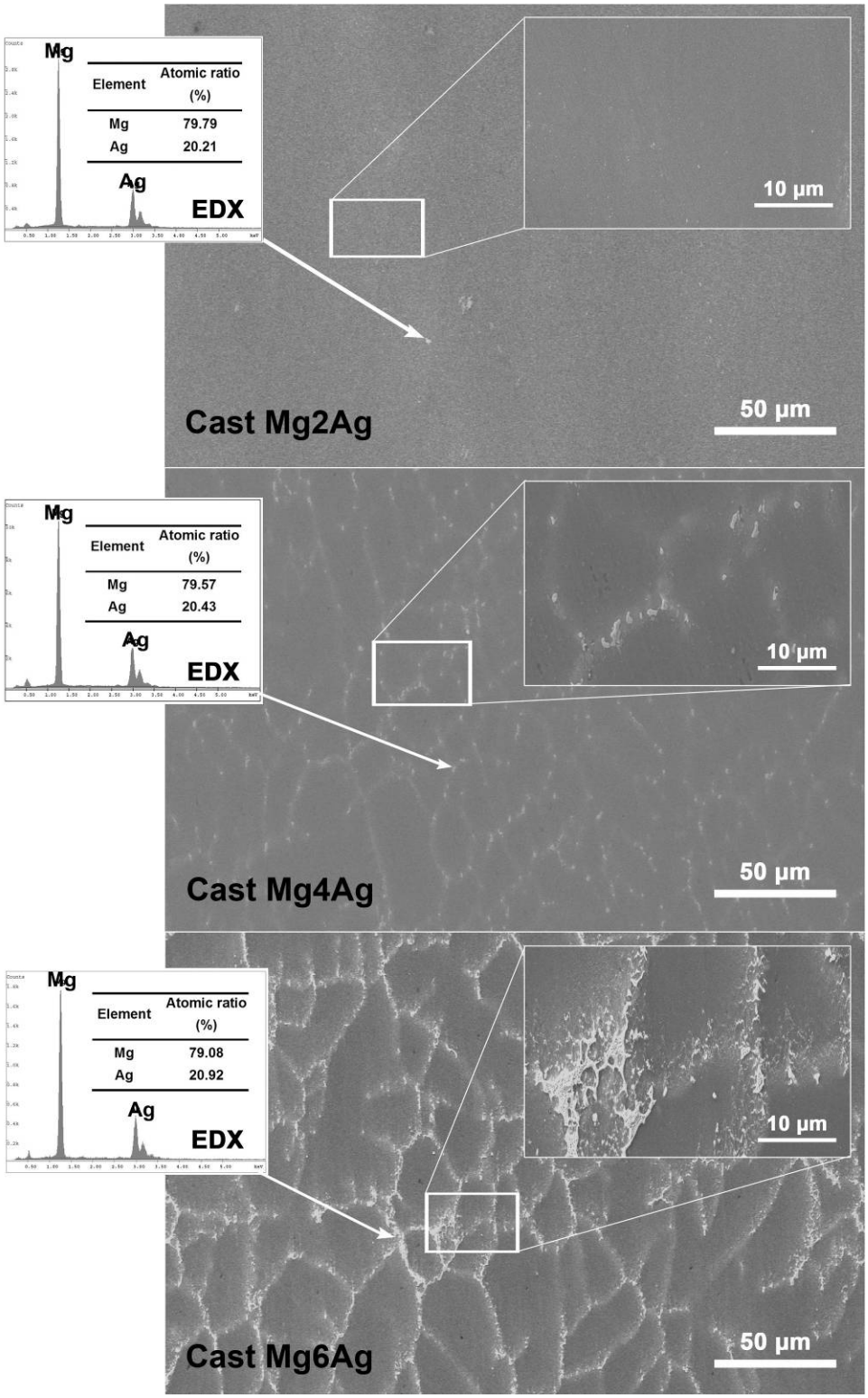

Fig. 10. SEM images and EDX analysis to cast Mg-Ag alloys. Combination of Mg_4Ag and $Mg_{54}Ag_{17}$ were identified as the main species of secondary phases in all Mg-Ag alloys.

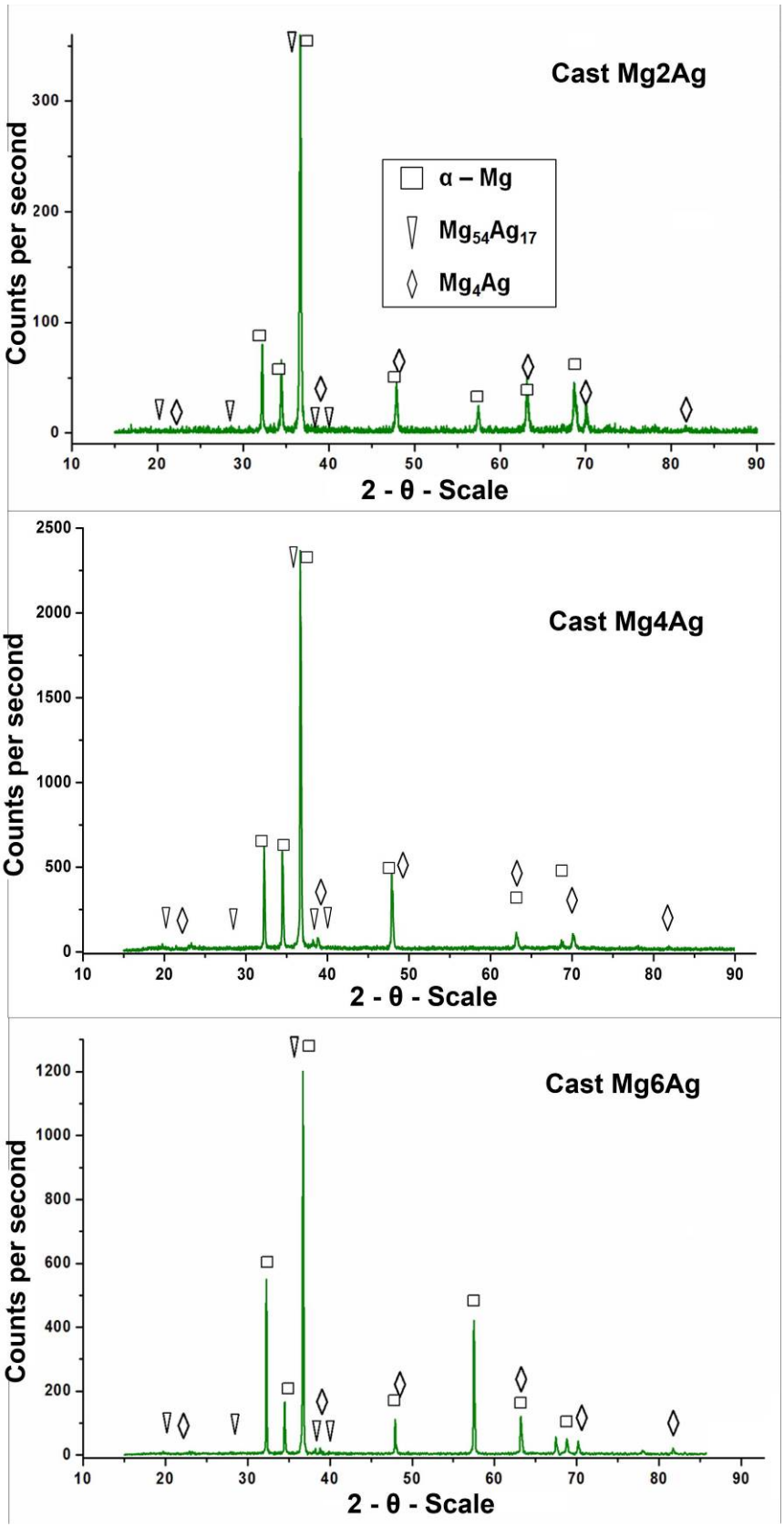

Fig. 11. XRD analysis to cast Mg-Ag alloys.

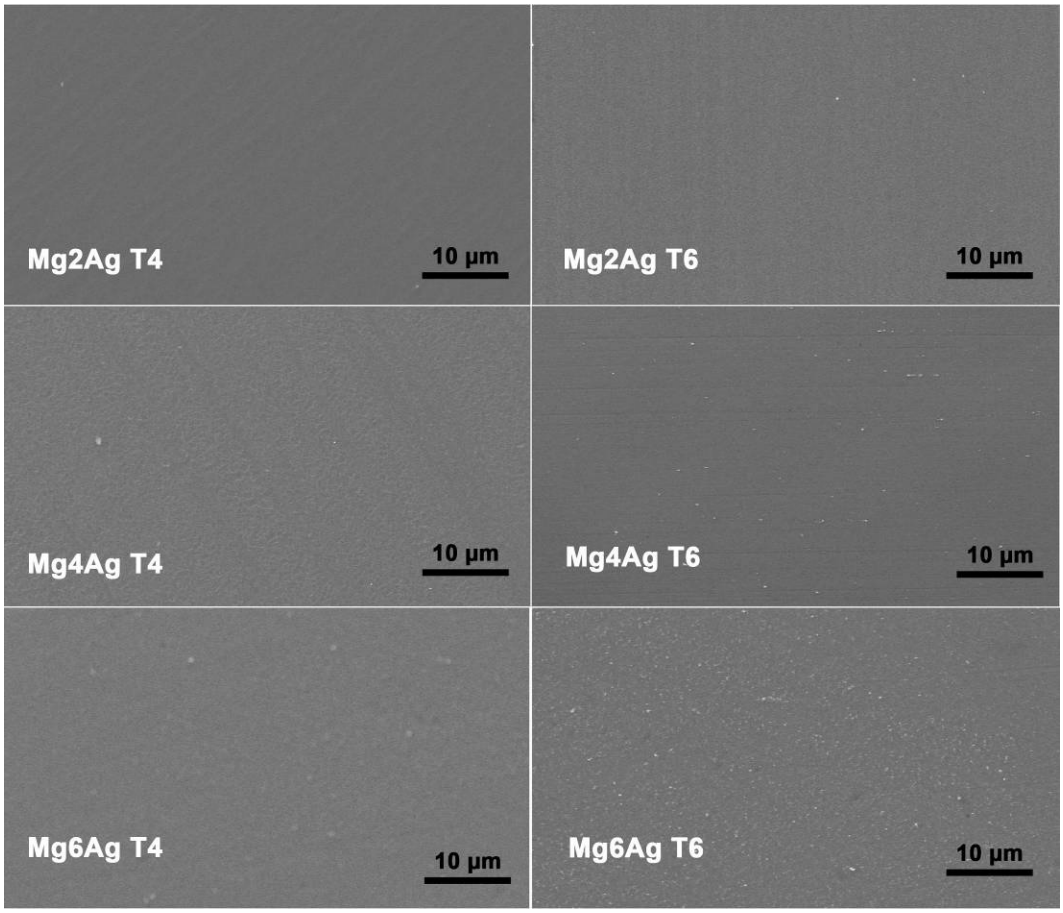

Fig. 12. SEM images of T4 and T6 treated Mg-Ag alloys. Small amount of re-precipitated secondary phases could be observed in T6 samples.

5.2. Mechanical properties

5.2.1. Mechanical properties of cast materials

The relationship between mechanical properties and material composition of cast materials is shown in Fig. 13. Hardness increased gradually with increasing silver content from pure magnesium to Mg6Ag. Compared to pure magnesium the increase was significant in all cases (Holm-Sidak against control group (Mg), significance level $p<0.05$; Mg2Ag: $t=5.07$; Mg4Ag: $t=7.81$; Mg6Ag: $t=8.157$). The material strength (tension and compression) showed an even more pronounced increase by silver addition. The Mg6Ag alloy reached more than double of the ultimate tensile strength (Rm) of pure magnesium, from 108.3 MPa to 215.9 MPa.

The differences for tension (T) and compression (C) were in all cases significant (Holm-Sidak against control group (Mg), significance level $p<0.05$; Mg2Ag: $t=17.26$ (T) and 46.09 (C); Mg4Ag: $t=21.32$ (T) and 27.17 (C); Mg6Ag: $t=21.98$ (T) and 25.17

(C), respectively). Mg6Ag was superior to the other materials with respect to the mechanical parameters.

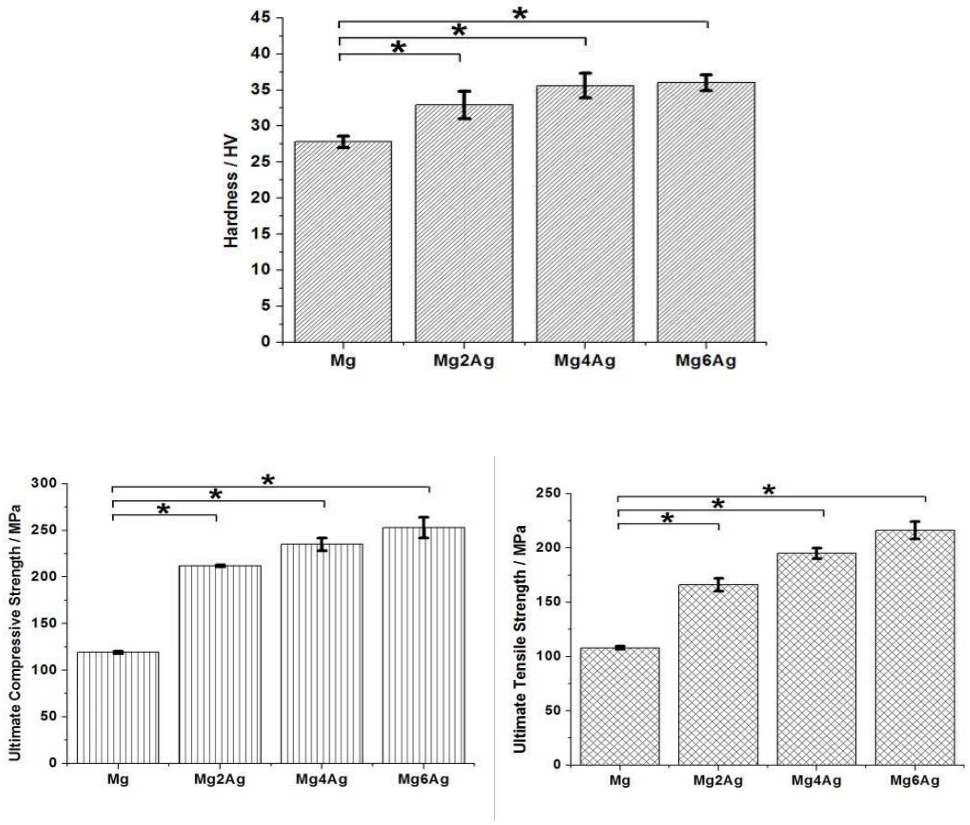

Fig. 13. Vickers hardness, compressive and tensile strength of cast Mg, Mg2Ag, Mg4Ag and Mg6Ag (mean ± SD, significance level *p < 0.05, #p > 0.05).

5.2.2. Mechanical properties after heat treatment

In Fig. 14 the mechanical properties of the materials are displayed. The average vickers hardness HV5 of pure magnesium was 27.8 ± 0.8 . The addition of silver leaded to a significant increase of the average HV5. For cast Mg2Ag, Mg4Ag and Mg6Ag values of 32.9 ± 2.0, 35.6 ± 1.7 and 35.9 ± 1.1 respectively were found. This can be explained by the increase of Mg_4Ag β phases and dendrite structure regardless of heat treatment status.

T4 treated alloys exhibited slight decrease in hardness for Mg2Ag (30.0 ± 2.5) and Mg4Ag (34.3 ± 2.1) while a mild increase was found for Mg6Ag (40.1 ± 2.2), which were resulted in dissolving of β phases. T6 samples had higher hardness values (40.1 ± 2.0 for Mg2Ag, 38.8 ± 0.86 for Mg4Ag and 43.3 ± 1.4 for Mg6Ag) than cast materials because of the β phases' re-precipitation

Tension and compression values also increase with increased silver content (Fig. 14, lower row). The ultimate tensile strength (UTS) of the casted Mg6Ag alloy doubled from from 108.3 ± 3.1 MPa (pure Mg) to 215.9 ± 11.3 MPa, and the ultimate compressive strength (UCS) changed from 119 ± 1.5 MPa for pure magnesium to 244 ± 9.2 MPa for Mg6Ag. Like for the hardness results, T4 and T6 treatment did not influence these parameters.

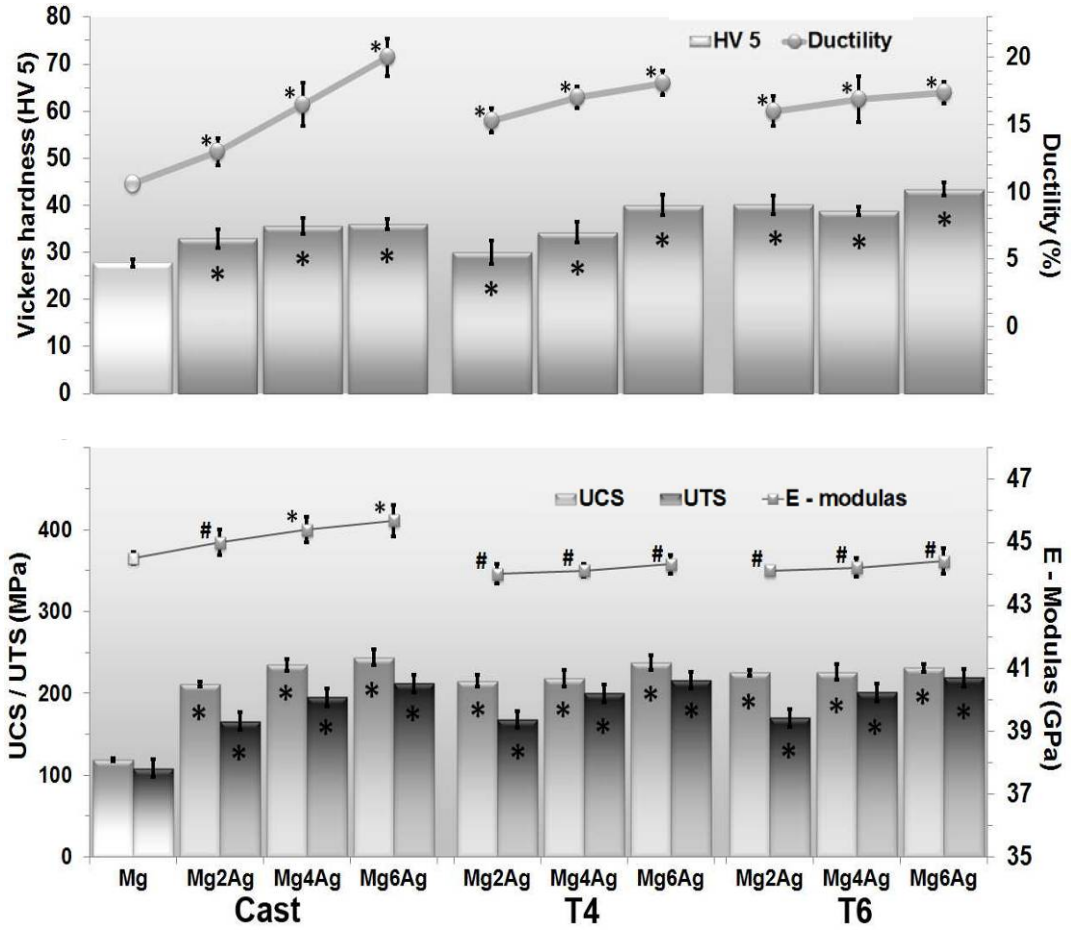

Fig. 14. Vickers hardness (HV5), ultimate tensile strength, ultimate compressive strength, the Young's modulus and (tensile) ductility of magnesium and Mg-Ag alloys. All the HV5, UTS and UCS values of both cast and heat treated Mg-Ag alloys were found to be significantly different (marked by an asterisk '*'; significance level $p < 0.05$) when compared with pure magnesium group.

The Young's modulus of the alloys was derived from the compressive strength curve, and the tensile ductility of the alloys was calculated via the tensile strength curve. For all materials the Young's modulus was in the range of 45 ± 1 GPa which is roughly double the value for bone. Ductility results demonstrated that the presence of silver provided a notable improvement in tensile ductility, which was most apparent in the cast material and grew from 10.6% for pure magnesium to 20.0% for Mg6Ag. After T4 treatment, the average tensile ductility value dropped for Mg6Ag (from 20.0% to

18.1%) while it grew in Mg2Ag (from 13.0% to 15.3%). T6 treatment minimized the difference between the alloys' ductility further leading to 16.0% for Mg2Ag, 16.9% for Mg4Ag, and 17.4% for Mg6Ag.

In summary the mechanical parameters showed that heat treated Mg-Ag alloys exhibited a significant improvement in the mechanical parameter as compared to pure magnesium, while Mg6Ag was slightly superior to the other materials due to its highest silver content.

5.3. Optimum of *in vitro* corrosion testing methods

5.3.1. Comparison and choosing of Corrosion media

5.3.1.1. Effects of Rinsing

Surface elements distribution of samples with and without rinsing after immersion experiments are shown in Table 5. It can be clearly observed that Na, as well as Cl almost disappeared after rinsing, which illustrates that all the corrosion products containing Na and Cl are soluble in water. P and Ca were also reduced by rinsing. In general, there were fewer visible elements left after rinsing, which proves that rinsing procedure is effective in removing soluble salts and contamination left by corrosion medium. It is very important for surface layer analysis.

Table 5. Surface element distributions by atom of magnesium samples immersed in DMEM, HBSS and SBF, with and without rinsing before XPS measurements

Element	DMEM		HBSS		SBF	
	Unrinsed [%]	Rinsed [%]	Unrinsed [%]	Rinsed [%]	Unrinsed [%]	Rinsed [%]
Mg	12.8	20.6	25.5	22.8	9.4	24.1
Ca	8.6	4.2	1.8		5.2	
Na	1.0	0.2	0.8	0.6	13.1	0.7
O	61.0	60.4	58.7	63.7	57.6	62.0
C	9.5	11.1	8.8	7.3	8.8	13.2
P	6.8	3.3	2.0	5.6	4.0	
Cl	0.3	0.2	2.4		2.0	

5.3.1.2. Distribution of Surface Elements

In table 5, elemental distributions for sample surfaces exposed to different corrosion media are listed by atom ratio. By using XPS survey spectra, different element distributions on the surface of immersed samples can be observed (Fig. 15).

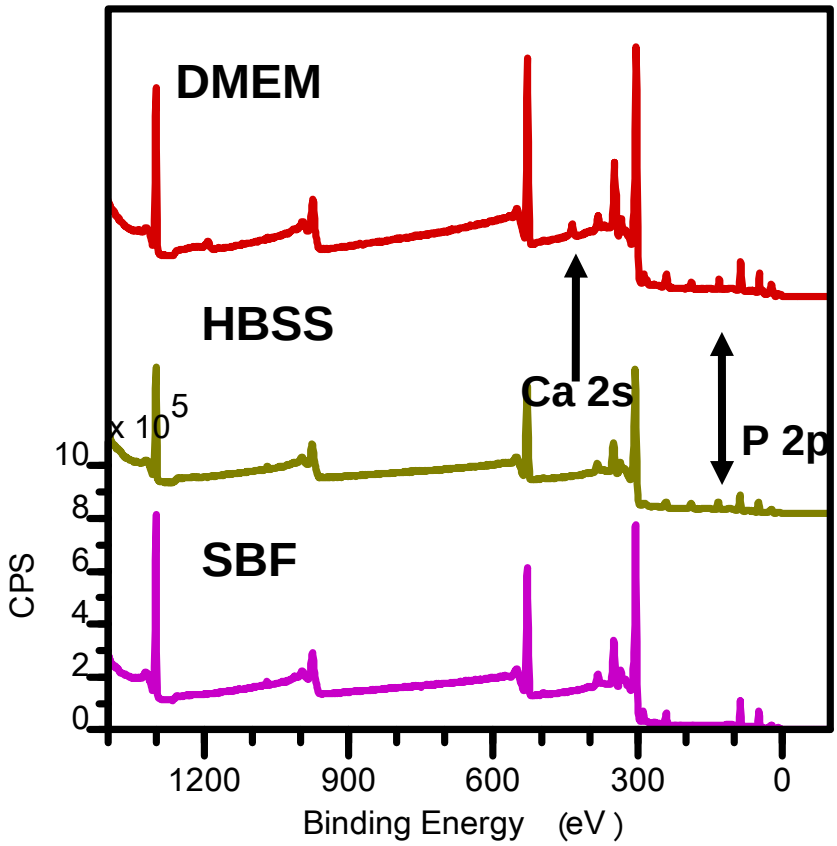

Fig. 15. Comparison of XPS survey spectra of Mg surface after immersion in DMEM, HBSS and SBF

5.3.1.3. Identification of Surface Products

Mg 2p peak spreads from 47.0eV to 52.8eV, which can be fitted by Mg(OH) at 49.3eV, MgO at 50.8eV and $MgCO_3$ at around 52.0 eV. The ratio of $Mg(OH)_2$ to MgO and $Mg(CO)_3$ can be calculated by fitting models.

O 1s peak appears from 526.7eV to 535.9eV, having two groups of sub-peaks at 528.4eV and 530.7eV. The sub-peak at 528.4eV can be fitted to MgO, and the sub-peak centered at 530.7eV reflects appearance of OH^-. PO^{4-} and CO_3^{2-} can be fitted at around 531.5eV, which can also be proven by P 1s and C 1s spectra.

In the C 1s spectra the sub-peak located at 284.6eV is background simple substance C 1s peak formed from contamination by organic compounds. This peak is used for calibration. The C 1s peak at around 289ev to 290eV represents the appearance of CO_3^{2-} on the surface, corresponding to $MgCO_3$ and $CaCO_3$ in the corrosion products.

In Ca 2p spectra the higher sub-peak centered at 350eV corresponds to Ca 2p1/2 peak, proving the appearance of Ca salts. The other sub-peak centered at 346.5eV is 2p3/2 peak which can give more details about the structure of the corrosion products.

P 2p peak at 132.9eV, the exact binding energy of P in Ca-PO_4 and Mg-PO_4, further proves appearance of $Ca_3(PO_4)_2$. It can be also determined from the peak width that there is small amount of $(OH)_m(PO_4)_n^{a-}$.

5.3.2. Protein's effects on corrosion of Mg-Ag alloys

5.3.2.1. Electrochemical analysis

The average results, and the corresponding standard deviation (S. D., in parentheses), obtained for the alloys in DMEM are presented in Table 6 and Table 7. Current densities and corrosion rates were generally reduced when medium with FBS was used.

Table 6. Average results ± S.D. of the electrochemical parameters for the alloys in DMEM.

Alloys	Corrosion Rate (mm/year)	R_p (Ω/cm^2)	i_0 (A/cm^2)	E_0 vs SHE (V)
Mg	0.53 ± 0.09	1116 ± 59	$2.34\times10^{-5} \pm 2.02\times10^{-6}$	-1.50 ± 0.07
Mg2Ag	1.13 ± 0.02	541 ± 6	$4.82\times10^{-5} \pm 7.51\times10^{-7}$	-1.43 ± 0.05
Mg4Ag	1.29 ± 0.03	492 ± 5	$5.30\times10^{-5} \pm 9.02\times10^{-6}$	-1.41 ± 0.07
Mg6Ag	1.43 ± 0.02	458 ± 4	$5.96\times10^{-5} \pm 5.57\times10^{-7}$	-1.40 ± 0.04

Table 7. Average results ± S.D. of the electrochemical parameters for the alloys in DMEM with 10% FBS.

Alloys	Corrosion Rate (mm/year)	R_p (Ω/cm^2)	i_0 (A/cm^2)	E_0 vs SHE (V)
Mg	0.40 ± 0.05	1270 ± 52	$2.05\times10^{-5} \pm 2.02\times10^{-6}$	-1.50 ± 0.06
Mg2Ag	0.88 ± 0.01	668 ± 3	$3.88\times10^{-5} \pm 7.00\times10^{-7}$	-1.42 ± 0.05
Mg4Ag	1.01 ± 0.03	504 ± 22	$5.18\times10^{-5} \pm 3.03\times10^{-6}$	-1.41 ± 0.03
Mg6Ag	1.18 ± 0.02	495 ± 5	$5.34\times10^{-5} \pm 1.10\times10^{-6}$	-1.38 ± 0.05

In the anodic polarization curves of the materials (Fig. 16 and Fig. 17), it is possible to observe, especially in the linear plot presence of FBS led to a lower slope of the anodic curve of the materials, and also moved the pitting corrosion potential to

anodic direction, which demonstrates that the homogeneous and pitting corrosion both decreased. Anodic behavior of magnesium did not change much indicating that FBS affects pure magnesium less than alloys.

Mg4Ag and Mg6Ag shows no signs of pitting corrosion in DMEM + FBS viewed from their cyclic voltammograms (Fig. 20 and Fig. 21). As the distance between the breakdown potential and the repassivation potential widens, the pitting corrosion effect caused by the difficulty of repassivation of the partially activated surface is stronger for the material corroded in DMEM without FBS addition.

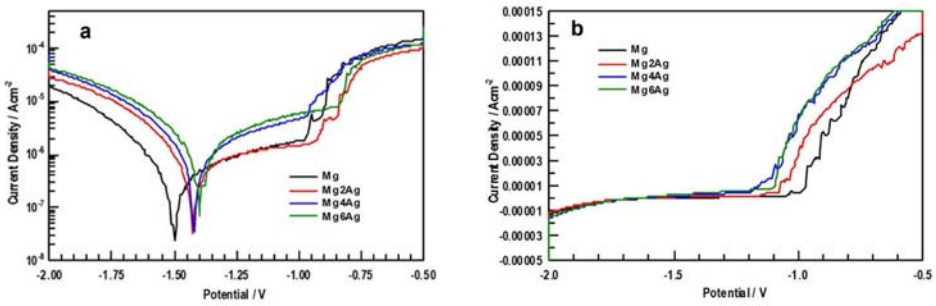

Fig. 16. Current density vs. potential (SHE) curves in logarithmic (a) and linear (b) scale for studied materials in DMEM.

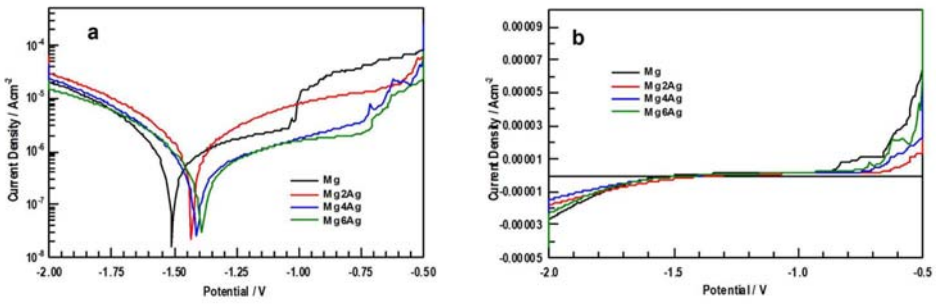

Fig. 17. Current density vs. potential (SHE) curves in logarithmic (a) and linear (b) scale for studied materials in DMEM + 10% FBS.

5.3.2.2. XPS analysis

N element determination is a key parameter to show if protein or ammonic salt present, yet there is no N element present on all samples' surface even in trace amount. In this case, all of N element related peaks are checked (Fig.18).

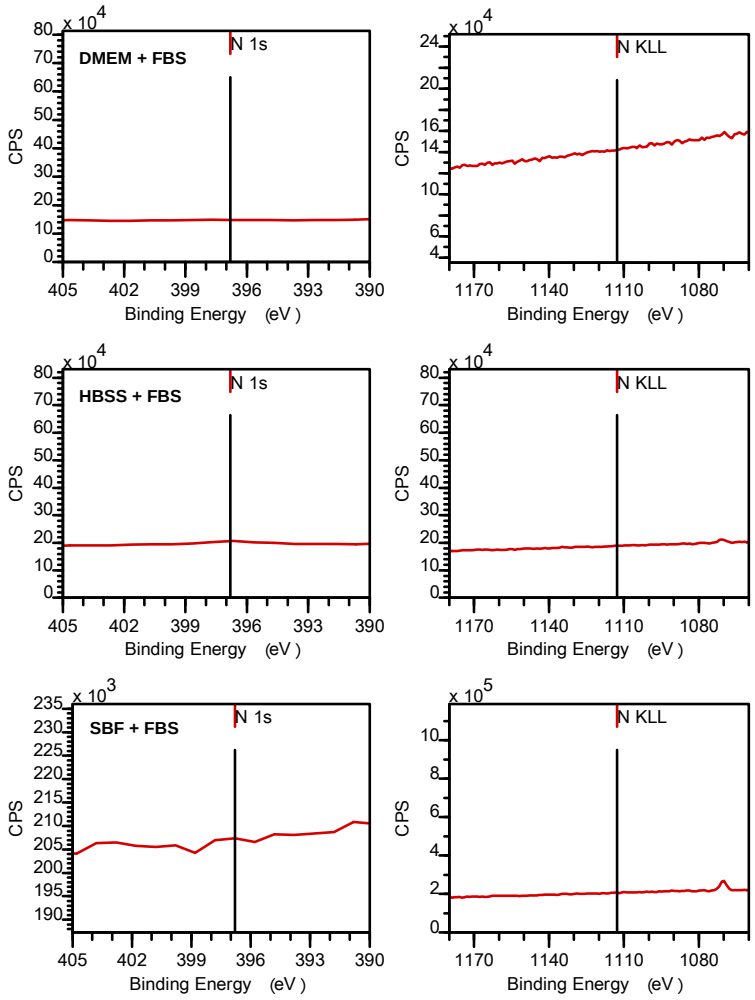

Fig. 18. N 1s and N KLL peaks of samples immersed in 3 kinds of media

Table 8. Surface element distributions by atom of magnesium samples immersed in DMEM, HBSS and SBF, with and without 10% (V/V) FBS addition

Element	DMEM [%]	DMEM +FBS [%]	HBSS [%]	HBSS +FBS [%]	SBF [%]	SBF +FBS [%]
Mg	20.6	31.6	22.8	30.7	24.1	33.6
Ca	4.2	2.7				
Na	0.2		0.6	0.3	0.7	1.2
O	60.4	53.5	63.7	49.2	62.0	51.1
C	11.1	10.2	7.3	12.0	13.2	13.3
P	3.3	2.0	5.6	7.8		0.6
Cl	0.2					0.2

Comparisons of C 1s peak before and after FBS addition can be seen in Fig. 19. Quantitative analysis also neither shows hints of protein or ammonic products

present. From the spectra of C 1s, amount of C element in carbonate form can be also calculated.

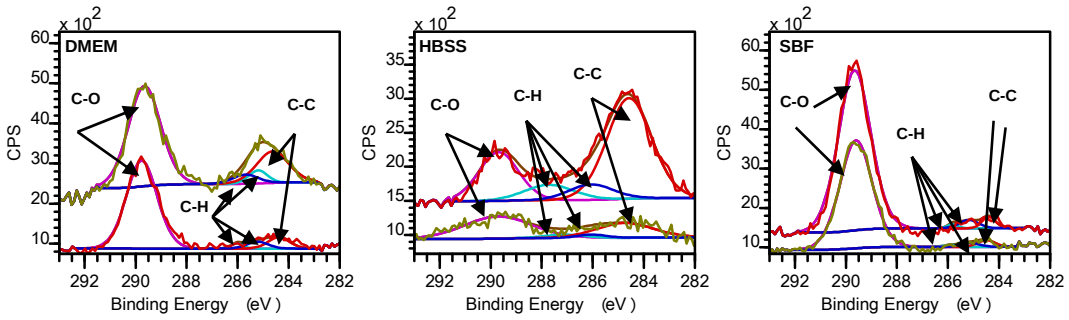

Fig. 19. Comparisons of C 1s spectrum before and after FBS's addition
* Lines in red are samples in pure media (without FBS).

5.4. Corrosion properties of Mg-Ag alloys

5.4.1. Corrosion properties of cast materials

5.4.1.1. Electrochemical tests

The average results, and the corresponding standard deviation (S. D., in parentheses), obtained for the alloys in DMEM +FBS are presented in Table 6 and Table 7. The highest corrosion rate, exchange current density and lowest polarization resistance was observed for Mg6Ag. This means that Mg6Ag has the highest general corrosion rate. With increasing silver content, Mg-Ag alloys become less resistant from the homogeneous corrosion's point of view.

The cyclic voltammograms of the studied alloys in DMEM (Fig. 20) show that magnesium and Mg-Ag alloys both have hysteresis behavior. This indicates that the material underwent pitting corrosion to some extent in cell culture circumstance. However, it is possible to see that as more silver content added, the alloys acquire more pitting corrosion susceptibility.

In the anodic polarization curves of the materials (Fig. 16 and Fig. 17), it is possible to observe, especially in the linear plot, that the anodic behavior of the alloys Mg4Ag and Mg6Ag are similar, whilst Mg2Ag is more similar to that of pure magnesium, as the curve slope is identical. A gradually changed slope from Mg to Mg6Ag is related to increasing content of Ag in alloys. Oxidation state changes are responsible for the shift of break down potential in the anodic direction near -0.9 V of all alloys.

The cyclic voltammograms of the studied alloys in DMEM + FBS are depicted in Fig. 21. Different from the corrosion behavior in DMEM, Mg4Ag and Mg6Ag shows no signs of pitting corrosion in DMEM + FBS, whilst Mg and Mg2Ag both have slight increases in the current density of the reverse scan, which hints their hysteresis

behavior is more pronounced than Mg4Ag and Mg6Ag. The pitting potential of Mg and Mg2Ag as well as the repassivation potential are more cathodic than Mg4Ag and Mg6Ag. This means that they are less susceptive to pitting corrosion than Mg and Mg2Ag.

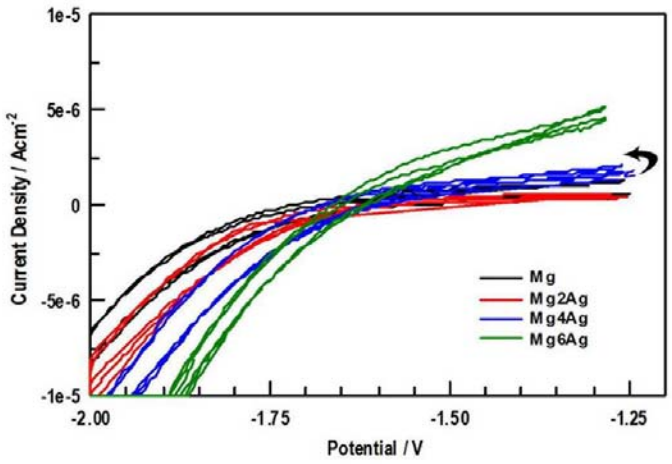

Fig. 20. Comparison of the cyclic voltammetry curves for the studied alloys in DMEM. The arrow shows the direction of current after changing the polarization direction.

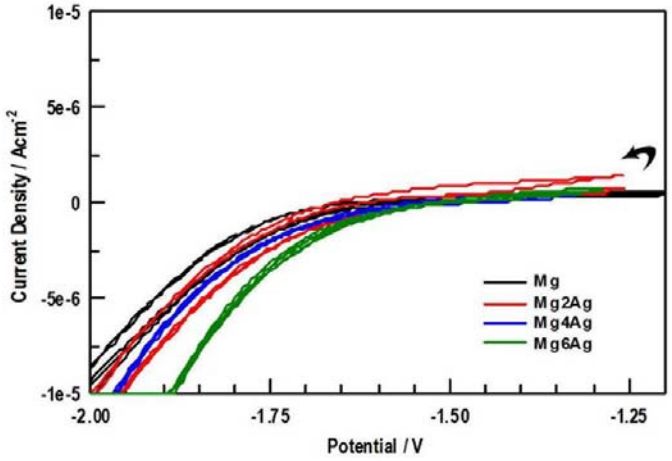

Fig. 21. Comparison of the cyclic voltammetry curves in DMEM + 10% FBS. The arrow shows the direction of current after changing the polarization direction.

The typical micrographs of cast Mg-Ag alloys taken by optical microscopy are shown in Fig. 22. The alloys have fine grains of a size of 0.2 mm to 0.6 mm. In the grains, the secondary dendrites are also observed. Some eutectic phases formed during the solidification along the grain boundaries. Representative SE images of the specimen surface morphology before (reference) and after corrosion testing are illustrated in

Fig. 22. Corroded surfaces showed light parallel scratches due to the grinding process. Second phases were identified as mainly $Mg_3Ag/Mg_{54}Ag_{17}$, and corrosion products around pits and cracks consist of MgO and $Mg(OH)_2$.

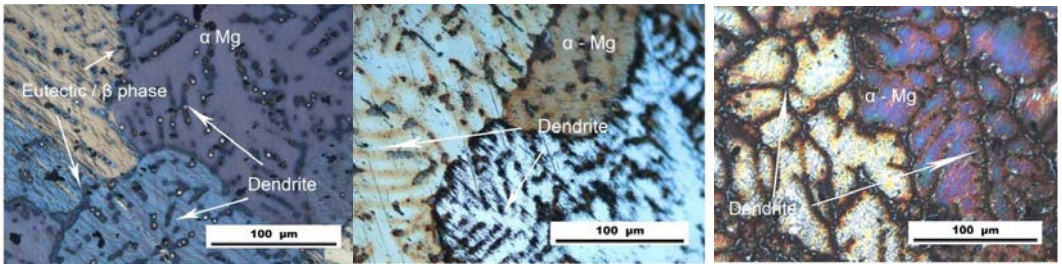

Fig. 22. Metallic microstructure of the alloys analysed by optical microscopy: Mg2Ag, Mg4Ag and Mg6Ag from the left.

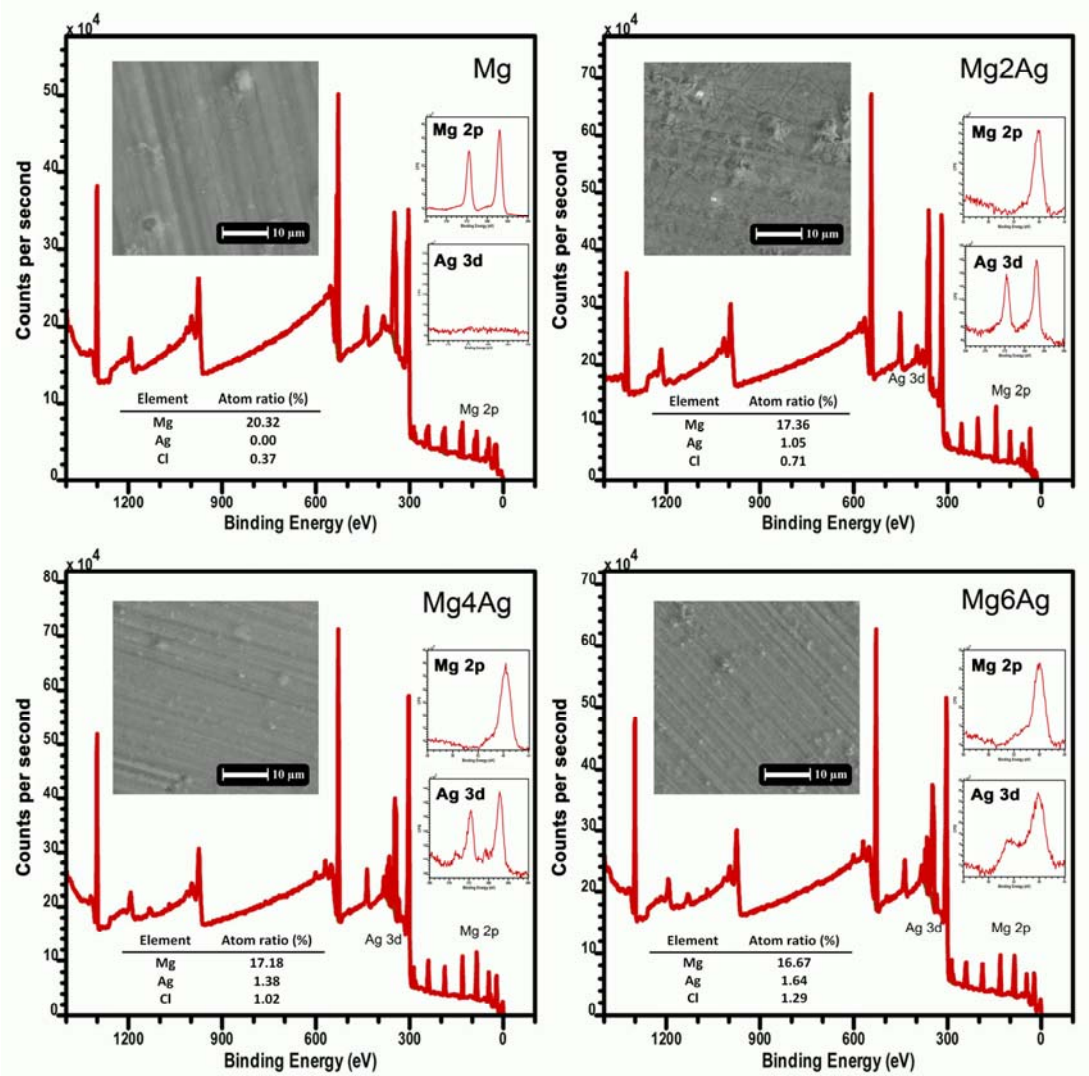

Fig. 23. XPS survey spectra of experimental surfaces after exposure in DMEM + 10% FBS. Mg 2p and Ag 3d core level spectra, Mg, Ag and Cl elemental distribution and typical corrosion surface SEM patterns are presented together.

All the 4 materials displayed an irregularly distributed non-circular concavity pattern after corrosion testing in DMEM, while Mg and Mg2Ag demonstrated deepened surface. Homogeneous and pitting corrosion were both observable after immersion for Mg2Ag in DMEM with FBS, while Mg4Ag and Mg6Ag show only minor signs of pitting corrosion.

5.4.1.2. Corrosion products analysis

In Fig. 23 elemental distributions for sample surfaces after exposure to DMEM + 10% FBS are illustrated by using XPS survey spectra, in which Mg 2p and Ag 3d peaks were selected to make a high resolution scanning. Mg, Ag and Cl atom ratio was calculated by peak signal integration.

For magnesium products on the surface of all materials, Mg 2p peak spreads from 47.0eV to 52.8eV, which can be fitted by Mg(OH) at 49.3eV, MgO at 50.8eV. Besides, $MgCO_3$ and Cl- Mg-(OH) are also present. AgCl as the dominant silver containing corrosion product is present in the corrosion layer of each alloy. With increasing amount of silver in the alloys the atomic ratio found in the corrosion layer rises from 1.05% in Mg2Ag to 1.64% in Mg6Ag. When more silver was added, the amount of magnesium products drops to around 17 at% in alloys compared with pure magnesium. While most alloyed silver in α phase formed AgCl as corrosion product, a certain proportion of silver remained in metallic compound status during the electrochemical corrosion acting as dispersed cathodes.

5.4.2. Effects of heat treatment on corrosion properties

5.4.2.1. Electrochemical tests

The single sweep voltamograms of the materials (Fig. 25) and their average corrosion rate (Fig. 26), while the SEM images of treated samples obtained from the materials measured in DMEM with 10% FBS at 37° C and 5% CO_2 (cell culture conditions) are presented in Fig. 24.

The highest corrosion rate, exchange current density and lowest polarization resistance was observed for casted Mg6Ag, which showed a corrosion rate of 1.43 mm/year. With increasing silver content, Mg-Ag alloys become more susceptible to corrosion regardless of heat treatment status. However, the corrosion properties were significantly improved especially by T4 treatment. The lowest degradation was observed for T4 treated Mg2Ag which exhibits a corrosion rate of 0.343 mm/year which is much lower than pure casted magnesium (0.534 mm/year). As there was no phase transformation in pure magnesium, its corrosion rate did not vary after T4 heat treatment (from 0.534 mm/year to 0.519 mm/year).

In the anodic polarization curves of the materials (Fig. 25) show that the anodic behavior of the casted Mg4Ag and Mg6Ag alloys were similar, while the Mg2Ag curve was more comparable to pure magnesium.

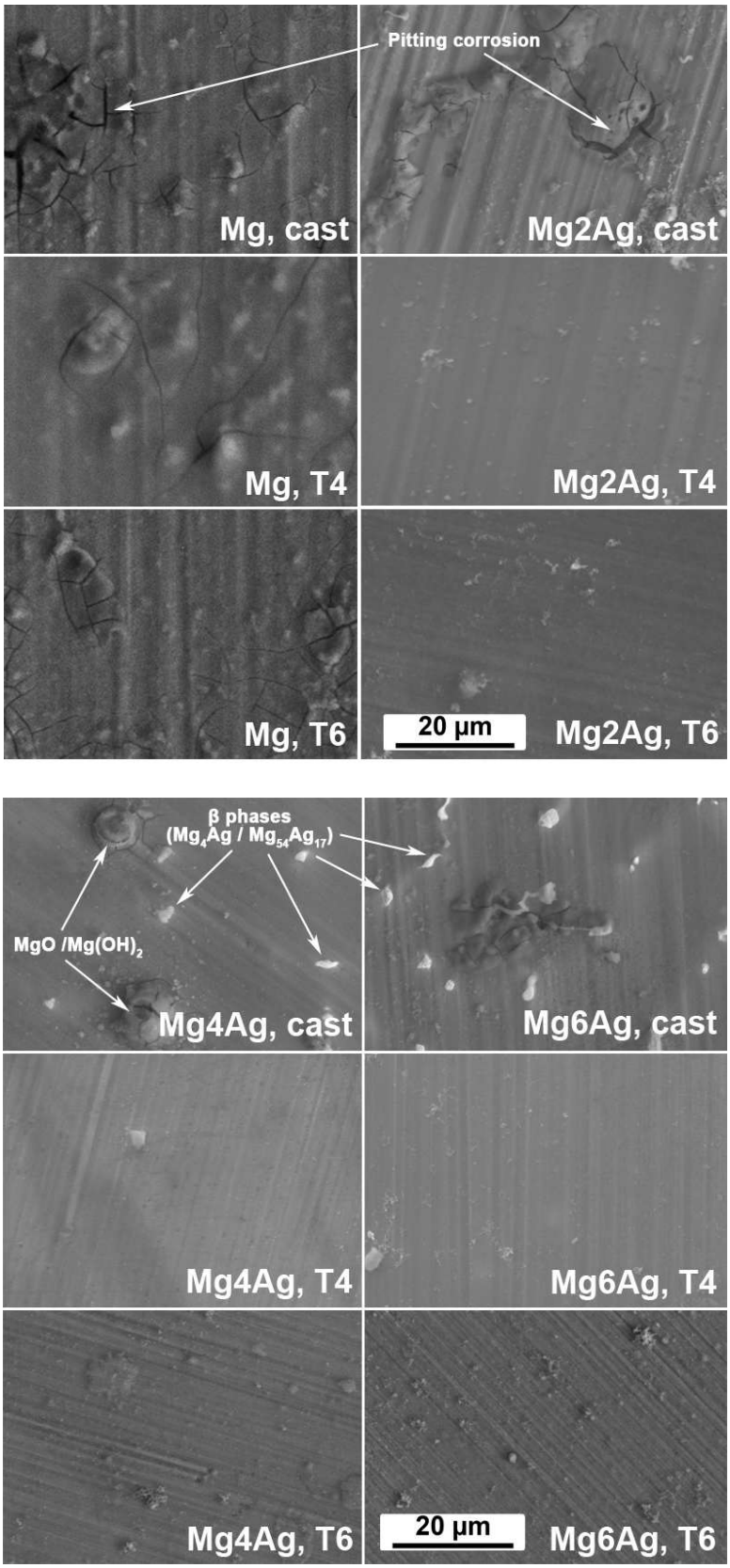

Fig. 24. SEM images after electrochemical tests. Susceptibility to localized corrosion was reduced as increasing content of silver. T4 treatment was proved greatly effective on decreasing alloys' corrosion rate.

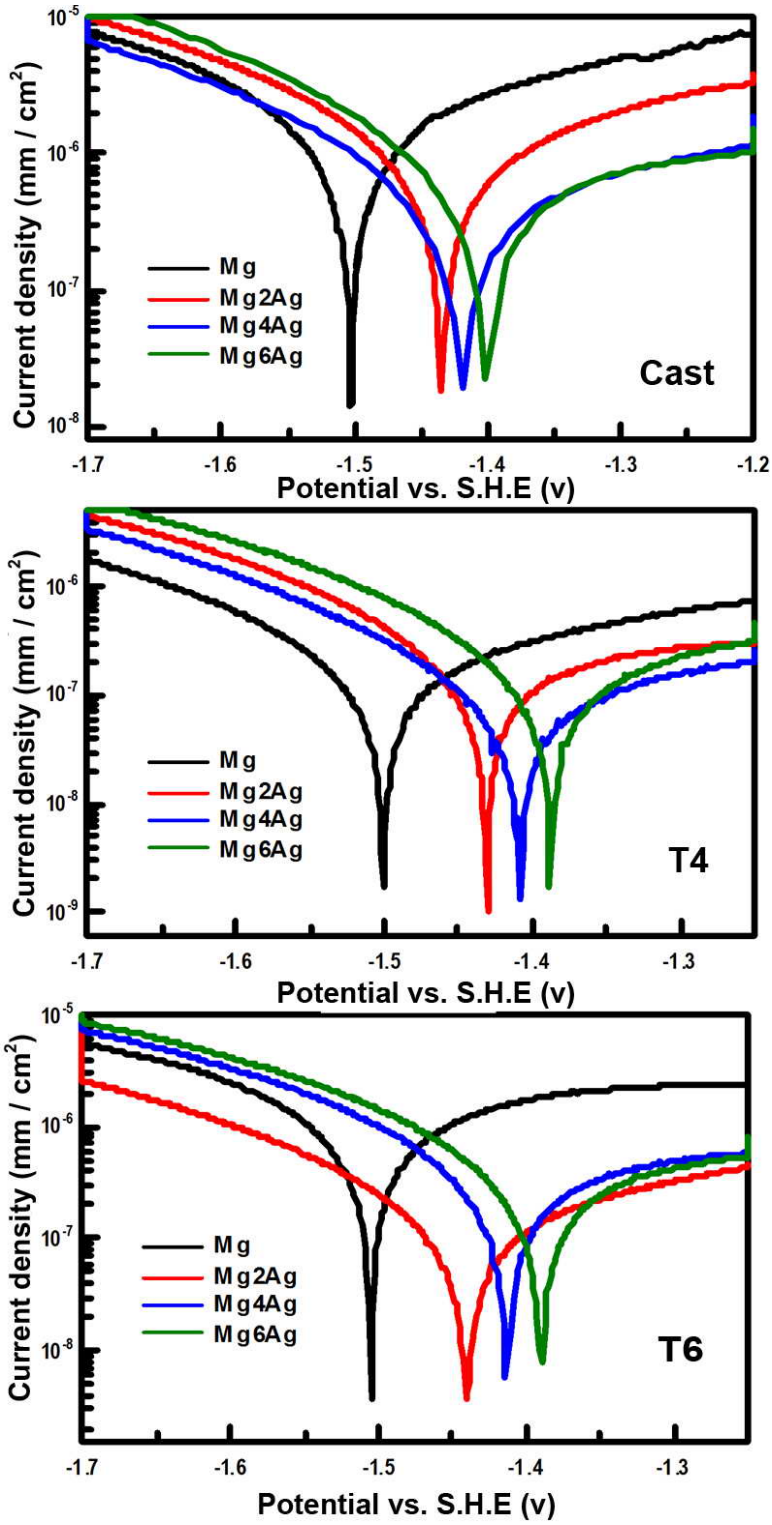

Fig. 25. Single sweep voltammograms of the tested materials. Susceptibility to localized corrosion was reduced with increasing content of silver. T4 treatment was proved greatly effective on decreasing alloys' corrosion rate.

A gradually changed slope from Mg to Mg6Ag was related to increasing content of Ag in alloys. Oxidation state changes were responsible for the shift of break down

potential in the anodic direction near -0.9 V of all alloys. Heat treatment showed no significant influence on open circuit potential of all materials, but the exchanging current density was shifted to lower level, which stands for the change in the corrosion rate.

The combination of representative SEM (SE) images (Fig. 24) with EDX analysis showed that the corrosion products around the pits and cracks mainly consist of MgO and $Mg(OH)_2$. All the four cast materials display irregularly distributed non-circular concavity patterns after corrosion testing. In addition Mg and Mg2Ag also show deep cavities. Both, homogeneous and pitting corrosion were observed after immersion of casted Mg2Ag, while casted Mg4Ag and Mg6Ag showed only minor signs of pitting corrosion. Both T4 and T6 treatment exhibited evident effects on reducing pitting corrosion especially to Mg4Ag and Mg6Ag. Compared to T4 treatment, T6 treated samples presented less smooth surface due to small amount of re-precipitated β phases.

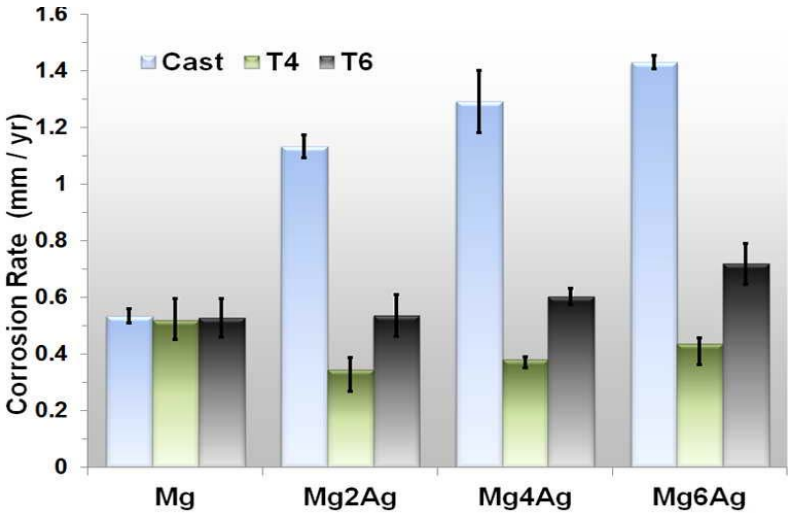

Fig. 26. Fitted corrosion rate of the tested materials. T4 treatment was proved greatly effective on decreasing alloys' corrosion rate.

From the corrosion point of view the T4 treated Mg2Ag was the best material. Though from a mechanical point of view Mg6Ag was the most promising material we consider corrosion the more crucial. Therefore we continued the following experiments with T4 samples only.

5.4.2.2. Corrosion products analysis

In order to better understand the corrosion behaviour of the materials under near physiological conditions a detailed composition analysis of the corrosion layer of T4 treated materials was performed.

As an example Fig. 27 shows a SEM image of a perpendicular cut (side-view) through the corrosion layer of T4 treated Mg2Ag. In order to acquire in-depth information about the composition of the surface corrosion layer, XPS analysis and ion gun ablation was used. Thus three levels were produced: The first level was the original specimen surface after immersion in DMEM. After removal of two times approximately 3 µm a second and a third XPS analysis respectively was performed. We thus obtained XPS spectra for 0, 3 and 6 µm depth of the corrosion layer (Fig. 27 and 29). The elemental distributions were illustrated by using XPS survey spectra. In addition Mg 2p Ag 3d and C 1s peaks were selected for higher resolution scanning to identify corrosion products' compositions (Fig. 28). The vertical distribution of corrosion products in T4 treated Mg2Ag was calculated by peak signal integration (Fig. 29) using the software Casa 2.3.15.

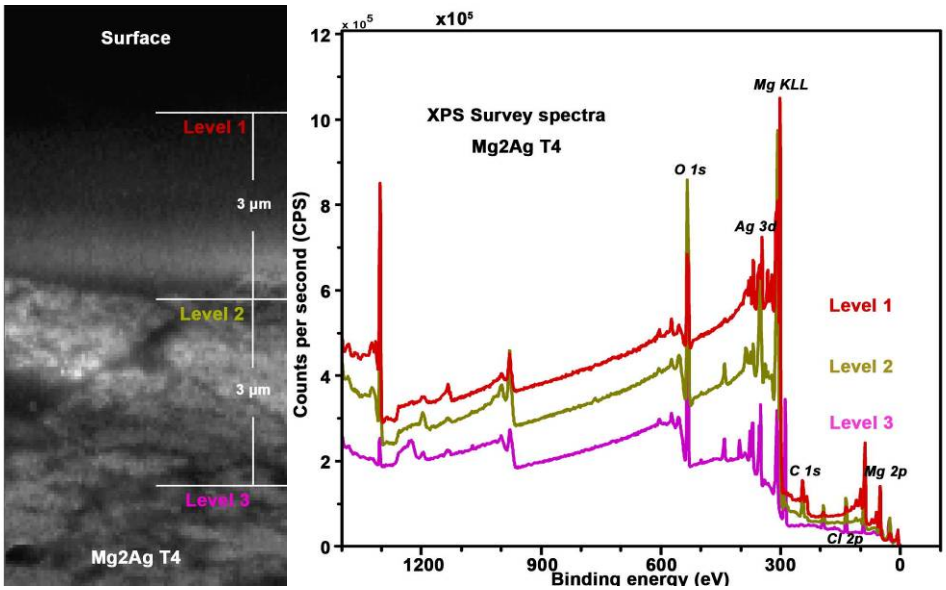

Fig. 27. Side view SEM images of T4 treated Mg6Ag corrosion layer after immersion in DMEM with FBS for 72 h. The corrosion layer's thickness was ca. 35 µm, of which the top three layers with ca. 0 µm, 3 µm and 6 µm depth from the surface were analyzed by XPS depth profiling measurement.

Two notable trends can be seen in the surface corrosion layer of all materials: (1) carbonate salts are only found at the very surface and (2) the atomic ratio of magnesium corrosion products increase in deeper levels. A summary of the surface XPS analysis of all T4 treated materials are presented in Fig. 30. For magnesium corrosion products on the surface of all materials, the Mg 2p peak spreads from 47.0eV to 52.8eV, which can be fitted by $Mg(OH)_2$ at 49.3eV and MgO at 50.8eV [183]. Besides, $MgCO_3$ and Mg (OH)Cl were also present. AgCl as the dominant silver containing corrosion product is present in the corrosion layer of each alloy. With increasing amount of silver in the alloys the atomic ratio found in the corrosion

layer rises from 1.5% in Mg2Ag to 5.8% in Mg6Ag. This is a little less than originally found in the alloy. With higher silver content the amount of magnesium products dropped to around 83 at% in Mg6Ag. While the majority of the alloyed silver in the α phase formed AgCl as corrosion product, a small proportion of metallic silver remained acting as dispersed cathodes during the electrochemical corrosion.

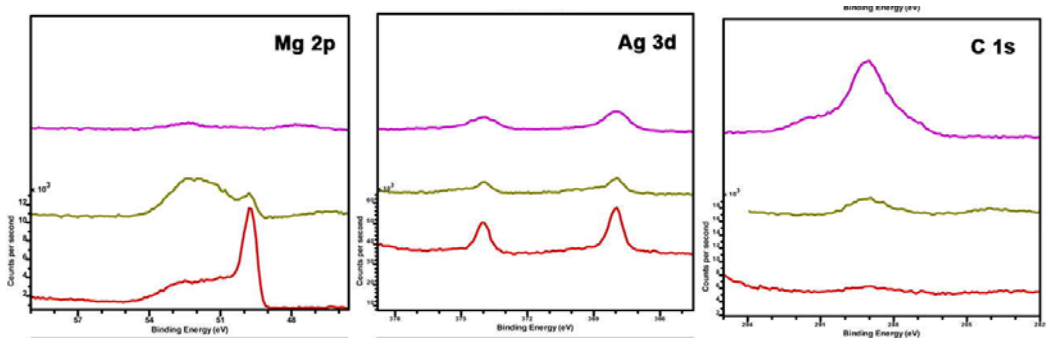

Fig. 28. High resolution XPS depth profiling spectra of Mg 2p, Ag 3d and C 1s core energy levels for the corrosion layer of Mg2Ag.

	$Mg(OH)_2$	MgO	$MgCO_3$	$Mg\text{-}(PO_4)$	$CaCO_3$	$Ca\text{-}(PO_4)$	AgCl
	(At%)	(At%)	(At%)	(At%)	(At%)	(At%)	(At%)
Level 1	33.2	18	4.9	2.1	23.3	16.7	1.8
Level 2	54.1	20.2	0.3	5.2	5.9	8.9	5.4
Level 3	58.4	20	0.1	4.6	4.3	6.8	5.8

Fig. 29. Corrosion products vertical distribution counted by Mg/Ca atom amount in the corrosion layer of Mg2Ag.

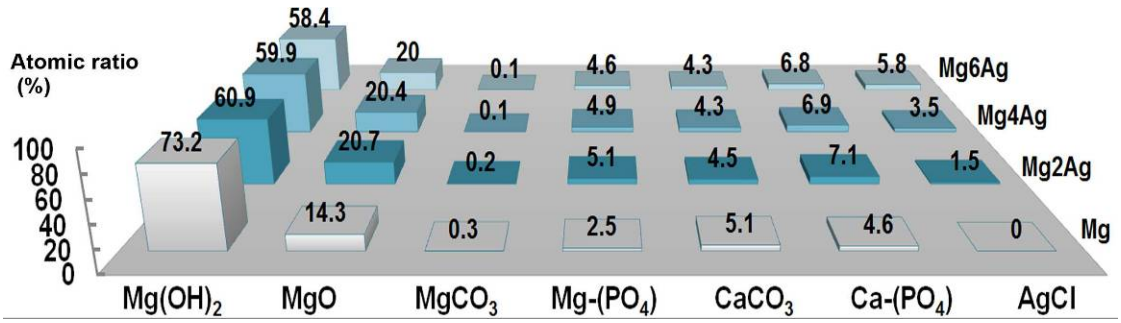

Fig. 30. Compositions of surface corrosion products counted by Ca / Mg atom in all four T4 treated materials derived from XPS surface layer analysis.

5.4.3. Immersion tests

Gas bubbles gathered and released from the samples' surface at the first hours, however quite few gas bubbles could be observed after 12 hours of immersion. The gross morphology and comparison of the corrosion surfaces via SEM BSD patterns of the T4 treated samples after immersion tests is depicted in Fig. 31. All Mg-Ag samples showed black corrosion layers with white precipitates of various sizes while the magnesium sample surface was almost completely white.

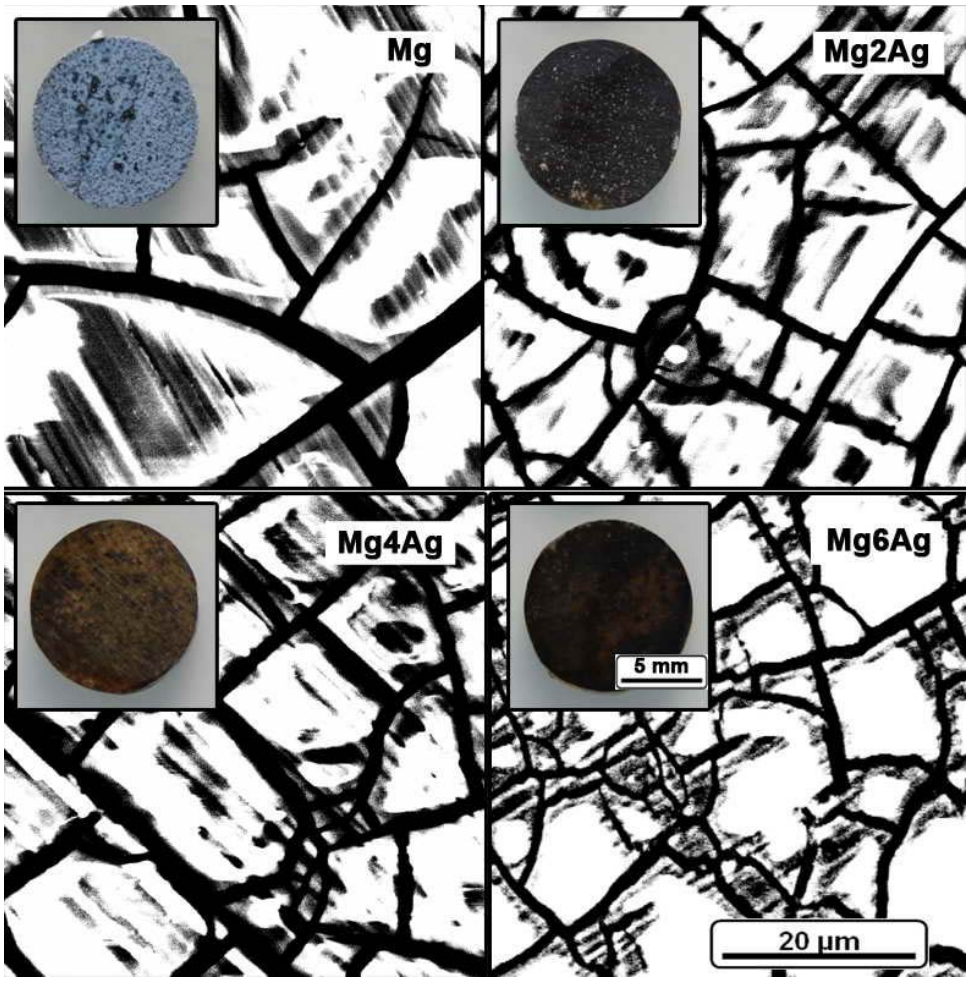

Fig. 31. Corrosion morphology of the T4 treated samples immersed in DMEM with FBS for 72 h and SEM (BSD) images for corroded surfaces of according material.

The outer corrosion layers of the samples mainly consisted of MgO / $Mg(OH)_2$ by EDX, and the different outlooks were formed by different density and thickness of the corrosion products.

The precipitates were not water-soluble as rinsing with deionized water did not alter the morphology. Viewed from SEM images, the corrosion product "blocks" on the magnesium surface were bigger than those of the Mg-Ag alloys, as a result of finer grain size in alloys than pure magnesium. The osmolality, pH and magnesium and silver ion concentration of the corrosion media were measured prior and after the

immersion period. The results are exhibited in Fig. 32 and 33. The value of pH and increase in magnesium ion concentration of the media after immersion with alloys were quite similar to the corresponding value for pure magnesium, while the osmolality value decreased compared to pure magnesium which hinted the corrosion rate was reduced with presence of silver content. The silver ion concentrations in the corrosion media were negligible and showed a small increase corresponding to the higher content of silver in the alloys.

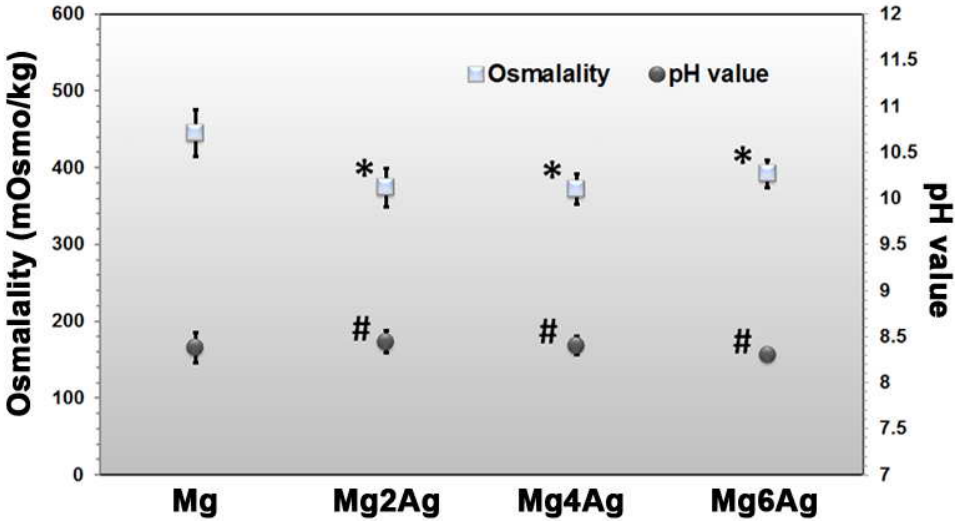

Fig. 32. Summary of pH and osmolality value after immersion tests. '*' means significance level $p < 0.05$ while '#' stands for significance level $p > 0.05$.

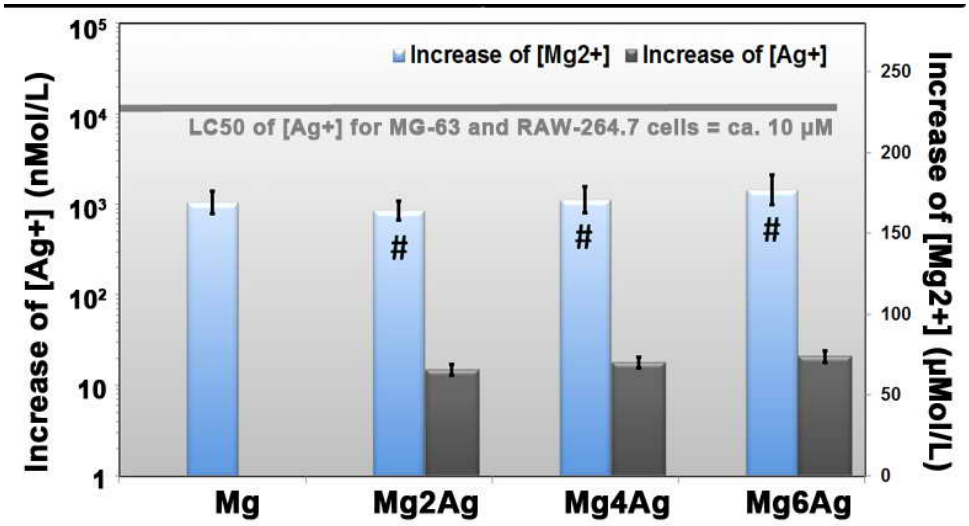

Fig. 33. Summary of changes in Mg^{2+} ion concentration and Ag^{+} ion concentration after immersion tests. The differences of Mg^{2+} concentration increase between alloys and pure magnesium group were not significant (marked by a number sign '#'; significance level $p > 0.05$). Ag^{+} concentrations after immersion with the alloys were all far lower than the LC50 of MG-63 and RAW 264.7 cells.

5.5. Cytocompatibility

5.5.1. Silver ion cytotoxicity testing

Silver nitrate was used to examine differences in reaction of the different cell types and concentrations from 1 nM up to 100 mM were tested. Viability of the cells was calculated as percent of control group (n=16 for each concentration). LC50 were determined to be at 11.0 µM for MG-63, 9.0 µM for RAW 264.7 and 400 µM for HUCPV (Fig. 34). Presence of nitrate showed no influence on cell viability according to MTT test, which warranted the cytotoxicity results only reflected the cellular response to silver ions. The following long term cytotoxicity tests under the LC50 confirmed the LC50 concentrations got from MTT tests. Considering the silver ion release results from immersion tests (Fig. 34), the silver ion concentrations in media after immersion were lower than LC50 of tested cells for several orders of magnitude.

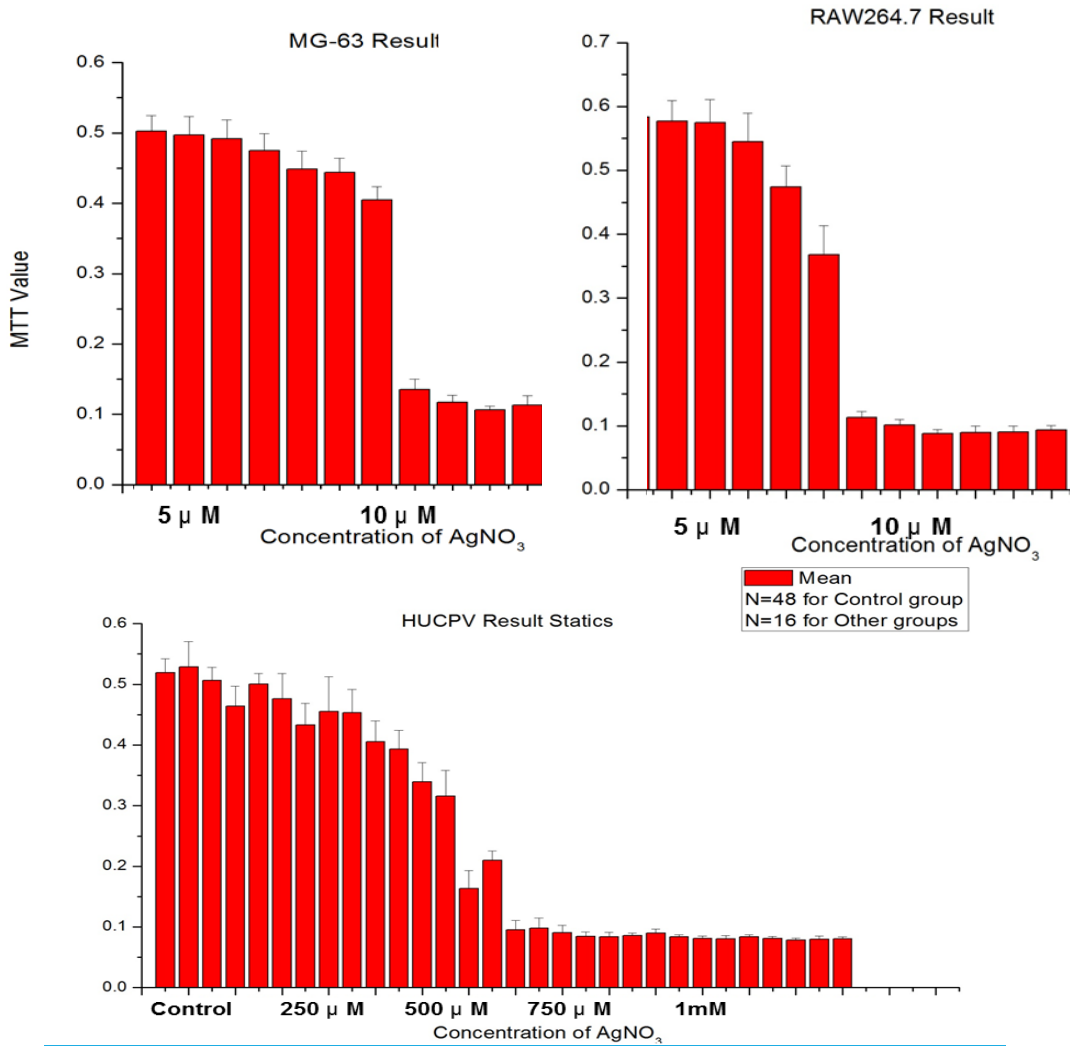

Fig. 34. Cytotoxicity of silver ion result. LC50 was determined to be at 11.0 µM for MG-63 cells, 9.0 µM for RAW 264.7 cells and ca. 500 µM for HUCPV cells by MTT cellular viability tests

From this point of view, T4 treated Mg-Ag alloys exhibited no cytotoxicity to MG-63, RAW 264.7 and HUCPV cells when immersed in cell culture media under cell culture conditions.

5.5.2. Cell adhesion tests

A long term cytotoxicity and cell adhesion test over 14 days where human osteoblasts were grown directly on the specimen (Fig. 35) showed survival rates between 95 and nearly 100% (on Mg2Ag). Recalculating the silver ion release results from the immersion tests we find ca. 10 nM , the silver ion concentrations in media were by several orders of magnitude lower than the LC50 of MG-63 and RAW 264.7 cells. From this point of view, T4 treated Mg-Ag alloys can be considered to be non-cytotoxic.

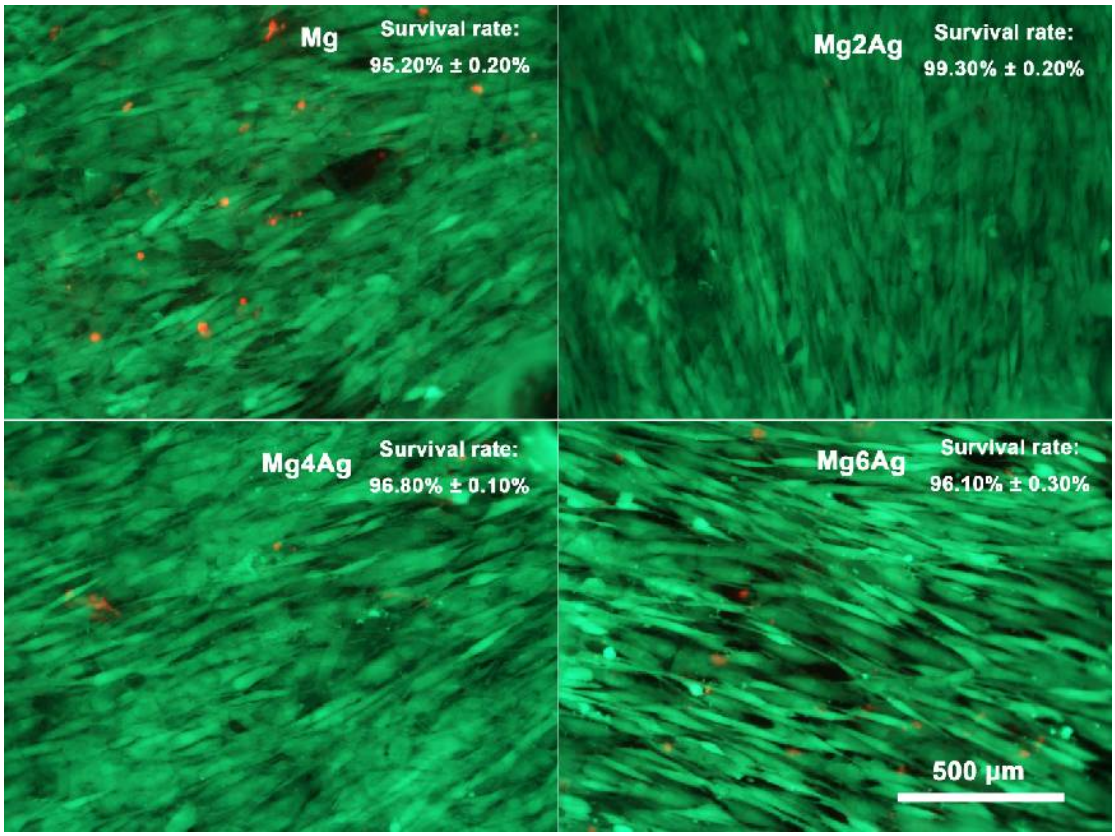

Fig. 35. Fluorescent microscope images and survival rates of human osteoblasts cells after 72 hs incubation on tested materials. Cells were stained with a LIVE/DEAD cell assay, where living cells are labeled green and dead cells red.

Furthermore, cell adhesion is directly related to cells reaction to material surface. Fig. 36 represent the SEM micrographs of human osteoblast cells on T4 treated Mg-Ag samples. Cell attachment and spreading on alloys was even better than on magnesium surface as can be seen from the SEM figures. From the SEM patterns, it could also be revealed that viability and seeding density were considerably higher on Mg-Ag alloys than pure magnesium.

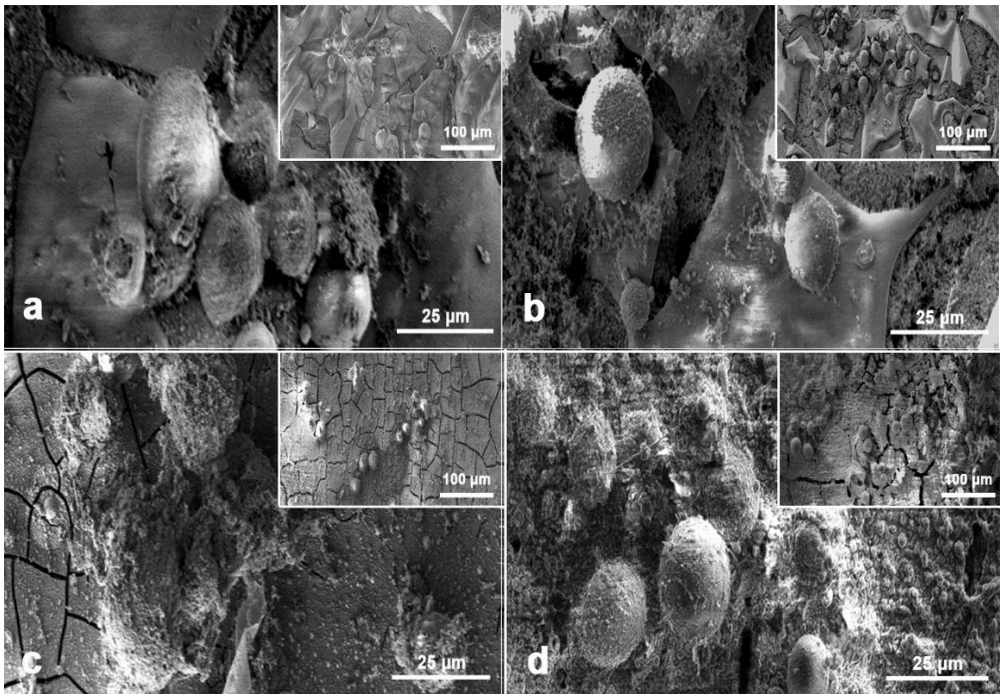

Fig. 36. SEM micrographs of human osteoblast cells adhesion on T4 treated samples (a, b, c and d).

Although Mg6Ag samples had higher corrosion rate than the other two alloys, it did not show more negative effects on cells' adhering according to the range of cellular extension.

5.6. Antibacterial properties

To analyse if the silver concentrations were still high enough to have an antibacterial effects the amount of adhering bacteria and their vitality on Mg-Ag alloys were compared with the corresponding values on Ti, glass and pure magnesium. The viability of the bacteria was calculated as percent of the total adhering amount. In average for titanium, glass, magnesium, Mg2Ag, Mg4Ag and Mg6Ag 49.8%, 52.2%, 36.0%, 27.5%, 21.4% and 16.5% respectively viable adhesive bacteria were found (Fig. 39). Compared to titanium and glass, Mg-Ag alloys showed a 50-75% reduction of adherent bacteria. The tendency of increased antibacterial activity with increased silver atomic ratio in alloys was observed and Mg6Ag was identified as most potent antibacterial material.

The CLSM micrographs visualizing life/dead stained adherent bacteria on the materials in the bioreactor are shown in Fig. 37 and 38. The bacterial colonization was relatively homogenous over the entire sample surface which ensured representative micrographs.

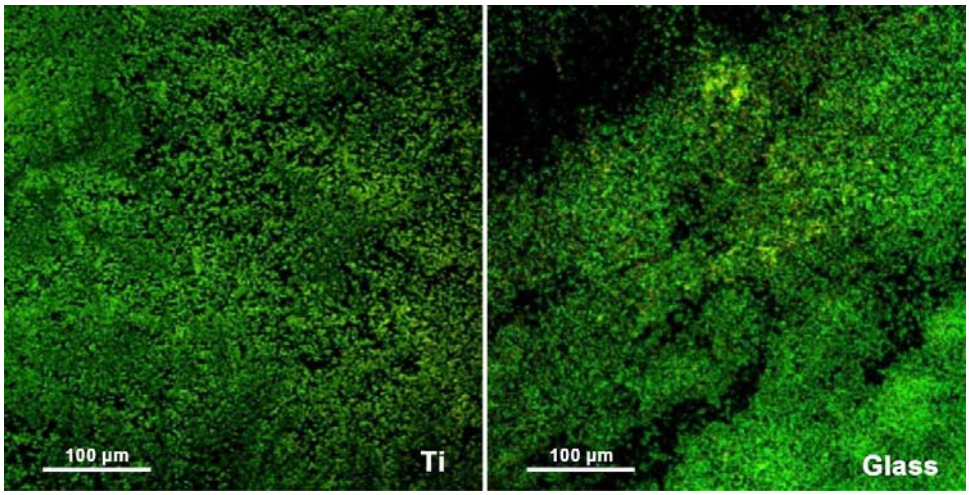

Fig. 37. Morphology of reference materials, Ti and glass, surfaces after bacteria adhering tests in the bioreactor by CLSM (wave length = 488 nm) analysis. Bacterial films were fluorescence stained: green color for living bacteria; red color for dead bacteria.

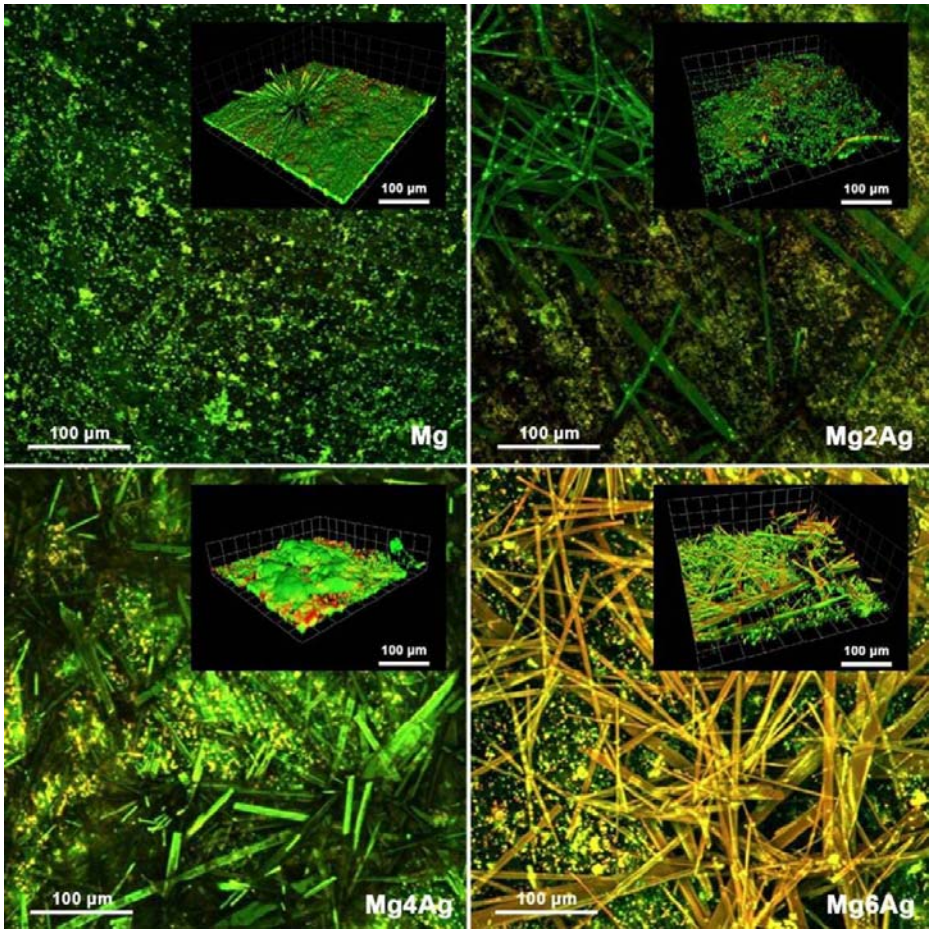

Fig. 38. Morphology of T4 treated material surfaces after bacteria adhering tests in the bioreactor by CLSM (wave length = 488 nm) analysis, with according 3D reconstruction images. Bacterial films were fluorescence stained: green color for living bacteria; red color for dead bacteria. Crystal structures were generated by corrosion products.

Crystal-like structures were observed on some samples which were generated by corrosion products. Ti and glass samples exhibited little visible influence on bacteria's viability, while had flatter surface due to no corrosion happened. The CLSM patterns also confirmed that the antibacterial activity is correlated with the silver content. Mg6Ag was more effective than Mg4Ag > Mg2Ag > magnesium, and all alloys demonstrated far higer effectivity than glass and titanium.

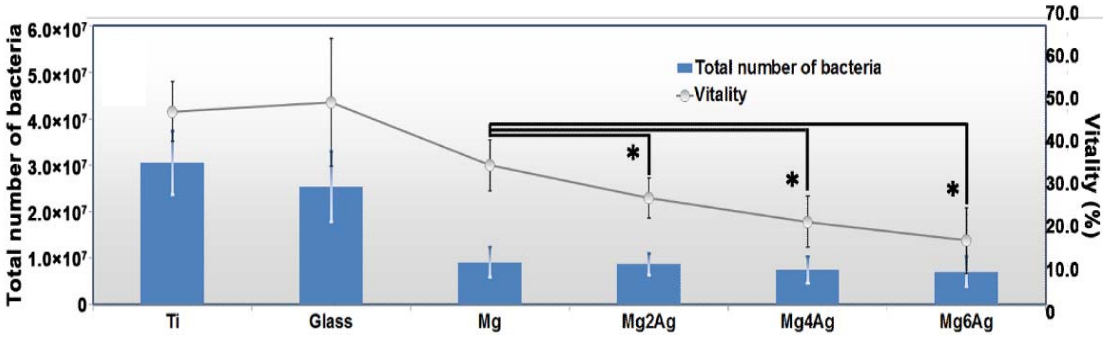

Fig. 39. Comparison of adhering bacteria number and their viability on studied materials.

6 Discussion

Degrading Mg-Ag alloys so far have not been used for biomedical applications. Therefore the newly produced materials had to be characterized for their mechanical and corrosion properties and selective toxicity with respect to bacteria.

6.1. Microstructure of Mg-Ag alloys

The improved cooling processing at the end of the casting ensured a grain-refined and purified material was produced [184]. Due to the relatively slow cooling rate of the casting process, the structure of the sample consists of coarse equiaxed grains rather than columnar grains. Viewed from microstructure pictures, silver had a grain refining effects itself. As a result, the microstructure of the investigated cast Mg-Ag alloys consisted of small grains of a size of 350-600 μm which were much smaller than cast pure magnesium [185], and heat treatments did not bring visible grain growing. Fig. 9 depicts the microstructure of the cast alloys, in which Mg-Ag secondary phases are indicated. Compared with pure magnesium the grain size was reduced which could bring better mechanical properties [186], and this effect was also proven by mechanical results (Fig. 13 and 14). The secondary phases and dendrites can be observed inside the grains, and additionally eutectic phases. This distribution indicates that the corrosion properties of the alloys could be further improved by heat treatment including solidification and aging [187].

The as-cast Mg-Ag alloys microstructures had typically a primary α-Mg matrix and eutectic phases distributed along the grain boundaries (Fig. 10). Besides the influence of secondary phases and eutectic structure, the bigger grain size in pure magnesium compared to alloys also made it more corrosion resistant than the other cast alloys [188]. Phase identification analysis via both EDX and XRD were carried out towards cast alloys because they contained higher ratio of secondary phases than heat treated materials. XRD results showed no visible formation of other secondary phases besides Mg_4Ag and $Mg_{54}Ag_{17}$ phases, between which Mg_4Ag was dominant because of magnesium rich environment. The close-up SEM patterns in Fig. 10 and 12 clearly demonstrate that the eutectic consists of large β-Mg_4Ag/$Mg_{54}Ag_{17}$ phase particles and the eutectic α-Mg phase. Microstructure of the alloy was changed during the process of heat treatment. The T4 heat treatment dissolved the β phases and produced a microstructure consisting of the saturated α-Mg phase, while quite few tiny residual β phases were still observed especially in T4 treated Mg6Ag (Fig. 12). During T6 process, β phases precipitated randomly along the grain boundaries and inside grains of the α-Mg phase. Despite of the large atomic size of silver atoms, aging treatment still made some silver atoms diffuse

towards grain boundaries to form precipitates of β phases. This process reduced the silver concentration in the α-Mg matrix, which induced changing of mechanical and corrosive properties.

6.2. Mechanical properties

The presented measurements show that silver containing secondary phases have positive effects on mechanical properties. Hardness, tensile and compressive strength of Mg-Ag alloys achieved significant improvement compared to pure magnesium in both cast and heat treated status. The lowest hardness was observed in pure magnesium, while more secondary phases and dendrite structure (Fig. 10) led to higher hardness with increasing silver content regardless of heat treatment status. Compared to pure magnesium the increase was significant in all cases. This phenomenon revealed that size and distribution of the secondary Mg-Ag phase could reinforce the overall hardness. Mechanical performance of T4 treated alloys is attributed to effects of solution strengthening, while the loss of some mechanical performance is due to dissolving of β phases [189]. This is confirmed by the increase of hardness after T6 treatment by the re-precipitated secondary phases.

The Young's modulus of Mg-Ag alloys maintained nearly constant regardless of compositions and heat treatment. The uniform Young's modulus of all tested materials reduces difficulties when choosing proper materials for specific use for bone applications [4]. Ductility of all Mg-Ag alloys was higher than for magnesium either before or after heat treatment due to the presence of silver atoms in the metallic matrix [190]. Since the Vickers hardness of cortical bone is reported to be about 49.8 [191], the T4 and T6 treated Mg-Ag alloys are approaching the characteristics of the natural bone with an ultimate compressive strength of 130-180 MPa [4]. However, tensile tests exhibited for Mg6Ag an ultimate tensile strength of almost double value (220-230 MPa) than cortical bone [4]. The mechanical characteristics indicate that heat treated Mg-Ag alloys could be suitable as biomaterials for larger degradable implants especially in load bearing applications. According to the microstructure of T6-treated alloys (Fig. 9 and Fig. 12), further improvement in tensile and compressive strength could be expected via increasing amount of re-precipitates, which could be achieved by prolonging aging time. This option extends the application range of Mg-Ag alloys and makes them more adjustable for specific needs.

6.3. Optimum of *in vitro* corrosion testing methods

6.3.1. Corrosion media

6.3.1.1. Effects of Rinsing

The pure Mg sample without rinsing in water gives a more fluctuant XPS spectrum than the sample with a cleaning procedure prior to the measurement (Fig. 40). The Mg 2p peak of unrinsed samples distributes in a very wide range from 46.9eV to 54.2eV binding energy, with obvious impurity background and a lot of sub-peaks. The peak can be fitted by many different supposed binding types including $Mg(OH)_2$, MgO and other salts. For the Mg 2p spectrum of the rinsed sample, the peak is much smoother and sharper and locates from 47.0eV to 51.8eV. This peak sharply splits to only 2 sub-peaks, which can be fitted exactly by $Mg(OH)_2$ at 49.3eV and MgO at 50.8eV.[192] From the comparison, it is obvious that rinsing after immersion experiments is a necessary procedure to remove surface soluble products and other contaminations formed during immersion, and the all of the following analyses are based on rinsed samples.

6.3.1.2. Comparison of corrosion products in different media

Compared with the sample in DMEM, the sample in HBSS has no calcium products on its surface. This is due to the choice of calcium and magnesium free HBSS. The element distribution on the sample immersed in SBF showed there is only very few Na and P on its surface, besides which only Mg, O and C elements appears. An interesting observation is the total clearance of Ca by rinsing on SBF-treated samples, whereas on the surface of samples treated with DMEM still a high amount of calcium can be found.

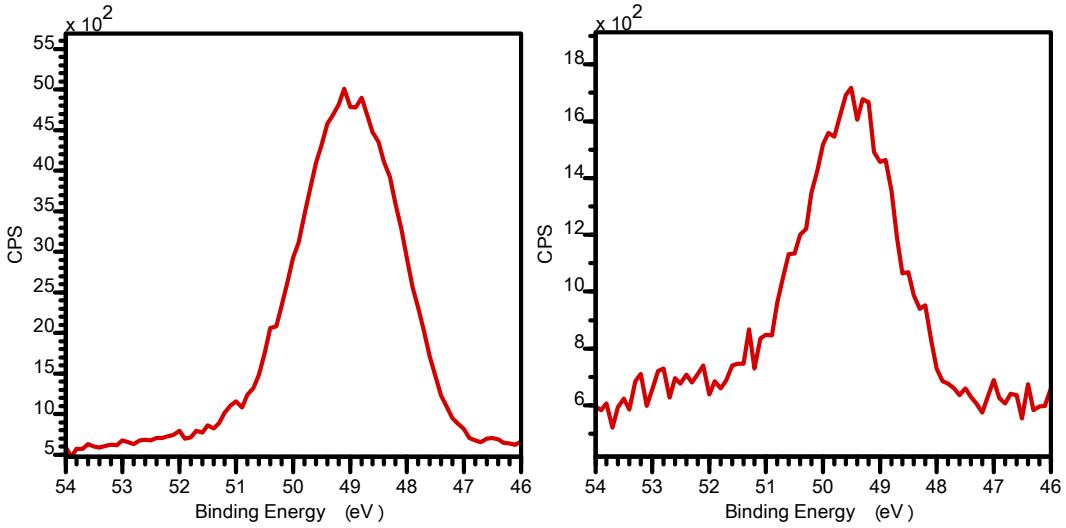

Fig. 40. Comparison of Mg 2p XPS spectra between Mg surfaces after rinsing (left) and not rinsed (right) after immersion in DMEM

The appearance of MgO on all samples is due to the formation of a thin $MgO/Mg(OH)_2$ layer, which is transparent to electrons and allowing the electrons to reach the conduction band of water.[193] The formation of $Mg(OH)_2$ is a normal corrosion product if magnesium gets in contact with aqueous solutions.[194] Moreover, in all samples the formation of $MgCO_3$ could be observed, which can be attributed to the environmental conditions. Fitting models to Mg 2p peaks of different samples are compared in Fig. 41.

The cations of those phosphates and carbonates can be determined from their binding energy. In most of cases $Mg(OH)_2$ appears as dominant surface product due to its low solubility compared to Mg phosphates and carbonates.

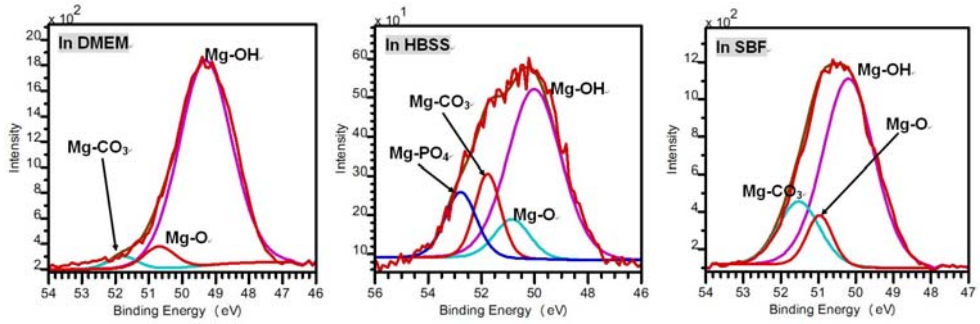

Fig. 41. Mg 2p spectra of Mg sample immersed in DMEM, HBSS and SBF

Due to magnesium corrosion the medium becomes alkaline, therefore CaO and $CaHPO_3$ cannot be generated, while $CaHCO_3$ and $Ca(OH)_2$ can neither be left on the surface because of their solubility. Alkaline Ca salt in the form of Ca^{2+} in $Ca_m(PO_4)_n(OH)_x$ and $CaCO_3$ are the most possible corrosion products on the surface, which can also be supported by O 1s and C 1s spectra.

6.3.1.3. Quantitative Analysis

According to Mg 2p spectrum of Mg sample immersed in DMEM, three observable compound peaks were fitted to $Mg(OH)_2$, MgO and $MgCO_3$, with the ratio of 71%:8%:5%. The rate of CO_3^{2-} to Carbon C is 69%:31% by C atom. As the total C element takes 11% by atom out of all surface products, the CO_3^{2-} form of C takes 7% by atom out of all surface products. The rate of PO_4^{3-} and CO_3^{2-} is 12%:9% calculated by P 2p and C 1s peak fitting. This rate exactly meets the element distribution of the survey spectrum.

Samples immersed in HBSS show 4 measurable elements on the sample surface: C, O, Mg and P. According to Mg 2p and O 1s spectra, $MgCO_3$, $Mg_m(PO_4)_n$ and $Mg(OH)_2$ are present on the surface as dominant corrosion products, at the rate of 13%:24%:55% by Mg/Ca atom, while a small amount of MgO (8%) is also present. In HBSS the original pH value is around 7.4. During immersion under cell culture conditions it first drops to around 6.6 and as immersion is proceeding, the pH value

will go higher to alkaline direction, which leads to the formation of $MgCO_3$. Yamamotos calculation also proved it. [195] The ratio of $MgCO_3/Mg_m(PO_4)_n$ by $Mg(OH)_2$ is supported by O1s spectra as well, the peak model has been published before.[183]

From sample element distribution immersed in SBF (Table 9), it can be determined that only Mg, O and C elements are present on the sample surface (with a trace amount of Na and P within error tolerance). Using the same fitting model as for the samples immersed in HBSS and DMEM, the Mg surface products are fitted to $Mg(OH)_2$, MgO and $MgCO_3$ according to Mg 2p and O 1s spectra, at the rate of 71%:10%:19% ($Mg(OH)_2$:MgO: $MgCO_3$). It can be calculated from C 1s spectrum that, C in carbonate form takes 5% of overall atoms on the surface, and this amount matches the $MgCO_3$ calculation as well. Surface product species and their ratio are summarized in Table 9.

Generally, it is usually found that the corrosion is slowed down in animal trials by several orders of magnitude as compared to in vitro tests with standard laboratory corrosion solutions [8]. *In vitro* corrosion experiments with relatively simple corrosion solutions show the formation of a layer containing calcium, phosphorous, magnesium, and oxygen, which is assumed to be corrosion protective and osteoinductive. [196-197]

Table 9. Surface products components by Ca/Mg atom in different media

Media	$Mg(OH)_2$ [%]	MgO [%]	$MgCO_3$ [%]	Mg-(PO_4) [a] [%]	$CaCO_3$ [%]	Ca-(PO_4) [a] [%]
DMEM	71%	8%	5%		4%	12%
HBSS	55%	8%	13%	24%		
SBF	71%	10%	19%			

[a] Mg-(PO_4) and Ca-(PO_4) here referring to Mg/Ca atoms binding to PO_4^{3-}.

The corrosion behaviour in SBF (Simulated Body Fluid) or other standard electrolyte solutions (Hank's balanced salt solution HBSS, phosphate buffered saline PBS etc.) was explained by the high amount of chloride in the corrosion media which leads to high corrosion rates.[154, 198] Already the composition of SBF may lead to different results and despite its abundance in literature there is an ongoing discussion about the usefulness of such fluids. However, not only the choice of the corrosion solution, but also the corrosion environment is very important. Therefore we choose cell culture conditions with a continuous supply of CO_2. This approach takes into account the buffering system based on the sodium bicarbonate system, which is present in all three solutions. Under standard cell culture condition with CO_2 flow addition, pH value's changing of samples immersed in different corrosion medium was monitored

by an online system, and the results can be drawn in Fig. 42. pH value varied in a very small range (difference around 0.5 to 0.7), and this stable pH environment is crucial to keep immersion results credible. In this experimental condition, carbon dioxide introduces the formation of H_2CO_3, which is the substrate for magnesite formation:

$$H_2 + CO_2 \leftrightarrow H_2CO_3^- + H^+ \quad \text{(Eq. 7)}$$

$$Mg(s) + H_2CO_3(aq) \leftrightarrow MgCO_3 + H_2(g) \quad \text{(Eq. 8)}$$

Due to the dissociation of sodium bicarbonate:

$$NaHCO_3 \leftrightarrow Na^+ + HCO_3^- \quad \text{(Eq. 9)}$$

The equilibrium of the carbon dioxide system is shifted to H_2CO_3 giving rise to further magnesite production. Due to this fact the buffering capacity even of small amounts of immersion medium is higher than for experiments performed without CO_2.

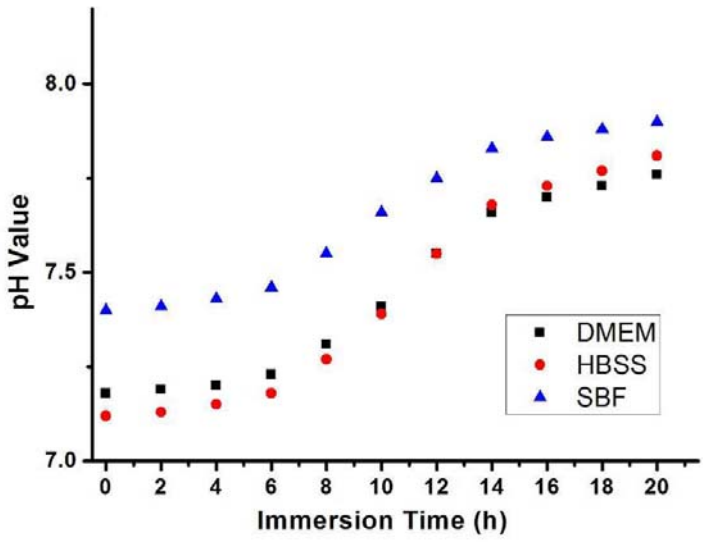

Fig. 42. The change of pH values in three corrosion media as a function of immersion time

Still these experiments are far away from the realistic environment of e. g blood which is a very complex mixture of organic and inorganic molecules. Thus, the *in vitro* corrosion results obtained from different literature are not really comparable with data obtained *in vivo*, even for the same material. Further studies should include the analysis of e.g. proteins or the introduction of flowing conditions to maintain a stable pH, and the direct comparison of *in vivo* with *in vitro* data have to be performed to eventually find a correlation.

Contamination during immersion and soluble salts covering the surface may induce inaccurate XPS results. It was proven that rinsing is a necessary procedure after immersion experiments before carrying out surface analysis. MgO, $Mg(OH)_2$, and $MgCO_3$ species as the dominant corrosion products are present in all specimens despite of the different corrosion media. However the ratio of corrosion products depends on the medium composition. Compared with immersion in DMEM, surface products after immersion in HBSS and SBF exclude Ca; while compared with immersion in DMEM and HBSS, surface products after immersion in SBF nearly exclude P. HBSS is the simplest solution and by far not comparable with tissue fluids or blood, whereas SBF only reflects the inorganic part of blood. DMEM could be a more reliable medium due to the addition of organic compounds. Moreover, the influence of proteins has to be taken into account. These results may help predict magnesium corrosion behaviour and corrosion products in an *in vitro* biomaterial test, and also provide a standard to evaluate which medium is more proper when applied in a certain test.

6.3.2. Effects of protein

6.3.2.1. XPS analysis

Compared with samples in pure media, elemental Mg is present besides MgO, $Mg(OH)_2$ and $MgCO_3$. An increase in Mg can be determined after addition of FBS, regardless of different media. Fitting models of Mg 1s peak of each sample in media with FBS can be seen in Fig. 43. Elemental Mg may be present because corrosion layers became thinner when serum was added. In this measurement, the products in ca. 70nm depth were determined. While little elemental Mg can be found in samples with pure media, much more Mg was detectable in samples with media and FBS. The thinner the corrosion layer was, the more element Mg can be found; this can be proven by the samples immersed in human blood with profile measurement (depth scan).

Addition of FBS decreased the amount of oxygen but did not change its compound species and ratio in each medium. Real C element amount (in CO_3^{2-}) neither change in each medium after FBS addition, although in HBSS overall C element increased (Fig. 43).

Calcium is only present in DMEM (Fig. 44), and after addition of FBS, only Ca-PO_4 was left while $CaCO_3$ totally disappeared. This is maybe because magnesium became much more released after FBS addition, and all carbonate generates $MgCO_3$ instead. The reason for in SBF P element is missing despite of big amount of PO_4^{3-} in the SBF, maybe related to the chemical form of PO_4^{3-}. According to the three media's compositions and XPS analysis result, generation of phosphate was mostly related with the concentration of $H_2PO_4^-$ rather than HPO_4^{2-}. Ca-PO_4 is generated prior to Mg-HPO_4^{3-} and in case of DMEM, it did not matter whether FBS was added or not.

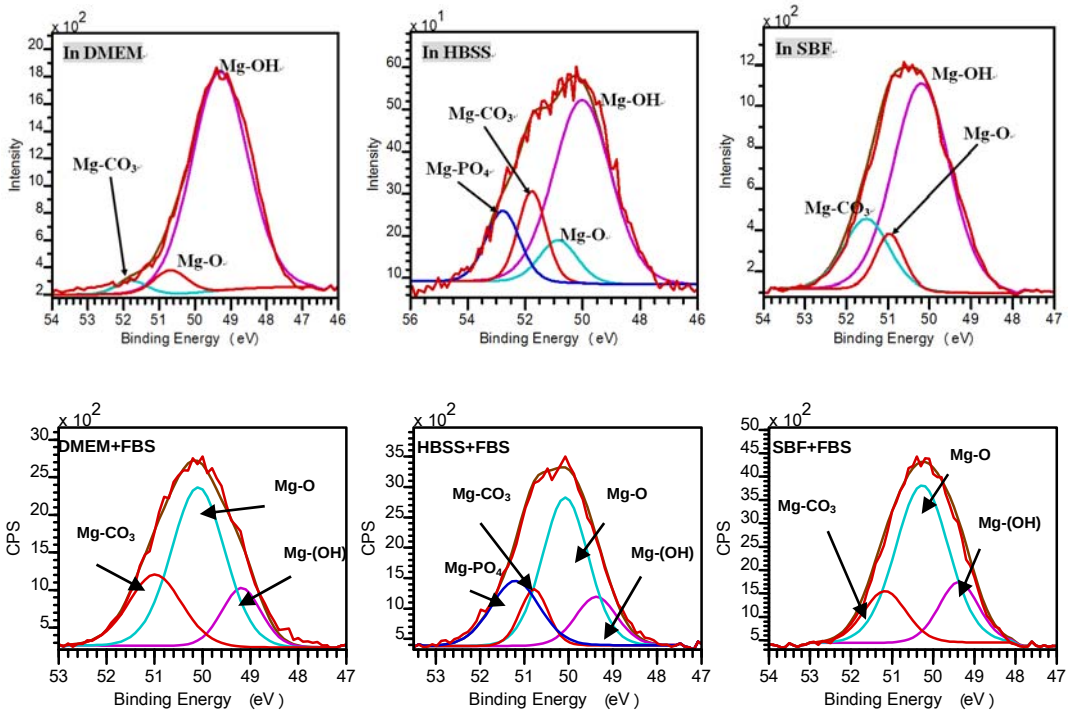

Fig. 43. Fitting models of samples Mg 2p spectrum in media without and with FBS

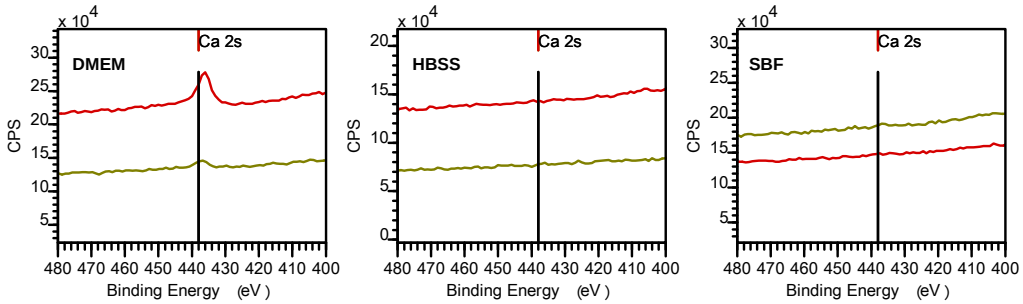

Fig. 44. Ca 2s spectra in DMEM, HBSS and SBF

* Lines in red are samples in pure media (without FBS).

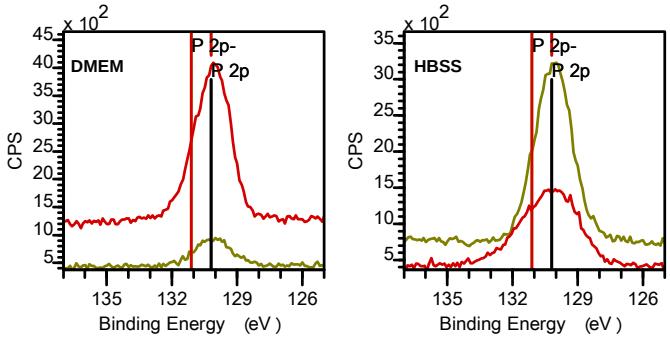

Fig. 45. Comparisons of P 2p spectra in DMEM and HBSS

* Lines in red are samples in pure media (without FBS).

The amount of P is always strictly following Ca amount in fixed rate of ca. 1:1.4, and analysis of P 2p spectra proved that all phosphate is incorporated to Ca-PO_4 binding, and P 2s peak at 189 eV also support this. To the case of HBSS, absence of Ca made Mg-PO_4 generated and protein seems to increase this trend. Comparisons of P 2p spectra in DMEM and HBSS can be seen in Fig. 45.

Na element in surface products of all samples is lower than 1.2%, due to media remnants. According to element distribution they may belong to NaCl and Na_2CO_3.

The possible principle how FBS decreases corrosion rate is that: attachment of protein made effective anodic areas smaller, therefore the exchanging current became less and the corrosion rate was slower than in pure cell culture media. As a result, corrosion layer became thinner due to less corrosion product generated. There was another interesting point that metallic Mg rised next to the other corrosion products. This phenomenon showed that the corrosion happened inhomogeneously on the surface, and cracks and gullies were generated during corrosion.

6.3.2.2. Electrochemical analysis

From the electrochemical and microscopy results obtained, it is clear see that presence of protein (FBS) reduced homogeneous corrosion and pitting corrosion simultaneously

The corrosion experiments with proper electrolytes are recognized as key factor by many studies, especially for an *in vitro* test of a biomaterial. Different electrolytes may introduce much incommensurable results from different experiment [38]. In this study, addition of FBS into DMEM was chosen as physiologically relevant environment, as serum containing protein was shown to play a quite important role in bio-corrosion [199-200]. Presence of FBS decreased the materials general corrosion rate regardless of their component. In terms of pitting corrosion, the introduction of FBS also inhibits pitting dramatically. Hypothetically, a layer of protein could be formed above the corrosion oxidation layer, which restrains exchange of ions between electrolyte and material surface. Due to lack of electron supply, the cathodic area would be slowed down, and consequently the anodic area is beneficial for lower corrosion rate. While the ionization process is controlled, the fresh anodic area in the bottom of the pits gains time to regenerate a new oxidation layer, therefore pitting corrosion is minimized when protein is present. This result may also explain why some *in vitro* and *in vivo* corrosion studies show much lower corrosion rates in the presence of proteins or when corrosion tests were performed in an animal [10, 199].

DMEM and FBS applied in this study could be a more reliable medium due to the addition of organic compounds in comparison of other electrolyte in an *in vitro* test. Compositions of electrolyte have also been verified as an important factor to evaluate corrosion properties of degradable materials [201].

6.4. Corrosion properties of Mg-Ag alloys

Beside the mechanical parameter two additional aspects are important: the corrosion of the material which of course is correlated to the microstructure and its selective antibacterial activity which should only be caused by the Ag release and not by a too high corrosion rate which results in high pH values and an intolerable increase of ion concentration in general.

6.4.1. Corrosion properties of cast materials

6.4.1.1. Electrochemical behavior

From the electrochemical and microscopy results obtained, the following points are essential: (1) both the cathodic and anodic behaviors of the alloys are mostly due to the silver content of the alloys; (2) the general corrosion rates of the four alloys increases as follows: Mg < Mg2Ag < Mg4Ag < Mg6Ag; (3) the pitting corrosion susceptibility of the four alloys increases as follows: Mg >Mg2Ag >Mg4Ag > Mg6Ag, which may be a hint that higher silver content may retard pitting corrosion in cell culture medium. The pitting corrosion resistance seems to be related to higher silver content. The lower pitting susceptibility of Mg4Ag and Mg6Ag is easier to visualize in comparison to the other two alloys especially in DMEM with FBS, as in Fig. 20 and 21, where the cyclic voltammograms of the four alloys in DMEM and FBS are presented together.

Pure magnesium as a reference material exhibited the lowest corrosion rate in both media. However, magnesium was observed to be more sensitive to pitting corrosion than the other three Mg-Ag alloys. Compared with pure magnesium, Mg-Ag alloys have different electrochemical behavior due to their silver component. Mg2Ag has the lowest silver content of the three alloys and in the curve a slope in the anodic area (Fig. 16 and Fig. 17), but it still has an intense current density increase over pure magnesium.

Mg4Ag and Mg6Ag are obviously influenced by the content of silver by an acceleration of the general corrosion rate. Considering that Mg6Ag contains thrice the silver amount of Mg2Ag, their general corrosion rates are not exceeding 40% either in DMEM or in DMEM + 10% FBS (table 6 and table 7). This trend indicates that the correlation of silver amount to general corrosion is generally linear, and the fitting results can be found in Fig. 46.

For the assessment of the electrochemical behavior of biodegradable alloys it is necessary to go beyond the anodic polarization measurements to the cyclic measurements as it is then possible to evaluate the pitting corrosion susceptibility. The single sweeps are necessary because they are the tool that gives the knowledge about corrosion behavior and how silver content of the alloy affect it [202]. From the pitting corrosion point of view, it seems that the higher the silver content of an alloy,

the more possible it is to conceive a stable material. Therefore, it seems advisable to pay attention to the principle how silver affects the electrochemical corrosion process.

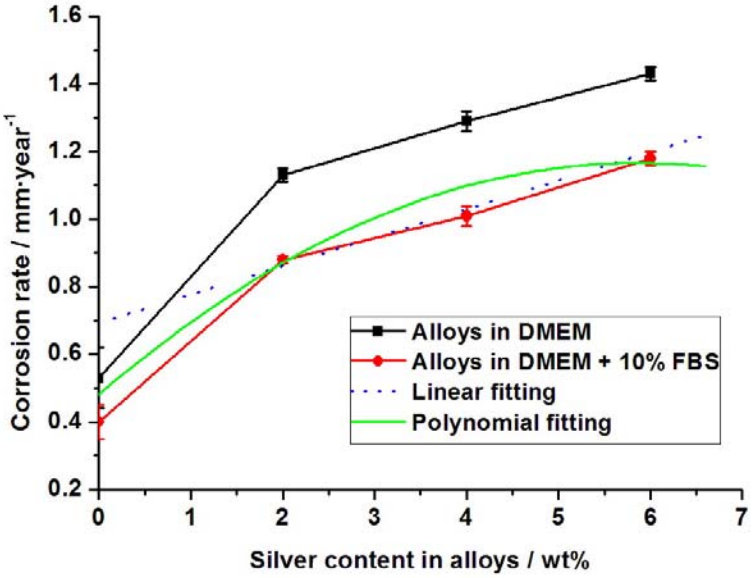

Fig. 46. Influence of silver content on corrosion rate of Mg-Ag alloys

6.4.1.2. Identification of corrosion products

Based on the XPS results (Fig. 23), the appearance of MgO on all samples is due to the formation of a thin MgO/$Mg(OH)_2$ layer, which is transparent to electrons and allowing the electrons to reach the conduction band of water [193]. The formation of $Mg(OH)_2$ is a normal corrosion product if magnesium gets in contact with aqueous solutions [194]. The chloride peak at 203.2 eV is only present when silver is available, because there is no chloride products appearing in pure Mg corrosion.

6.4.1.3. Mechanism of localized corrosion

Apart from the silver in AgCl left in the corrosion layer, around 30% of silver generated β phases mainly consist of Mg_3Ag permeated in α Mg phase or formed eutectic phases. These stable compounds then emerged due to lower corrosion rate on the material surface, which could be observed by SEM (Fig. 47). The different corrosion rate between α and β phases then affected the pitting corrosion process. Mg-Ag metallic compounds' corrosion potential is shifted to the anodic direction due to addition of silver [203], which could provide better corrosion property for the second phases. The mixed corrosion potential of the alloy is varied positively as well, which is also supported by the E_0 data shown in Table 7. Yet at the same time, these more corrosion-resistant second phases permeated in the alloys provide highly active microcathodes, which form numerous micro corrosion cells on the material surface. These micro corrosion cells make the electrochemical corrosion reaction more

severe, as a result the general corrosion rate is accelerated although the mixed E_0 could be even positive [204]. On the other hand, these areas are more corrosion-resistant; therefore the cathode area like oxidation layer in homogeneous material will turn to anode in this case. Hence, as what is illustrated before, the surface corrosion cell is transferred to a situation that the anode area is bigger than the cathode area, which could lead to faster homogeneous corrosion whilst minimizing pitting corrosion [187]. Material imperfections like pores or cracks which may cause pitting corrosion in more homogeneous material afford less current distribution, so the pitting corrosion was controlled or even erased by this effect.

The electrochemical corroded surface of the alloys can be illustrated well by representative BE images (Fig. 47). It is quite clear that magnesium suffered the most serious pitting corrosion in comparison with the other alloys, despite of its lowest general corrosion rate. On the contrary, with an increasing content of silver, Mg-Ag alloy gain a higher resistance to pitting corrosion, while holding a higher homogeneous corrosion rate.

It is easy to visualize that on corroded magnesium surface, the pitting corrosion cracks developed adequately and sub-cracks spread to form network under the oxidation layer. As for Mg-Ag alloys, the pitting corrosion has to compete against surface oxidation, so that pitting corrosion's dimension is controlled to minimum level and cracks do not have sufficient space to grow. It is also much apparent that due to faster homogeneous corrosion, Mg-Ag intermetallic phases were exposed to the corrosion surface as a result of oxidation of the surrounding anodic area, and then restrained the pitting corrosion from developing.

The results of the mechanical measurement in last section illustrate that Mg-Ag alloys have much better mechanical properties than pure magnesium at human body temperature (Fig. 13), which ensures a potential application of Mg-Ag alloys according to their mechanical performances. Thereafter, the corrosion test results show that the three cast Mg-Ag alloys are acceptable according to their general corrosion rate compared with currently applied biodegradable materials [5, 15]. Furthermore, from an applied point of view, localized corrosion is much more harmful than homogeneous corrosion in most of cases, because it leads to a loss of mechanical performance in a very short time, which could be quite problematic especially for biomaterials [205]. Hence, as an innovative antibacterial material, Ag-Mg binary alloy shows good resistance of pitting corrosion, with a corrosion rate comparable to other magnesium alloys [15]. In ongoing work it was preliminary proven that heat treatment is highly efficient to improve the mechanical and corrosion properties of the alloys by reducing secondary phase particles, which would be applied for further improvement.

Furthermore, the mini-cell system applied in this study as a setup with enough sensitivity to analyze composition factors by electrochemical behavior, gives the

precise individual characterization to the studied materials [38]. The next step following the determination of the material properties will be the evaluation of improvement brought by heat treatment.

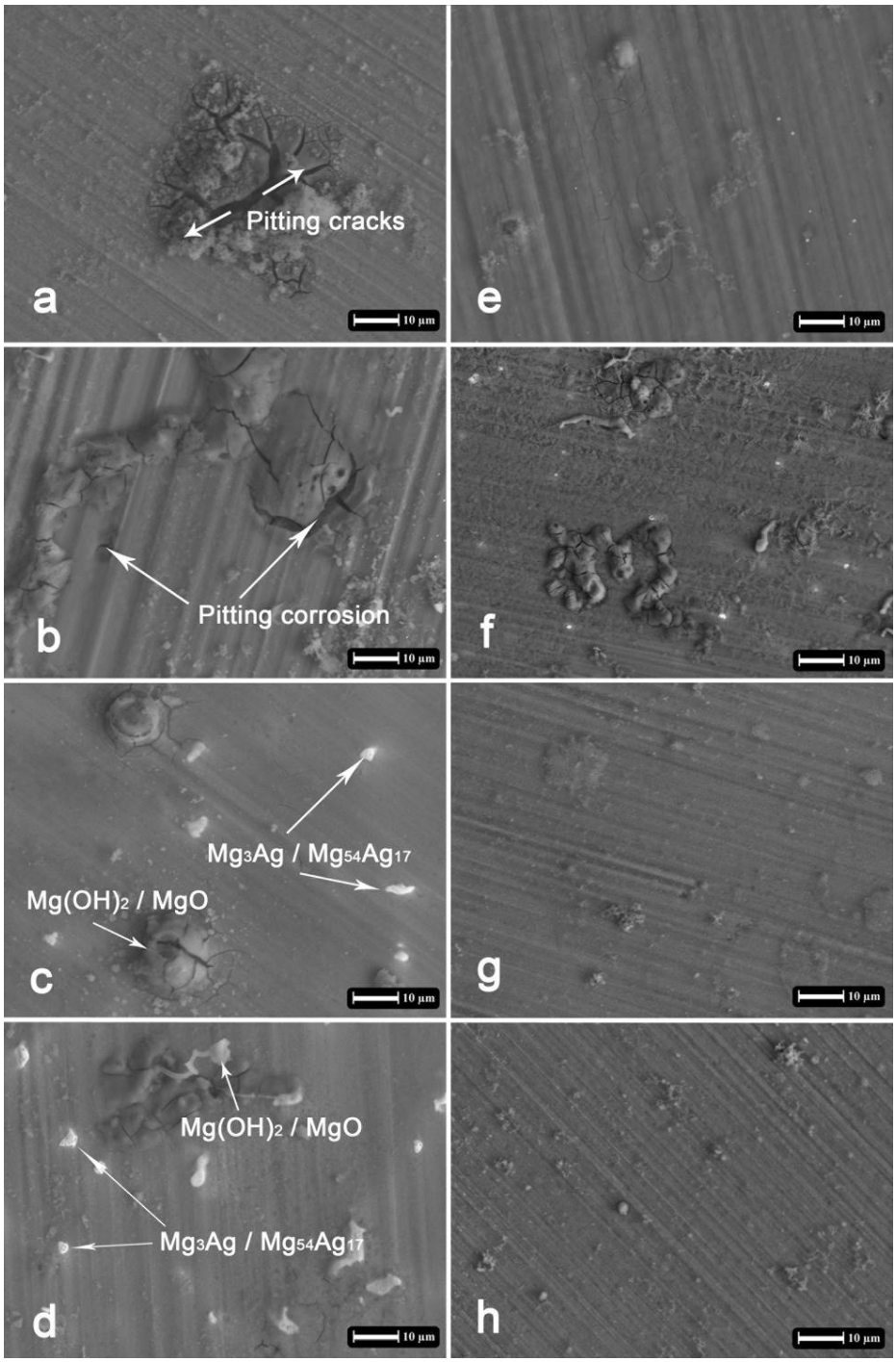

Fig. 47. Secondary electron (SE) images from corroded surface of materials tested in DMEM (a, b, c and d) and DMEM + 10% FBS (e, f, g and h): Mg (a and e), Mg2Ag (b and f), Mg4Ag (c and g) and Mg6Ag (d and h).

6.4.2. Corrosion properties of heat treated materials

6.4.2.1. Behavior and principles of electrochemical corrosion

Corrosion media choosing was proved a crucial factor for *in vitro* corrosion tests [38], so DMEM was selected as the corrosion medium in this research for its better representativeness according to former studies on media choosing for *in vitro* corrosion tests [154, 206]. Previous studies reported presence of protein (FBS) may result in different corrosion behavior [207-208], and induce increases in osmolality of corrosion media while reducing the corrosion rate of materials [209]. In the last section, our study also showed that DMEM is more credible when carrying out *in vitro* corrosion tests and protein's effects on corrosion of magnesium alloys. Therefore in this study, 10% FBS (by volume) was added to DMEM to simulate realistic *in vivo* corrosion environment, and to make the corrosion results more comparable with cytocompatibility tests. Therefore, DMEM supplemented with FBS has been chosen as corrosion media in the following experiments. Cell culture conditions provided ion buffer system as well as the human body like atmosphere; therefore the two corrosion testing methods employed in this study were both performed under cell culture conditions to assure experimental accuracy.

From the electrochemical and SEM microscopy results obtained, the following points are essential: (1) both the cathodic and anodic behaviour of the alloys are mostly due to the silver content of the alloys; (2) the general corrosion rates of the four alloys in all three heat treatment status increases as follows: Mg < Mg2Ag < Mg4Ag < Mg6Ag (Fig. 26); (3) the pitting corrosion susceptibility of the four alloys in all three heat treatment status increases as follows: Mg >Mg2Ag >Mg4Ag > Mg6Ag, which may be a hint that higher silver content could restrain pitting corrosion in cell culture medium; (4) heat treatment reduced corrosion rates of Mg-Ag alloys dramatically by dissolving dendrites and secondary phases. T4 treatment led to a lower corrosion rate of the Mg-Ag alloys than observed for pure magnesium. The pitting corrosion resistance seems to be related to higher silver content. The lower pitting susceptibility of Mg4Ag and Mg6Ag is easier to visualize in comparison to the other two alloys as in Fig. 24, where the single sweep voltammograms of are presented together (Fig. 25).

The electrochemically corroded surface of the alloys is shown in Fig. 24. It is obvious that magnesium suffered the most serious pitting corrosion in comparison with the other alloys, despite of its lowest general corrosion rate. On the contrary, an increasing content of silver leads to a higher resistance to pitting corrosion, despite of inducing a higher general corrosion rate. It is easy to visualize that on the corroded magnesium surface, pitting corrosion cracks (consisting of $Mg(OH)_2$ and MgO according to EDX analysis) developed and sub-cracks spread to form network under the oxidation layer. Pitting corrosion on Mg-Ag alloys has to compete against surface oxidation, so that its dimension is controlled to minimum level and cracks do not have sufficient space to grow. Apparently, due to faster homogeneous corrosion

secondary phases were exposed to the corrosion surface as a result of oxidation of the surrounding anodic area, also reducing pitting corrosion. After T4 and T6 treatment, pitting corrosion as well as other type of localized corrosion was greatly reduced due to the solving of secondary phases. T6 treated samples were slightly more susceptible to localized corrosion according to SEM patterns (Fig. 24) due to the re-precipitates. In pure magnesium no phase transformation occurs during heat treatments, so the corrosion rate did not vary significantly after heat treatment.

As most of silver content enriched in β phases, their corrosion potential was shifted towards the anodic direction (Fig. 24) due to presence of silver [203], which could make β phases more resistant to corrosion [58]. Therefore, electrochemical corrosion cells formed between α-Mg and β phases as Fig. 48 shows. To cast materials, most of β phases separated from α-Mg and concentrated in dendrites and grain boundaries (Fig. 9 and 10). In this case, corrosion cells grew completely all over the surface, and induced electrochemical corrosion between α-Mg and β phases.

At the first stage of electrochemical corrosion, hydrogen gas generated from cathode areas (Eq. 10). As corrosion layer grew thicker, oxygen absorption corrosion became dominant cathode reaction due to pH's change on the surface (Eq. 11). That is why much less gas bubbles could be found after 12h immersion.

The cathodic reaction: $2H^+ + 2e^- \rightarrow H_2\uparrow$ Eq. 10

$$O_2 + 2H_2O + 4e^- \rightarrow 4OH^-$$ Eq. 11

Fig. 48 exhibits the electrochemical corrosion scheme happened on cast materials, in which much bigger area of anode formed by α-Mg than small sized cathode formed by β phases could be observed. As a result of more negative corrosion potential, α-Mg were corroded more severely and faster than β phases. Therefore, β phases emerged on the surface due to lower corrosion rate, which could be clearly observed in SEM images (Fig. 24). Hence, general corrosion rates of cast materials were considerably high due to the fact that electrochemical corrosion was dominant in their corrosion processes. More content of silver generated a higher amount of β phases, as a result the general corrosion rate increased while the mixed open circuit potential (E_0) could be even more positive (Fig. 25) [204].

Conversely, T4 and T6 treated materials suffered much lighter corrosion thanks to most of β phases were dissolved by heat treatment (Fig. 9). As lack of potential difference between areas, corrosion was mainly by the means of chemical corrosion

rather than electrochemical corrosion. Therefore, the corrosion rates of heat treated materials were greatly decreased and generated more homogeneous corrosion layer (Fig. 24 and 48). Similar influence of heat treatment on corrosion process can be found on other magnesium alloys as well [210], and this trend became more obvious when more silver content was added like in Mg6Ag (Fig. 24),

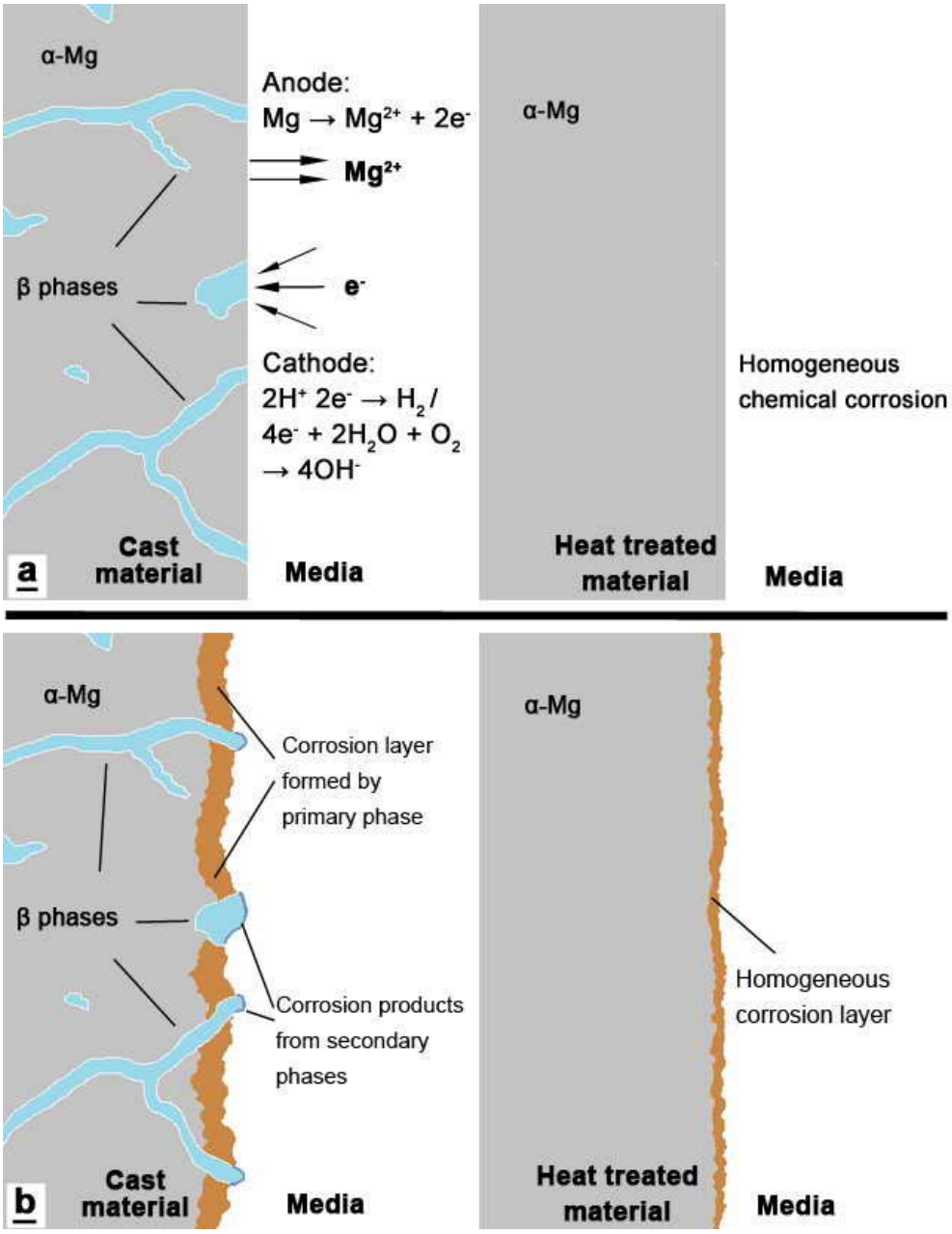

Fig. 48. Schematic diagram of the corrosion interface before (a) and after (b) corrosion in cell culture media. Cast material was corroded mainly by means of electrochemical corrosion, which resulted in higher corrosion rate, thicker and more inhomogeneous corrosion layer than heat treated material. Chemical corrosion was the primary corrosion style happened on heat treated material due to lack of potential difference between areas.

The different corrosion rate between α-Mg and β phases affected the pitting corrosion process as well. It can be visualized from Fig. 24 that on the corroded magnesium surface, pitting corrosion cracks (consisting of $Mg(OH)_2$ and MgO) and sub-cracks spread under the oxidation layer. As the general corrosion rate went higher with increasing silver content, general corrosion governed the whole surface, which made localized corrosion like pitting have little time and space to grow [211]. Therefore, less pitting corrosion could be observed in Mg4Ag and Mg6Ag despite of higher general corrosion rate (Fig. 24). After T4 and T6 treatment, pitting corrosion as well as other type of localized corrosions was greatly reduced due to the dissolving of β phases.

T4 treated samples demonstrated the best corrosion properties compared to the other two treatments during the electrochemical tests. To obtain the correlation between silver content and corrosion rate of T4 samples, Origin software (Origin 8.6, Originlab, Northampton, USA) was applied for fitting the corrosion rate data versus silver content. The following equation (Eq. 12) was derived as practical equation for estimating the general corrosion rate of T4 treated binary Mg-Ag alloys under cell culture conditions:

$$CR = 2.28 \times C_{Ag} + 0.2926 \quad \text{Eq. 12}$$

where CR stands for corrosion rate; CAg stands for mass concentration of silver in alloy; $0.02 \leq CAg \leq 0.06$; unit is mm per year.

According to mechanical and electrochemical testing results, T4 treated samples presented balanced mechanical performance and the best corrosion properties, which can meet the needs for biomedical applications better than the other two treatments. Therefore, T4 treated samples were selected for the following tests.

6.4.2.2. Corrosion products analysis and ion release

Based on the XPS analysis of the corroded surface (Fig. 27 and 29), the appearance of MgO on all samples is due to the formation of a thin $MgO/Mg(OH)_2$ layer, which is transparent to electrons and allowing the electrons to reach the conduction band of water [193]. Therefore, thickness of the corrosion product blocks were much higher than the real corrosion interface, which formed the barrier between material and media and then decreased the general corrosion rate (Fig. 49) [193]. The formation of $Mg(OH)_2$ is a normal corrosion product if magnesium gets in contact with aqueous solutions [194].

The chloride peak at 203.2 eV is only present when silver is available, and increasing silver products did not affect the distribution of magnesium corrosion products,

because most of silver content was enriched in β phases and corroded separately from α-Mg like specified above.

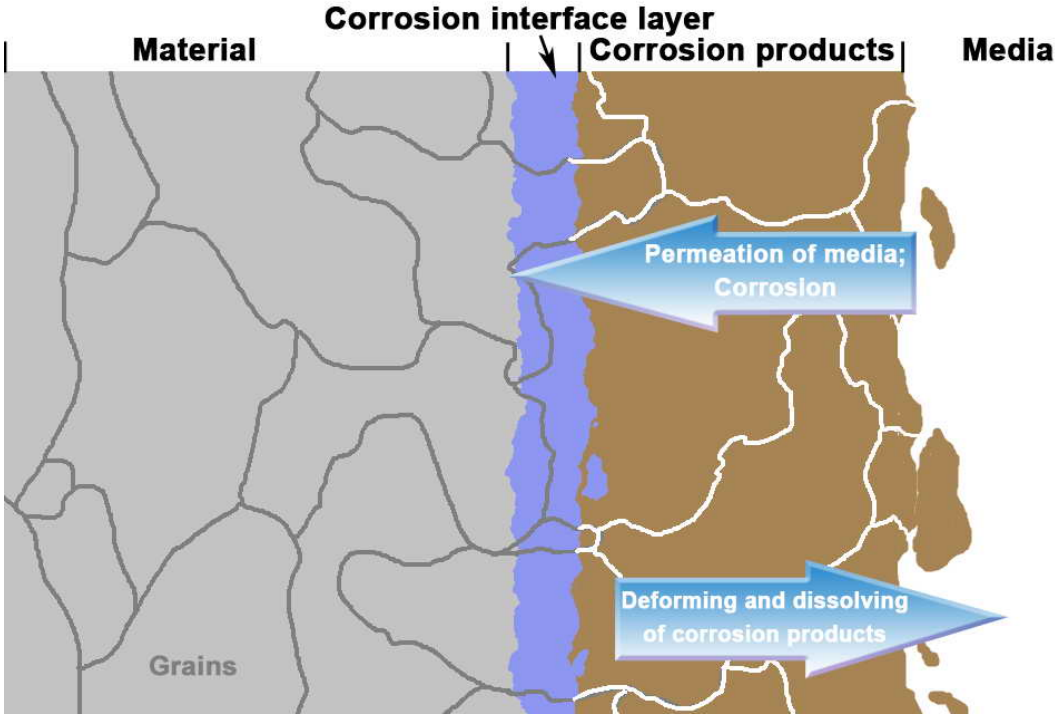

Fig. 49. Scheme of surface structure after bio-corrosion

Due to the same reason, silver content had little influence on increases in osmolality and pH of the corrosion media, the two key parameters for biocorrosion (Fig. 32). The increases in magnesium ion release of T4 materials were not significant either (Fig. 33). Compared to inner levels, the surface corrosion level contained a notably higher amount of carbonates which could be hardly found in inner levels. It was generated by the reaction of magnesium / calcium hydroxide and carbon dioxide (Eq. 13), and the reaction only happened on the very surface due to carbon dioxide's low diffusion capability in the solid corrosion layer [212].

$$Mg(OH)_2 / Ca(OH)_2 + CO_2 \rightarrow MgCO_3 / CaCO_3 \qquad \text{Eq. 13}$$

During the corrosion tests, cell culture conditions provided constant pH and concentration of CO_2, without which carbonate on the surface could not be generated. It was already proved that the steady and realistic circumstance provided by cell culture conditions is crucial for *in vitro* corrosion tests to simulate *in vivo* conditions [209]. Considering all facets of corrosion properties of the tested materials, T4 treated alloys seemed to be preferable as potential implant materials for their low general corrosion rate, slight susceptibility to pitting corrosion and low ion release, especially for T4 treated Mg2Ag and Mg4Ag alloys.

6.5. Cytocompatibility and antibacterial properties

The cytocompatibility tests were performed to clarify two important issues to Mg-Ag alloys designed as implant materials: cytotoxicity of the released ions and cellular response to the interfaces. As pure magnesium has been proven as a low cytotoxic biomaterial [18, 213], the toxicity tests of the alloys focused firstly on the cytotoxicity of silver ions since their magnesium ion release level were no higher than pure magnesium (Fig. 33). Comparing the silver ion release results shown in Fig. 33 and the cells' LC50 concentrations in Fig. 34, ion release was several orders of magnitude lower than the LC50. The silver ion release level of T4 Mg-Ag alloys should therefore not induce cytotoxic effects. According to literatures on cytocompatibility of ionic silver, 3T3 fibroblast cell could even survive at concentrations of over 10 mM [214].

For bone biomaterial interaction testing, osteoblast adhesion is an essential requirement. The interaction between cells and implant materials are governed by a number of physical and chemical processes, among which surface condition is a major factor [215-216]. The interaction between the alloys and the osteoblasts in this study showed even better cell adhesion and higher cell viability than pure magnesium (Fig. 35. The influence of the corrosion layers on cell adhesion were not explicitly studied, but will be subject of further studies. Absorbance of proteins is the first stage prior to adhesion of cells. However, it is not yet clear whether proteins adhere to degrading magnesium in the same way as they do on permanent materials.[209], and remnants of proteins were hardly found in the corrosion layer [206]. It is highly important to understand the interaction of proteins with the permanently changing surface during degradation and this will be analyzed in further studies. However, it was shown already that for materials with low corrosion rates good protein absorbance ability of magnesium alloys [9] may be responsible for the improvement of cytocompatibility. Presence of silver decreased the corrosion process while brought no additional toxicity, which provided better environment for cell adhesion than pure magnesium. The effects were also proven by the higher seeding density and better range of extension of osteoblasts on Mg-Ag alloys.

The antibacterial testing using the dynamic flow bioreactor was carried out to determine the antibacterial properties under human body like environment. Alloy degradation was observed in both chambers of the flow accompanied with bacterial colonization (Fig. 37 and 38) as expected. Different from the immersion in DMEM with FBS, crystal structures formed by precipitation of corrosion products were clearly presented in CLSM pictures. Despite the significant surface changes the viable bacteria numbers could still be accurately quantified by counting of bacterial colonization. Pure magnesium also showed antibacterial ability during the tests, however, considering its relatively higher corrosion rate, some of the effects attributed to increasing pH and osmolality which could reduce cellular viability as well

[39]. Fig. 50 gives a comparison of corrosion rate and bacteria viability between each T4 treated materials, in which it could be clearly drawn that Mg-Ag alloys demonstrated significantly higher antibacterial property than pure magnesium while keeping lower corrosion rate. Bacteria viability decreased with more silver presence, however considering the influence by increasing corrosion rate, Mg2Ag and Mg4Ag has already achieved satisfactory antibacterial performance.

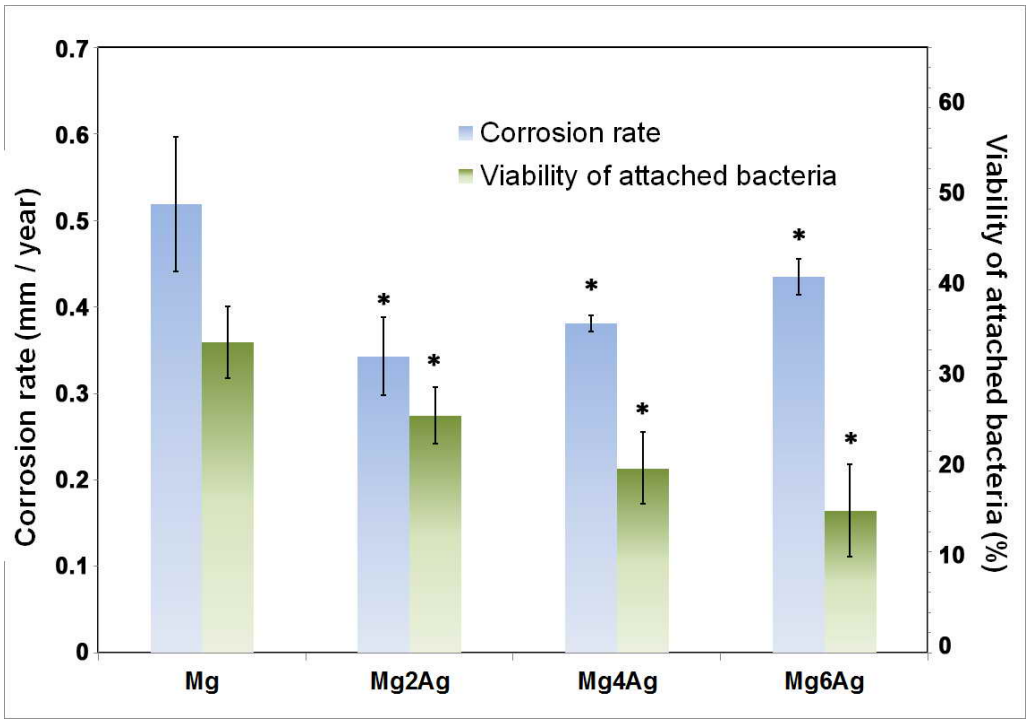

Fig. 50. Comparison of corrosion rate and viability of adhering bacteria on the surface between T4 treated pure magnesium and Mg-Ag alloys. Mg-Ag alloys presented improved antibacterial properties while maintaining lower corrosion rate than pure magnesium. '*' means significance level $p < 0.05$. The differences between alloys and pure magnesium in corrosion rate and viability of adhering bacteria were both significant.

As newly developed biodegradable materials, Mg-Ag alloys exhibited a stronger antibacterial capability than the permanent implant material titanium and the biodegradable implant material pure magnesium, which was correlated to the silver content. The CLSM pictures (Fig. 38) support the bacteria counting results very well, in which the trend of stronger antibacterial ability brought by increasing content of silver was clearly presented. These results confirmed the well-known antibacterial effects of silver could be also expressed in magnesium after alloying. Based on this study, the long term distribution, migration, vitality and stability of bacterial films still need to be further studied. Compared to the widely used reference materials titanium and glass, Mg-Ag alloys reduced viable bacterial counts significantly, which is much helpful to reduce probability of infections during an implant surgery. Further studies will focus on *in vivo* antibacterial properties of these alloys.

6. Discussion

The accumulation and metabolism of silver in human body is still being studied [217]. Some investigations on wound treatment with ionic silver reported that the accumulation and metabolism by skin and hairs was the possible mechanism [71]. Metallic silver was proved to pose minimal risk to health [71], so the silver content utilized in these alloys was safe to human body considering their low silver ion release (Fig. 33). The low cytotoxicity, low ion release and harmonious interaction with cells of T4 treated Mg-Ag alloys warranted their low risk when used as implant materials especially compared with other heavy metal containing magnesium alloys.

In this study we have demonstrated that Mg-Ag alloys, especially for T4 treated Mg2Ag and Mg4Ag, had appropriate mechanical, corrosive, cytocompatible and antibacterial properties. Since the control of *in vivo* corrosion and minimizing probability of infection are both of major importance, the use of Mg-Ag alloys provides an ideal option for bone implant surgery in the future.

7. Conclusions

1. From mechanical properties' point of view, 2% - 6% Ag-Mg alloys (abbr. as Mg-Ag) have quite nice performance as binary alloys, while T6 treatment make it even better.
2. T4 treated Mg-Ag alloys are more corrosion resistant than pure magnesium and less susceptible to pitting corrosion. Their corrosion and mechanical properties are highly adjustable.
3. Mg-Ag alloys's cytotoxicity is similar to pure magnesium due to their low Ag+ ion release. The alloys neither change pH nor Mg2+ ion release significantly.
4. Compared with pure magnesium, Mg-Ag alloys show significantly better antibacterial properties accompanied by a lower corrosion rate.
5. As content of silver increases, mechanical and antibacterial properties become better, while for corrosion properties and cytocompatibility the trend is just opposite.
6. Heat treated Mg-Ag alloys exhibit adjustable improved mechanical, corrosive, biocompatible and antibacterial properties. In summary, T4 treated Mg2Ag and Mg4Ag alloys show the biggest potentials as antibacterial biodegradable materials because they show an excellent balance in their property profile.

Reference

[1] Witte F. The history of biodegradable magnesium implants: A review. Acta Biomaterialia. 2010;6:1680-92.

[2] Witte F, Hort N, Vogt C, Cohen S, Kainer KU, Willumeit R, et al. Degradable biomaterials based on magnesium corrosion. Current Opinion in Solid State & Materials Science. 2008;12:63-72.

[3] Pollock TM. Weight Loss with Magnesium Alloys. Science. 2010;328:986-7.

[4] Staiger MP, Pietak AM, Huadmai J, Dias G. Magnesium and its alloys as orthopedic biomaterials: A review. Biomaterials. 2006;27:1728-34.

[5] Hort N, Huang Y, Fechner D, Störmer M, Blawert C, Witte F, et al. Magnesium alloys as implant materials - Principles of property design for Mg-RE alloys. Acta Biomaterialia. 2010;6:1714-25.

[6] Zhang SX, Zhang XN, Zhao CL, Li JA, Song Y, Xie CY, et al. Research on an Mg-Zn alloy as a degradable biomaterial. Acta Biomaterialia. 2010;6:626-40.

[7] Erbel R, Di Mario C, Bartunek J, Bonnier J, de Bruyne B, Eberli FR, et al. Temporary scaffolding of coronary arteries with bioabsorbable magnesium stents: a prospective, non-randomised multicentre trial. Lancet. 2007;369:1869-75.

[8] Witte F, Fischer J, Nellesen J, Crostack HA, Kaese V, Pisch A, et al. In vitro and in vivo corrosion measurements of magnesium alloys. Biomaterials. 2006;27:1013-8.

[9] Witte F, Feyerabend F, Maier P, Fischer J, Stormer M, Blawert C, et al. Biodegradable magnesium-hydroxyapatite metal matrix composites. Biomaterials. 2007;28:2163-74.

[10] Zberg B, Uggowitzer PJ, Loffler JF. MgZnCa glasses without clinically observable hydrogen evolution for biodegradable implants. Nat Mater. 2009;8:887-91.

[11] Xin YC, Jiang J, Huo KF, Tang GY, Tian XB, Chu PK. Corrosion resistance and cytocompatibility of biodegradable surgical magnesium alloy coated with hydrogenated amorphous silicon. Journal of Biomedical Materials Research Part A. 2009;89A:717-26.

[12] Wong HM, Yeung KWK, Lam KO, Tam V, Chu PK, Luk KDK, et al. A biodegradable polymer-based coating to control the performance of magnesium alloy orthopaedic implants. Biomaterials. 2010;31:2084-96.

[13] Zeng RC, Dietzel W, Witte F, Hort N, Blawert C. Progress and challenge for magnesium alloys as biomaterials. Advanced Engineering Materials. 2008;10:B3-B14.

[14] Drynda A, Deinet N, Braun N, Peuster M. Rare earth metals used in biodegradable magnesium-based stents do not interfere with proliferation of smooth muscle cells but do induce the upregulation of inflammatory genes. Journal of Biomedical Materials Research Part A. 2009;91A:360-9.

[15] Kirkland NT, Lespagnol J, Birbilis N, Staiger MP. A survey of bio-corrosion rates of magnesium alloys. Corrosion Science. 2010;52:287-91.

[16] Zhang S, Zhang X, Zhao C, Li J, Song Y, Xie C, et al. Research on an Mg–Zn alloy as a degradable biomaterial. Acta Biomaterialia. 2010;6:626-40.

[17] Palmer RJ, Butenhoff JL, Stevens JB. Cytotoxicity of the rare earth metals cerium, lanthanum, and neodymium in vitro: Comparisons with cadmium in a

pulmonary macrophage primary culture system. Environmental Research. 1987;43:142-56.
[18] Yun YH, Dong ZY, Lee N, Liu YJ, Xue DC, Guo XF, et al. Revolutionizing biodegradable metals. Materials Today. 2009;12:22-32.
[19] Atiyeh BS, Costagliola M, Hayek SN, Dibo SA. Effect of silver on burn wound infection control and healing: Review of the literature. Burns. 2007;33:139-48.
[20] McBride ED. Absorbable metal in bone surgery. J Am Med Assoc. 1938;111:7.
[21] Silver S, Phung LT, Silver G. Silver as biocides in burn and wound dressings and bacterial resistance to silver compounds. J Ind Microbiol Biotechnol. 2006;33:627-34.
[22] Kwakye-Awuah B, Williams C, Kenward MA, Radecka I. Antimicrobial action and efficiency of silver-loaded zeolite X. J Appl Microbiol. 2008;104:1516-24.
[23] Sintubin L, De Gusseme B, Van der Meeren P, Pycke BFG, Verstraete W, Boon N. The antibacterial activity of biogenic silver and its mode of action. Appl Microbiol Biotechnol. 2011;91:153-62.
[24] Sreekumari KR, Nandakumar K, Takao K, Kikuchi Y. Silver containing stainless steel as a new outlook to abate bacterial adhesion and microbiologically influenced corrosion. Isij International. 2003;43:1799-806.
[25] Saravanana M, Nanda A. Extracellular synthesis of silver bionanoparticles from Aspergillus clavatus and its antimicrobial activity against MRSA and MRSE. Colloid Surface B. 2010;77:214-8.
[26] Nanda A, Saravanan M. Biosynthesis of silver nanoparticles from Staphylococcus aureus and its antimicrobial activity against MRSA and MRSE. Nanomed-Nanotechnol Biol Med. 2009;5:452-6.
[27] Paton BE, Kaleko DM, Koval YM, Slipchenko VM, Musienko RY, Neganov LM, et al. Influence of Alloying with Silver and Tantalum on Features of Medical-Purpose Ti-Ni Alloy. Metallofiz Nov Tekhnol-Met Phys Adv Techn. 2010;32:1691-703.
[28] Necula BS, Apachitei I, Tichelaar FD, Fratila-Apachitei LE, Duszczyk J. An electron microscopical study on the growth of TiO2-Ag antibacterial coatings on Ti6Al7Nb biomedical alloy. Acta Biomaterialia. 2011;7:2751-7.
[29] Huang CF, Chiang HJ, Lan WC, Chou HH, Ou KL, Yu CH. Development of silver-containing austenite antibacterial stainless steels for biomedical applications Part I: microstructure characteristics, mechanical properties and antibacterial mechanisms. Biofouling. 2011;27:449-57.
[30] Hardes J, Streitburger A, Ahrens H, Nusselt T, Gebert C, Winkelmann W, et al. The Influence of Elementary Silver Versus Titanium on Osteoblasts Behaviour In Vitro Using Human Osteosarcoma Cell Lines. Sarcoma. 2007;2007.
[31] Bosetti M, Massè A, Tobin E, Cannas M. Silver coated materials for external fixation devices: in vitro biocompatibility and genotoxicity. Biomaterials. 2002;23:887-92.
[32] ATSDR. Toxicological Profile for Silver. 1990, TP-90-24. Atlanta, GA: Agency for Toxic Substances and Disease Registry.
[33] Furst A, Schlauder MC.. Inactivity of two noble metals as carcinogens. J Environ Pathol Toxicol; 1978; 1: 51–7.
[34] Zemczuznyj SF. On the alloys of magnesium with silver. Z Anorg Chem. 1906;49:400-14.
[35] Zworykin VK, Ruedy JE, Pike EW. Silver-magnesium alloy as a secondary electron emitting material. Journal of Applied Physics. 1941;12:696-8.
[36] Fox FA. Equilibrium relations and some properties of magnesium lithium and magnesium silver lithium alloys. Journal of the Institute of Metals. 1946;72:540-2.

[37] Loveless JD, Alemohammad H, Li J, Gertsman V, Emadi D, Toyserkani E, et al. Laser-assisted maskless microdeposition of silver nano-particles on a magnesium substrate. Materials Letters. 2009;63:1397-400.
[38] Mueller WD, de Mele MFL, Nascimento ML, Zeddies M. Degradation of magnesium and its alloys: Dependence on the composition of the synthetic biological media. Journal of Biomedical Materials Research Part A. 2009;90A:487-95.
[39] Fischer J, Profrock D, Hort N, Willumeit R, Feyerabend F. Improved cytotoxicity testing of magnesium materials. Materials Science and Engineering B-Advanced Functional Solid-State Materials. 2011;176:830-4.
[40] Frant M, Stenstad P, Johnsen H, Dölling K, Rothe U, Schmid R, et al. Anti-infective surfaces based on tetraether lipids for peritoneal dialysis catheter systems. Materialwissenschaft Und Werkstofftechnik. 2006;37:538-45.
[41] Schierholz JM, Beuth J. Implant infections: a haven for opportunistic bacteria. Journal of Hospital Infection. 2001;49:87-93.
[42] STAMM WE. Infections Related to Medical Devices. Annals of Internal Medicine. 1978;89:764-9.
[43] Gristina A. Biomaterial-centered infection: microbial adhesion versus tissue integration. Science. 1987;237:1588-95.
[44] Roos J, aring, ker AM, Renvert S, Egelberg J. Treatment of peri-implant infections: a literature review. Journal of Clinical Periodontology. 2003;30:467-85.
[45] Adell R, Lekholm U, Rockler B, Brånemark PI, Lindhe J, Eriksson B, et al. Marginal tissue reactions at osseointegrated titanium fixtures: (I). A 3-year longitudinal prospective study. International Journal of Oral and Maxillofacial Surgery. 1986;15:39-52.
[46] Smedberg JI, Lothigius E, Bodin I, Frykholm A, Nilner K. A clinical and radiological two-year follow-up study of maxillary overdentures on osseointegrated implants. Clin Oral Implan Res. 1993;4:39-46.
[47] Jepsen S, Rühling A, Jepsen K, Ohlenbusch B, Albers HK. Progressive peri-implantitis. Incidence and prediction of peri-implant attachment loss. Clin Oral Implan Res. 1996;7:133-42.
[48] Weber HP, Buser D, Fiorellini JP, Williams RC. Radiographic evaluation of crestal bone levels adjacent to nonsubmerged titanium implants. Clin Oral Implan Res. 1992;3:181-8.
[49] Darouiche RO. Treatment of Infections Associated with Surgical Implants. New Engl J Med. 2004;350:1422-9.
[50] Darouiche RO. Antimicrobial Approaches for Preventing Infections Associated with Surgical Implants. Clin Infect Dis. 2003;36:1284-9.
[51] Costerton JW, Stewart PS, Greenberg EP. Bacterial Biofilms: A Common Cause of Persistent Infections. Science. 1999;284:1318-22.
[52] Weinstein RA, Darouiche RO. Device-Associated Infections: A Macroproblem that Starts with Microadherence. Clin Infect Dis. 2001;33:1567-72.
[53] Klug D, Lacroix D, Savoye C, Goullard L, Grandmougin D, Hennequin JL, et al. Systemic Infection Related to Endocarditis on Pacemaker Leads : Clinical Presentation and Management. Circulation. 1997;95:2098-107.
[54] Rose EA, Gelijns AC, Moskowitz AJ, Heitjan DF, Stevenson LW, Dembitsky W, et al. Long-Term Use of a Left Ventricular Assist Device for End-Stage Heart Failure. New Engl J Med. 2001;345:1435-43.
[55] Widmer AF. New Developments in Diagnosis and Treatment of Infection in Orthopedic Implants. Clin Infect Dis. 2001;33:S94-S106.
[56] Gabriel SE, Woods JE, O'Fallon WM, Beard CM, Kurland LT, Melton LJ. Complications Leading to Surgery after Breast Implantation. New Engl J Med. 1997;336:677-82.

[57] Donlan RM, Costerton JW. Biofilms: Survival Mechanisms of Clinically Relevant Microorganisms. Clinical Microbiology Reviews. 2002;15:167-93.
[58] Donlan RM. Role of Biofilms in Antimicrobial Resistance. ASAIO Journal. 2000;46:S47-S52.
[59] Qian Z, Sagers RD, Pitt WG. Investigation of the mechanism of the bioacoustic effect. J Biomed Mater Res. 1999;44:198-205.
[60] Nociti FH, Machado MÂN, Stefani CM, Sallum EA, Sallum AW. Absorbable versus nonabsorbable membranes and bone grafts in the treatment of ligature-induced peri-implantitis defects in dogs. Clin Oral Implan Res. 2001;12:115-20.
[61] Persson LG, Ericsson I, Berglundh T, Lindhe J. Osseintegration following treatment of peri-implantitis and replacement of implant components. Journal of Clinical Periodontology. 2001;28:258-63.
[62] Wetzel AC, Vlassis J, Caffesse RG, Hämmerle CHF, Lang NP. Attempts to obtain re-osseointegration following experimental peri-implantitis in dogs. Clin Oral Implan Res. 1999;10:111-9.
[63] Persson LG, Ericsson I, Berglundh T, Lindhe J. Guided bone regeneration in the treatment of peri-implantitis. Clin Oral Implan Res. 1996;7:366-72.
[64] Machado MAN, Stefani, C. M., Sallum, E. A., Sallum, A. W., Tramontina, V. A., Nogueria-Filho, G. R. & Nociti, F. H. Jr. (2000) Treatment of ligature-induced periimplantitis defects by regenerative procedures: a histometric study in dogs. Journal of Oral Science 42, 163–168.
[65] Hall, E. E., Meffert, R. M., Herrmann, J. S., Mellonig, J. T. & Cochran, D. L.. Comparison of bioactive glass to demineralized freeze-dried bone allograft in the treatment of intrabony defects around implants in the canine mandible. Journal of Periodontology 1999; 70, 526–535.
[66] Behneke A, Behneke, N., d'Hoedt, B. & Wagner, W. (1997a) Hard and soft tissue reactions to ITI screw implants: 3-year longitudinal results of a prospective study. International Journal of Oral and Maxillofacial Implants 12, 749–757.
[67] Khoury FB, R. (2001) Surgical therapy of peri-implant disease: a 3-year follow-up study of cases treated with 3 different techniques of bone regeneration. Journal of Periodontology 52, 1498-1508.
[68] Aughtun, M., Richter, E. J., Hauptmann, S. & Yildrim, M.. Untersuchungen zur Behandlung von tiefen periimplanta¨ren Knochentaschen mit ePTFE-Membranen. Zeitschrift fuer Zahnaerzliche Implantologie 1992; 8, 246–250.
[69] Nayeb-Hashemi A, Clark J. The Ag-Mg (Silver-Magnesium) system. Journal of Phase Equilibria. 1984;5:348-58.
[70] Lim M, Tibballs, J.E., Rossiter, P.L. (1997) Z. Metallkd. 88: 162.
[71] Okamoto H. Ag-Mg (silver-magnesium). Journal of Phase Equilibria. 1998;19:487-.
[72] Smirnow WJ, Kurnakow NS. Bestimmte Verbindungen mit veränderter Zusammensetzung der festen Phase. I. Leitfähigkeit und Härte des Systems: Magnesium—Silber. Z Anorg Chem. 1911;72:31-54.
[73] K.W. Andrews and W. Hume-Rothery, "The Constitution of Silver-Magnesium Alloys in the Region 0-40 Atomic Percent Magnesium", J. Inst. Met., 69, 485-493 (1943).
[74] W. Hume-Rothery and E. Butchers, "The Solubility of Silver and Gold in Solid Magnesium", J. Inst. Met., 60, 345-350 (1937).
[75] R. J.M. Payne and J.L. Haughton, "Alloys of Magnesium. Part IV-The Constitution of the Magnesium-Rich Alloys of Magnesium and Silver", J. Inst. Met., 60, 351-363 (1937).
[76] F. Saeftel and G. Sachs, Z. MetaUkd., 17, 258-264 (1925).

[77] Payne RJM, Haughton JL. Alloys of magnesium. Part IV. - The constitution of the magnesium-rich alloys of magnesium and silver. Journal of the Institute of Metals. 1937;60:351-64.
[78] N. V. Ageew and V. G. Kuznezow, Izv. Akad. Nauk SSSR Otd. (Khim.) Nauk, 289-309 (1937).
[79] M. Kogachi, "Alloying Behavior of Ag-Mg, Au-Mg, and Ag-A1 Alloys", J. Phys. Chem. Solids, 35, 109-115 (1974).
[80] Letner HR, Sidhu SS. An X-Ray Diffraction Study of the Silver-Magnesium Alloy System. Journal of Applied Physics. 1947;18:833-7.
[81] L. M. Clarebrough and J. F. Nicholas, "The Superstructure in the a Phase of Silver-Magnesium Alloys", Aust. J. Sci. Res., A3, 284-289 (1950).
[82] S. Kachi, "Thermodynamic Properties of Hume-Rothery Type Silver-Magnesium Alloys. I-Activity of Magnesium in the Alpha Phase, and the Free Energy, Entropy, and Heat Capacity of the Alpha and Beta Phases", J. Jpn. Inst. Met., 19 (6), 378-382 (1955).
[83] A. Gangulee and M. B, Bever, "The Silver-Rich Solid Solutions in the System Silver-Magnesium. I-Short-Range Order", Trans. Met. Soc. AIME, 242, 272-277 (1968).
[84] Ya. I. Grayevskaya, V. I. Iveronova, A. A. Katsnelson, and I. I. Popova, Proc. of IV All Union Conf. on Atomic Ordering and Its Influence on the Properties of Alloys, Vol. 2, Tomsk, 130 (1974).
[85] M. Hamalainen, E. Laine, and T. Tarns, "Thermal Expansion of the Ag3Mg Alloy in the Ordered and Disordered States", J. Appl. Crystallogr., 2, 95-101 (1969).
[86] Ya. I. Grayevskaya, V. I. Iveronova, A. A. Katsnelson, and I.I. Popova, "Short-Range Order in a Alloys of Silver and Magnesium", Fiz. Met. Metalloved., 40(1), 195-197 (1975).
[87] R.A. Buckley, H.J. Axon, and J. Conacher, "Lattice Spacing of Silver-Magnesium Solid Solutions in the Ordered and Random Conditions", J. Inst. Met., 88, 225-226 (1959-60).
[88] Nordberg G, Gerhardsson L. Silver. In Seiler HG, Sigel H, Sigel A, editors. Handbook on toxicity of inorganic compounds. New York: Marcel Dekker. pp. 619–24.(1988).
[89] Hill WR, Pillsbury DM. (1939) Argyria: the pharmacology of silver. Baltimore, MD: Williams & Wilkins Company.
[90] Gulbranson SH, Hud JA, Hansen RC. Argyria following the use of dietary supplements containing colloidal silver protein. Cutis; 2000(66): 373–6.
[91] Drake PL, Hazelwood KJ. Exposure-related health effects of silver and silver compounds: A review. Ann Occup Hyg. 2005;49:575-85.
[92] Etris SF. Silver and silver alloys. In Kirk-Othmer encyclopedia of chemical technology, 2001, 4th edn. New York: John Wiley & Sons, Inc.
[93] HSE. Metallic silver. HSE review 1996. Report no. 1998:D97. London, UK: Health and Safety Executive.
[94] Modak SM, Sampath L, Fox CL Jr. (1988) Combined topical use of silver sulfadiazine and antibiotics as a possible solution to bacterial resistance in burn wounds. J Burn Care ehabil; 9: 359–63.
[95] Fung MC, Bowen DL. Silver products for medical indications: risk-benefit assessment. Clin Toxicol; 1996, 34: 119–26.
[96] Weir FW. Health hazard from occupational exposure to metallic copper and silver dust. Am Ind Hyg Assoc 1979, J; 40: 245–7.
[97] James RC, Roberts SM, Williams PL. General principles of toxicology. In Williams PL, James RC, Roberts SM, editors. Principles of toxicology: environmental and industrial applications, 2nd edn. New York: John Wiley and Sons, Inc. pp. 3–4. 2000, ISBN 0-471-29321-0.

[98] Williams N, Gardner I. Absence of symptoms in silver refiners with raised blood silver levels. Occup Med; 1995, 45: 205–08.
[99] Breitstadt R. Occupational exposure limits for metallic silver. In Proceedings of the 2nd European Precious Metals Conference, Lisbon, Portugal. May 10–12, 1995; 1–13.
[100] Rongioletti F, Robert E, Buffa P et al. Blue nevi-like dotted occupational argyria. J Am Acad Dermatol; 1992. 27: 1015–16.
[101] Rosenman KD, Moss A, Kon S. Argyria: clinical implications of exposure to silver nitrate and silver oxide. J Occup Med; 1979. 21: 430–5.
[102] Venugopal B, Luckey TD, editors. Metal toxicity in mammals. In Chemical toxicology of metals and metalloids. New York: Acedemic Press. 1978. pp. 32–36.
[103] Espinal ML, Ferrando L, Jimenex DF. Asymptomatic blue nevus-like macule. Diagnosis: localized argyria. Arch Dermatol; 1996. 132: 461–4.
[104] Van Garsse L, Versieck J. Generalized argyria caused by administration of tobacco-withdrawal tablets containing silver acetate. Ned Tijdschr Geneeskd; 1995. 139: 2658–61.
[105] Watanabe K. Histopathological study of damage to periodontal tissues by silver alloy metals in rats. J Jpn Assoc Periodontal; 1989. 31: 1021–46.
[106] Scroggs MW, Lewis JS, Proia AD. Corneal argyrosis associated with silver soldering. Cornea; 1992. 11: 264–9.
[107] Greene RM, Su WPD. Argyria. Am Fam Physician; 1987. 36: 151–4.
[108] Buckley WR, Oster CF, Fasset DW. Localized argyria: II. Chemical nature of the silver containing particles. Arch Dematol; 1965. 92: 697–705.
[109] Egli KL. Argyria: consequences of using an antiquated medication. Dermatol Digest; 2000. 13: 103–07.
[110] Fisher NM, Marsh E, Lazova R. Scar-localized argyria secondary to silver sulfadiazine cream. J Am Acad Dermatol; 2003. 49: 730–2.
[111] Rosenblatt MJ, Cymet TC. Argyria: report of a case associated with abnormal electroencephalographic and brain scan findings. J Am Osteopath Assoc; 1987. 87: 509–12.
[112] Juberg DR, Hearne FT. Silver and gold. In Bingham E, Cohrssen B, Powell CH, editors. Patty's toxicology, 2001. 5th edn. New York: John Wiley & Sons.
[113] Brooks SM. Lung disorders resulting from the inhalation of metals. Clin Chest Med; 1981. 2: 235–54.
[114] Sue YM, Lee JYY, Wang MC et al. Generalized argyria in two chronic hemodialysis patients. Am J Kidney Dis; 2001. 37: 1048–51.
[115] Baldi C, Minoia C, Di Nucci A et al. Effects of silver in isolated rat hepatocytes. Toxicol Lett; 1988. 41: 261–8.
[116] Furchner JE, Richmond CR, Drake GA. Comparative metabolism of radionuclides in mammals-IV. Retention of silver-110m in the mouse, rat, monkey and dog. Health Phys; 1968. 15: 505–14.
[117] Klein DA, editor. Effects on humans. In Environmental impacts of artificial ice nucleating agents. Stroudburg, Dowden, Hutchinson, and Ross. 1978. pp. 169–75.
[118] Armitage SA, White MA, Wilson HK. The determination of silver in whole blood and its application to biological monitoring of occupationally exposed groups. Ann Occup Hyg; 1996. 40: 331–8.
[119] Grabowski BF, Haney WG. Characterization of silver deposits in tissue resulting from dermal application of a silver-containing pharmaceutical. J Pharm Sci; 1972, 61: 1488–90.
[120] OSHA. United States Code of Federal Regulations, 29CFR Part 1910.1000, Air contaminants, final rule. Vol. 54. Washington, DC: Occupational Safety and Health Administration. 1989. p. 2702.

[121] NIOSH. (2003) Registry of toxic effects of chemical substances (RTECS): silver. VW3500000 (last updated August 2003) Cincinnati, OH: National Institute for Occupational Safety and Health.
[122] NIOSH. (1992) Reports and Memoranda. NIOSH publication no. 92-100. U.S. Department of Health, Education, and Welfare.
[123] ACGIH. (1991) Documentation of the threshold limit values and biological exposure indices, 6th edn. Cincinnati, OH: American Conference of Governmental Industrial Hygienists.
[124] Hermans MH (2006). "Silver-containing dressings and the need for evidence". The American journal of nursing 106 (12): 60–8; quiz 68–9.
[125] Chopra I (April 2007). "The increasing use of silver-based products as antimicrobial agents: a useful development or a cause for concern?". The Journal of Antimicrobial Chemotherapy 59 (4): 587–90.
[126] Saint S, Elmore JG, Sullivan SD, Emerson SS, Koepsell TD (September 1998). "The efficacy of silver alloy-coated urinary catheters in preventing urinary tract infection: a meta-analysis". The American Journal of Medicine 105 (3): 236–41.
[127] Lansdown, Alan B.G. (2006). Silver in Health Care: Antimicrobial Effects and Safety in Use. "Biofunctional Textiles and the Skin". Current problems in dermatology. Current Problems in Dermatology 33: 17–34.
[128] http ://en.wikipedia.org/wiki/Medical_uses_of_silver.
[129] Over-the-counter drug products containing colloidal silver ingredients or silver salts. Department of Health and Human Services (HHS), Public Health Service (PHS), Food and Drug Administration (FDA). Final rule". Federal Register 64 (158): 44653–8. August 1999.
[130] http ://www. elastoplast.c o m.au.
[131] Lansdown A B G, Silver I: Its Antibacterial Properties and Mechanism of Action, J Wound Care 2002;11, 5, 173.
[132] Im K, Takasaki Y, Endo A, Kuriyama M, Antibacterial Activity of A-Type Zeolite Supporting Silver Ions in Distilled Water. J Antibacterial Antifungal Agents, 1996; 24, 269 - 274.
[133] Sondi I, Salopek-Sondi B, Silver Nanoparticles as Antimicrobial Agent: A Case Study on E coli as a Model for Gram-Negative Bacteria, J Colloid Interface Sci 2004; 275, 177 - 182.
[134] Elchiguerra J L et al, Interaction of Silver Nanoparticles with HIV-I, J Nanobiotechnology 2005; 3, 6.
[135] Morones J R et al. The Bactericidal Effect of Silver Nanoparticles, Nanotechnology 2005; 16, 2346 -2353.
[136] McDonnell G, Denver R, Antiseptics and Disinfectants: Activity, Action and Resistance, Clinical Microbiol Reviews, 1999; 12, 1, 147 - 179.
[137] Matsumura Y, Yoshikata K, Kunisaki S-I, Tsuschido T, Mode of Bactericidal Action of Silver Zeolite and Its Comparison with that of Silver Nitrate, App Env Micro 2003; 69, 7, 4278 - 4281.
[138] Bragg P D, Rannie D J, The Effect of Silver Ions on the Respiratory Chain of E coli Can J Microbiol, 1974; 20, 883 - 889.
[139] Batarseh K I. Anomaly and Correlation of Killing in the Therapeutic Properties of Silver (I) Chelation with Glutamic and Tartaric Acids, JAntimicrobial Chemotherapy 2004; 54, 546–548.
[140] Richards R M E, Taylor R B, Xing D K L, Effect of Silver on Whole Cells and Speroplasts of a Silver Resistant Pseudomonas aeruginosa, Microbios 1984; 39, 151 - 158.
[141] Russell A D , Hugo W B, Antimicrobial Activity and Action of Silver, Prog. Med. Chem, 1994; 31, 351 - 371.

[142] Wells T N, et al, Mechanism of Irreversible Inactivation of Phosphomannose Isomerases by Silver Ions and Flamazine, Biochemistry 1995; 34, 24, 896 - 903.
[143] Thurmann R B, Gerba C P, The Molecular Mechanisms of Copper and Silver Ion Disinfection of Bacteria and Viruses, Crit Rev Environ Control, 1989;18, 295 - 315.
[144] Dibrov P, et al, Chemiosmotic Mechanism of Antimicrobial Activity of Ag+ in Vibrio cholerae, Antimicrobial Agents and Chemotherapy, 2002; 46, 8, 2668 - 2670.
[145] Cooper R, A Review of the Evidence for the use of Topical Antimicrobial Agents in Wound Care, World Wide Wounds, February 2004.
[146] Klaus, T., Joerger, R., Olsson, E. & Granqvist, C. G.. Silver-based crystalline nanoparticles, microbially fabricated. Proc Natl Acad Sci U S A 2000; 96, 13611–13614.
[147] Fox, C. L., Jr. Silver sulphadiazine – a new topical therapy for Pseudomonas in burns. Therapy of Pseudomonas infection in burns Arch Surg 1968; 96, 184–188.
[148] Wright, J. B., Lam, K. & Burrell, R. E.. Wound management in an era of increasing bacterial antibiotic resistance: a role for topical silver treatment. Am J Infect Control 1998; 26, 572–577.
[149] Ross, D. A., Phipps, A. J. & Clarke, J. A.. The use of cerium nitrate-silver sulphadiazine as a topical burns dressing. Br J Plast Surg 1993; 46, 582–584.
[150] Karlsmark, T., Agerslev, R. H., Bendz, S. H., Larsen, J. R., Roed-Petersen, J. & Andersen, K. E.. Clinical performance of a new silver dressing, Contreet foam, for chronic exuding venous leg ulcers. J Wound Care 2003; 12, 351–354.
[151] Hilton, J. R., Williams, D. T., Beuker, B., Miller, D. R. & Harding, K. G. (2004). Wound dressings in diabetic foot disease. Clin Infect Dis 39 (Suppl. 2), S100–S103.
[152] White, R. J. (2001). An historical overview of the use of silver in wound management. Br J Nurs 10 (15 Suppl. 2), S3–S8.
[153] Klaus, T., Joerger, R., Olsson, E. & Granqvist, C. G.. Silver-based crystalline nanoparticles, microbially fabricated. Proc Natl Acad Sci U S A 1999; 96, 13611–13614.
[154] Silver, S.. Bacterial silver resistance: molecular biology and uses and misuses of silver compounds. FEMS Microbiol Rev 2003; 27, 341–353.
[155] Wadhera A, Fung M. Systemic argyria associated with ingestion of colloidal silver. Dermatology Online Journal 2005; 11 (1): 12.
[156] Okan D, Woo K, Sibbald RG. "So what if you are blue? Oral colloidal silver and argyria are out: safe dressings are in". Adv Skin Wound Care 2007; 20 (6): 326–30.
[157] van Hasselt P, Gashe BA, Ahmad J.. "Colloidal silver as an antimicrobial agent: fact or fiction?". Journal of Wound Care 2004; 13 (4): 154–5.
[158] Kalouche H, Watson A, Routley D. "Blue lunulae: argyria and hypercopprecaemia". Australas. J. Dermatol. 2007; 48 (3): 182–4.
[159] McKenna JK, Hull CM, Zone JJ. "Argyria associated with colloidal silver supplementation". International Journal of Dermatology 2003; 42 (7): 549.
[160] Burrell RE, Heggers JP, Davis GJ, Wright JB. Efficacy of silver-coated dressings as bacterial barriers in a rodent burn sepsis model. Wounds 1999; 11:64-71.
[161] Percival SL, Bowler PG, Dolman J. Antimicrobial activity of silver-containing dressings on wound microorganisms using an in vitro biofilm model. Int Wound J 2007; 4:186-191.

[162] Shahverdi AR, Fakhimi A, Shahverdi HR, Minaian S.. Synthesis and effect of silver nanoparticles on the antibacterial activity of different antibiotics against Staphylococcus aureus and Escherichia coli. Nanomedicine 2007; 3:168-171.
[163] Panacek A, Kvitek L, Prucek R, Kolar M, Vecerova R, Pizurova N, Sharma VK, Nevecna T, Zboril R. Silver colloid nanoparticles: Synthesis, characterization, and their antibacterial activity. J Phys Chem B 2006; 110:16248-16253.
[164] Pal S, Tak YK, Song JM.. Does the antibacterial activity of silver nanoparticles depend on the shape of the nanoparticle? A study of the Gram-negative bacterium Escherichia coli. Appl Environ Microbiol 2007; 73:1712-1720.
[165] Wiley B, Sun Y, Mayers B, Xia Y. Shape-controlled synthesis of metal nanostructures: The case of silver. Chem Eur J 2005; 11:454-463.
[166] Hatchett DW, Henry S.. Electrochemistry of sulfur adlayers on low-index faces of silver. J Phys Chem 1996; 100:9854-9859.
[167] Morones JR, Elechiguerra JL, Camacho A, Holt K, Kouri JB, Ramı´rez JT, Yacaman MJ. 2005. The bactericidal effect of silver nanoparticles. Nanotechnology 16:2346-2353.
[168] Kammer C. Magnesium Taschenbuch. Düsseldorf: Aluminium-Verlag; 2000.
[169] Huse EC. A new ligature? Chicago Med J Exam 1878:172-2.
[170] Payr E. Beiträge zur Technik der Blutgefäss- und Nervennaht nebst Mittheilungen über die Verwendung eines resorbirbaren Metalles in der Chirurgie. Arch Klin Chir 1900;62:67–93.
[171] Payr E. Blutgefäß- und Nervennaht (nebst Mittheilung über die Verwendung eines resorbirbaren Metalles in der Chirurgie). Centralblatt für Chirurgie 1901;28 (Beilage: Bericht über die erhandlungen der deutschen Gesellschaft für Chirurgie, XXIX Kongress, abgehalten vom 18.-21. April 1900 im Langenbeck-Hause); p. 31–37.
[172] Lambotte A. Technique et indications de la prothèse perdue dans la traitement des fractures. Presse Med Belge 1909;17:321–3.
[173] Verbrugge J. Le matériel métallique résorbable en chirurgie osseuse. Presse Med 1934;23:460–5.
[174] Troitskii VV, Tsitrin DN. The resorbing metallic alloy 'Osteosinthezit' as material for fastening broken bone. Khirurgiia 1944;8:41–4.
[175] Witte F, Kaese V, Haferkamp H, Switzer E, Meyer-Lindenberg A, Wirth CJ, et al. In vivo corrosion of four magnesium alloys and the associated bone response. Biomaterials. 2005;26:3557-63.
[176] Friedrichs O, Sanchez-Lopez JC, Lopez-Cartes C, Dornheim M, Klassen T, Bormann R, et al. Chemical and microstructural study of the oxygen passivation behaviour of nanocrystalline Mg and MgH2. Applied Surface Science. 2006;252:2334-45.
[177] ASTM B. Standard practice for temper designations of magnesium alloys, cast and wrought.
[178] Müller WD, Zeddies M, Córsico M. Magnesium and its alloys as degradable biomaterials. Corrosion studies using potentiodynamics and EIS electrochemical techniques. J Mater Res 2007;10(1):5–10.
[179] Avedesian MM. Magnesium and magnesium alloys. Materials Park, OH: ASM International; 1999.
[180] Bach FW, Schaper M, Jaschik C. Influence of lithium on hcp magnesium alloys. Mater Sci Forum 2003;419–422:1037–42.
[181] Ducheyne PL, Hasting GW. Functional behavior of orthopedic biomaterials applications. UK: CRC Press 1984; vol. 2: 3-45.
[182] Quach NC, Uggowitzer PJ, Schmutz P. Corrosion behaviour of an Mg-Y-RE alloy used in biomedical applications studied by electrochemical techniques. C R Chim 2008; 11: 1043-54.

[183] Li LC, Gao JC, Wang Y. Evaluation of cyto-toxicity and corrosion behavior of alkali-heat-treated magnesium in simulated body fluid. Surf Coat Technol 2004; 92: 185-93.
[184] Tian XB, Wei CB, Yang SQ, Fu RKY, Chu PK. Water plasma implantation/oxidation of magnesium alloys for corrosion resistance. Nucl Instrum Methods B 2006; 242: 300-8.
[185] Duan HP, Du KQ, Yan CW, Wang FH. Electrochemical corrosion behavior of composite MAO film on magnesium alloy AZ91D. Electrochim Acta 2006; 51: 2898-909.
[186] Zhang YJ, CW Yan, Wang FH, Li WF. Electrochemical behavior of anodized Mg alloy AZ91D in chloride containing aqueous solution. Corrosion Sci 2005; 47: 2816-24.
[187] Atrens A, Dietzel W. The negative difference effect and unipositive Mg+. Adv Eng Mater 2007;9(4):292–7.
[188] Song JW, Kim CW, Han JW, Kim MS, Hwang SK. Improvement in mechanical properties of magnesium alloy (AZ31) sheet fabricated by casting and subsequent plastic working. Eco-Materials Processing & Design. 2003;439:227-32.
[189] Zeng RC, Dietzel W, Chen J, Huang WJ, Wang J. Corrosion behavior of TiO2 coating on magnesium alloy AM60 in hank's solution. Surface Engineering (Icse 2007). 2008;373-374:609-12849.
[190] Zhao MC et al. Influence of pH and chloride ion concentration on the corrosion of Mg alloy ZE41. Corros Sci 2008;50(11):3168–78.
[191] Mueller W-D, Lucia Nascimento M, Lorenzo de Mele MF. Critical discussion of the results from different corrosion studies of Mg and Mg alloys for biomaterial applications. Acta Biomaterialia. 2010;6:1749-55.
[192] Kree V, Bohlen J, Letzig D, Kainer KU. The metallographical examination of magnesium alloys. Praktische Metallographie-Practical Metallography. 2004;41:233-46.
[193] PDF. The powder diffraction fileTM. International Center for Diffraction Data (ICDD), PDF Release 2002, web site: <w ww.icdd.com> 2002.
[194] ASTM E92-82. Standard Test Method for Vickers Hardness of Metallic Materials. Philadelphia PA. 2003.
[195] ASTM E8 / E8M. Standard Test Methods for Tension Testing of Metallic Materials. Philadelphia PA. 2009.
[196] Bohner M, Lemaitre J. Can bioactivity be tested in vitro with SBF solution? Biomaterials. 2009;30:9.
[197] Fischer J, Prosenc MH, Wolff M, Hort N, Willumeit R, Feyerabend F. Interference of magnesium corrosion with tetrazolium-based cytotoxicity assays. Acta Biomaterialia. 2010;6:1813-23.
[198] Nascimento ML, Mueller WD, Carvalho AC, Tomas H. Electrochemical characterization of cobalt-based alloys using the mini-cell system. Dent Mater. 2007;23:369-73.
[199] Sarugaser R, Lickorish D, Baksh D, Hosseini MM, Davies JE. Human Umbilical Cord Perivascular (HUCPV) Cells: A Source of Mesenchymal Progenitors. Stem Cells 2005;23:220-229.
[200] Schade R.. Development of an in vitro system for testing the initial Plaqueadhärenz of dental biomaterials. Diss 2005, Jena.
[201] Ardizzone S, Bianchi CL, Fadoni M, Vercelli B. Magnesium salts and oxide: an XPS overview. Applied Surface Science. 1997;119:253-9.
[202] Peng QM, Huang YD, Zhou L, Hort N, Kainer KU. Preparation and properties of high purity Mg-Y biomaterials. Biomaterials. 2010;31:398-403.
[203] Fu HM, Qiu D, Zhang MX, Wang H, Kelly PM, Taylor JA. The development of a new grain refiner for magnesium alloys using the edge-to-edge model. Journal of Alloys and Compounds. 2008;456:390-4.

[204] Zhao ZD, Chen Q, Chao HY, Huang SH. Microstructural evolution and tensile mechanical properties of thixoforged ZK60-Y magnesium alloys produced by two different routes. Materials & Design. 2010;31:1906-16.
[205] Zhou W, Shen T, Aung NN. Effect of heat treatment on corrosion behaviour of magnesium alloy AZ91D in simulated body fluid. Corrosion Science. 2010;52:1035-41.
[206] Hoog C, Birbilis N, Estrin Y. Corrosion of Pure Mg as a Function of Grain Size and Processing Route. Advanced Engineering Materials. 2008;10:579-82.
[207] Braun R. Nd : YAG laser butt welding of AA6013 using silicon and magnesium containing filler powders. Materials Science and Engineering a-Structural Materials Properties Microstructure and Processing. 2006;426:250-62.
[208] Kariya Y, Hosoi T, Terashima S, Tanaka M, Otsuka M. Effect of silver content on the shear fatigue properties of Sn-Ag-Cu flip-chip interconnects. Journal of Electronic Materials. 2004;33:321-8.
[209] Hodgskinson R, Currey JD, Evans GP. Hardness, an indicator of the mechanical competence of cancellous bone. J Orthop Res. 1989;7:754-8.
[210] Liu M, Zanna S, Ardelean H, Frateur I, Schmutz P, Song GL, et al. A first quantitative XPS study of the surface films formed, by exposure to water, on Mg and on the Mg-Al intermetallics: Al3Mg2 and Mg17Al12. Corrosion Science. 2009;51:1115-27.
[211] Santamaria M, Di Quarto F, Zanna S, Marcus P. Initial surface film on magnesium metal: A characterization by X-ray photoelectron spectroscopy (XPS) and photocurrent spectroscopy (PCS). Electrochimica Acta. 2007;53:1314-24.
[212] Song G, Atrens A. Understanding Magnesium Corrosion - A Framework for Improved Alloy Performance. Advanced Engineering Materials. 2003;5:837-58.
[213] Yamamoto A, Hiromoto S. Effect of inorganic salts, amino acids and proteins on the degradation of pure magnesium in vitro. Mater Sci Eng C-Biomimetic Supramol Syst. 2009;29:1559-68.
[214] Xu LP, Yu GN, Zhang E, Pan F, Yang K. In vivo corrosion behavior of Mg-Mn-Zn alloy for bone implant application. Journal of Biomedical Materials Research Part A. 2007;83A:703-11.
[215] Zhang EL, Xu LP, Yu GN, Pan F, Yang K. In vivo evaluation of biodegradable magnesium alloy bone implant in the first 6 months implantation. Journal of Biomedical Materials Research Part A. 2009;90A:882-93.
[216] Song G. Control of biodegradation of biocompatable magnesium alloys. Corrosion Science. 2007;49:1696-701.
[217] Xu LP, Pan F, Yu GN, Yang L, Zhang EL, Yang K. In vitro and in vivo evaluation of the surface bioactivity of a calcium phosphate coated magnesium alloy. Biomaterials. 2009;30:1512-23.
[218] Eliezer A, Witte F. Corrosion Behavior of Magnesium Alloys in Biomedical Environments. In: Eliezer A, editor. Corrosion, Processes and Advanced Materials in Industry. Stafa-Zurich: Trans Tech Publications Ltd; 2010. p. 17-20.
[219] Mueller WD, Nascimento ML, de Mele MFL. Critical discussion of the results from different corrosion studies of Mg and Mg alloys for biomaterial applications. Acta Biomaterialia. 2010;6:1749-55.
[220] Nascimento ML, Mueller WD, Carvalho AC, Tomas HM. Electrochemical characterization of titanium biomaterials using the Mini-cell System. Journal of Materials Science. 2006;41:3323-7.
[221] Rao RVS, Wolff U, Baunack S, Eckert J, Gebert A. Corrosion behaviour of the amorphous Mg65Y10Cu15Ag10 alloy. Corrosion Science. 2003;45:817-32.

[222] Xin YC, Hu T, Chu PK. Degradation behaviour of pure magnesium in simulated body fluids with different concentrations of HCO3. Corrosion Science. 2011;53:1522-8.
[223] Kannan MB, Raman RKS. In vitro degradation and mechanical integrity of calcium-containing magnesium alloys in modified-simulated body fluid. Biomaterials. 2008;29:2306-14.
[224] Tie D, Feyerabend F, Hort N, Willumeit R, Hoeche D. XPS Studies of Magnesium Surfaces after Exposure to Dulbecco's Modified Eagle Medium, Hank's Buffered Salt Solution, and Simulated Body Fluid. Advanced Engineering Materials. 2010;12:B699-B704.
[225] Williams RL, Brown SA, Merritt K. Electrochemical studies on the influence of proteins on the corrosion of implant alloys. Biomaterials. 1988;9:181-6.
[226] Williams RL, Williams DF. Albumin adsorption on metal surfaces. Biomaterials. 1988;9:206-12.
[227] Willumeit R, Fischer J, Feyerabend F, Hort N, Bismayer U, Heidrich S, et al. Chemical surface alteration of biodegradable magnesium exposed to corrosion media. Acta Biomaterialia. 2011;7:2704-15.
[228] Beldjoudi T, Fiaud C, Robbiola L. Influence of Homogenization and Artificial Aging Heat-Treatments on Corrosion Behavior of Mg-Al Alloys. Corrosion. 1993;49:738-45.
[229] Zhou WQ, Shan DY, Han EH, Ke W. Effect of T4 and T6 treatment on corrosion of,die cast AZ91D magnesium alloys in 3.5% NaCl. Transactions of Nonferrous Metals Society of China. 2006;16:S1793-S7.
[230] Sato Y, Takikawa T, Sorakubo A, Takishima S, Masuoka H, Imaizumi M. Solubility and Diffusion Coefficient of Carbon Dioxide in Biodegradable Polymers. Industrial & Engineering Chemistry Research. 2000;39:4813-9.
[231] Feyerabend F, Fischer J, Holtz J, Witte F, Willumeit R, Drucker H, et al. Evaluation of short-term effects of rare earth and other elements used in magnesium alloys on primary cells and cell lines. Acta Biomaterialia. 2010;6:1834-42.
[232] Drewa T, Szmytkowska K, Chaberski M. The short term exposition of AgNO3 on 3T3 mouse fibroblasts cell line. Acta Poloniae Pharmaceutica. 2007;64:4.
[233] Vehof JWM, Spauwen PHM, Jansen JA. Bone formation in calcium-phosphate-coated titanium mesh. Biomaterials. 2000;21:2003-9.
[234] van den Dolder J, Farber E, Spauwen PHM, Jansen JA. Bone tissue reconstruction using titanium fiber mesh combined with rat bone marrow stromal cells. Biomaterials. 2003;24:1745-50.
[235] Wijnhoven SWP, Peijnenburg WJGM, Herberts CA, Hagens WI, Oomen AG, Heugens EHW, et al. Nano-silver – a review of available data and knowledge gaps in human and environmental risk assessment. Nanotoxicology. 2009;3:109-38.

Appendix

I. **Symbols and abbreviations**

PTFE: Polytetrafluoroethylene

%wt: Weight percentage

%at: Atomic percentage

CCC: Cell culture conditions

LC50: 50% lethal concentration

XPS: X-ray induced photoelectron spectroscopy

DMEM: Dulbecco's Modified Eagle Medium

ISE: Ion Selective Electrode

SHE: Standard hydrogen electrode

SCE: Saturated calomel electrode (E_0 = 0.241 V vs. SHE)

HBSS: Hank's Buffered Salt Solution (without calcium and magnesium)

FBS: Fetal Bovine Serum

SBF: Simulated body fluid

MRSA: Methicillin-resistant *Staphylococcus aureus*

MRSE: Methicillin-resistant *Staphylococcus epidermidis*

II. Lebenslauf (curriculum vitae)

Name	Tie
Vorname	Di
Geburtsdatum	13. 05. 1983
Geburtsort	Shenyang, P. R. China
09.1998 - 06.2001	Shenyang No. 9 High School, China
09.2001 - 06.2005	Dalian University of Technology, China
	Abschluss: Bachelor (Chemical Engineering)
09.2005 - 06.2008	Dalian University of Technology, China
	Abschluss: Master (Electrochemical Engineering)
08.2008 - 02.2009	National University of Singapore, Singapore
	Research assistant
00.1900 - heute	Helmholtz-Zentrum Geesthacht
	Ph.D. Candidate

III. **Publikationsliste**

Journal:

Di Tie, et al. XPS Studies of Magnesium Surfaces after Exposure to Dulbecco's Modified Eagle Medium, Hank's Buffered Salt Solution, and Simulated Body Fluid. Advanced Engineering Materials, 2010, 12(12).

Di Tie, et al. *In vitro* Mechanical and Corrosion Properties of Biodegradable Mg-Ag Alloys. Materials and Corrosion, **DOI**: 10.1002/maco.201206903

Di Tie, et al. Antibacterial Biodegradable Mg-Ag Alloys. European Cells & Materials. (accepted)

Invited review: Di Tie, et al. Review: In vitro corrosion testing methods for medically used magnesium alloys. Journal of Biomedical Materials Research Part A. (submitted)

Conference contribution:

Di Tie, et al. XPS Studies of Magnesium Surfaces after Exposure to Three Simulated Body Fluid. MSE 2010, Darmstadt, Germany.

Di Tie, et al. Electrochemical Characterization of Magnesium-Silver Alloys Using the Mini-cell System. Bio-Mat 2011, Jena, Germany.

Di Tie, et al. Effects of the Heat Treatment on the Corrosion Behaviour of Mg-Ag Biodegradable Alloys. Bio-Metal 2011, Quebec, Canada.

1. Di Tie, et al. XPS Studies of Magnesium Surfaces after Exposure to Dulbecco's Modified Eagle Medium, Hank's Buffered Salt Solution, and Simulated Body Fluid. Advanced Engineering Materials, 2010, 12(12).

ADVANCED BIOMATERIALS

DOI: 10.1002/adem.201080070

XPS Studies of Magnesium Surfaces after Exposure to Dulbecco's Modified Eagle Medium, Hank's Buffered Salt Solution, and Simulated Body Fluid

By *Di Tie*, Frank Feyerabend, Norbert Hort, Regine Willumeit* and *Daniel Hoeche*

Magnesium-based biomaterials are gaining increasing interest, while in vitro corrosion tests are not standardized yet. Moreover, the effects of different corrosion media on the corrosion products are still not fully understood. To compare and evaluate the three main corrosion media applied in most in vitro studies, an XPS investigation of magnesium surfaces was carried out after exposure of the specimens to Dulbecco's modified eagle medium (DMEM), Hank's buffered salt solution (HBSS), and simulated body fluid (SBF). The effects of rinsing the specimens after immersion were also determined. XPS investigations especially on the Mg 2p state showed that MgO, Mg(OH)2, and MgCO3 species were the dominant corrosion products presenting in all specimens despite of the different corrosion media. However, the ratio of corrosion products depends on the medium composition. It was also shown that rinsing specimens after immersion experiments is a necessary procedure when surface analysis is employed afterward

In recent years, magnesium and its alloys have attracted much attention as a biodegradable implant material due to their good biocompatibility and biodegradability.[1,2] Much research has been done for bone implant application,[3,4] and vascular stent.[5] However, the high corrosion rate limits their practical application.[1] Several measurements have been adopted to improve the biodegradation property, such as element alloying,[6,7] Ti-coating,[8] and alkaline treatment.[9] Also some new magnesium alloys have been prepared for biomedical application.[5,7,10,11]

Electrochemical testing and weight loss are widely adopted methods to determine corrosion properties of biomaterials in vitro including magnesium alloys.[12] Three kinds of corrosion media are widely applied in these measurements, Dulbecco's modified eagle medium (DMEM), Hank's buffered salt solution (HBSS), and simulated body fluid (SBF).[6,13,14] Much research was reported on alloy development, corrosion properties, coating technology, and biocompatibility of magnesium alloys, whereas much less attention paid to the environmental factors used for in vitro tests.

X-ray photoelectron spectroscopy (XPS) is a powerful technique for quantitative analysis of time-dependent chemical changes occurring at the sample surface. For example, Yao[15] revealed that the film on pure Mg formed in distilled water was mainly a mixture of $Mg(OH)_2$ and MgO; $Mg(OH)_2$ was predominantly in the top layer and decreased gradually with depth whilst MgO exhibit the opposite behavior. Mixed oxy-hydroxide layers were also reported on scratched Mg after air exposure.[16] It was also found that the films formed after immersion in an aqueous electrolyte had a bi-layer structure, consisting of a thin MgO inner layer and a $Mg(OH)_2$ external layer.[17]

To accurately predict in vivo degradation behavior by in vitro experiments, the selection of an appropriate corrosion medium, and environment is crucial. Therefore, it is necessary to investigate the effects of different media when applied in immersion experiments. In our approach XPS measurements were employed to determine magnesium corrosion product species and ratio after exposure in three kinds of corrosion media under cell culture conditions, which resemble physiological conditions.

Experimental

Materials and Corrosion Media

Magnesium samples (99.98%, Hydro Magnesium, Norway) were prepared by permanent mold casting. The metal was molten under protective atmosphere (Ar+2% SF_6) at a temperature of 750 °C. Then the melt was stirred for 30 min with 200 rpm prior to casting the material into preheated

[*] *D. Tie, Prof. R. Willumeit, Dr. F. Feyerabend, Dr. N. Hort, Dr. D. Hoeche*
GKSS Forschungszentrum Geesthacht GmbH, Max-Planck-Str. 1 D-21502 Geesthacht, Germany
E-mail: di.tie@gkss.de

2. Di Tie, et al. In vitro Mechanical and Corrosion Properties of Biodegradable Mg-Ag Alloys. Materials and Corrosion, **DOI**: 10.1002/maco.201206903

In vitro mechanical and corrosion properties of biodegradable Mg–Ag alloys

D. Tie*, F. Feyerabend, N. Hort, D. Hoeche, K. U. Kainer, R. Willumeit and W. D. Mueller

Binary magnesium–silver (Mg–Ag) alloys were designed as antibacterial material to treat infections in an implant site. The mechanical and electrochemical measurements were performed on three casting Mg–Ag alloys under cell culture conditions. The composition and distribution of the corrosion layer was analyzed by microscopy and X-ray photoelectron spectroscopy. In cell culture media, Mg–Ag alloys show higher, but still acceptable general corrosion rates while less susceptibility to pitting corrosion than pure Mg with increasing content of silver. This study indicates that Mg–Ag alloys have satisfactory corrosion properties and much better mechanical properties than pure magnesium as a functional biodegradable material.

1 Introduction

As an exceptionally lightweight material, magnesium (Mg) is also one of the human bodies' fundamental elements. Interest in magnesium for biodegradable implant material applications, especially in vascular intervention and osteosynthesis has been increasing continuously over the past years [1–4]. Magnesium not only exhibits mechanical properties close to natural bone and outstanding biocompatibility [5–7], but it is also degrading at the pH level between 7.4–7.6 and in the high chloride environment of physiological systems [8]. From the clinical point of view, magnesium as fully biodegradable and load bearing material has many advantages compared to permanent devices: no second surgical intervention is needed to remove the material; the hazard of long term adverse reactions is reduced; and bone tissue growth is positively influenced [9, 10]. Therefore, these intriguing characteristics have attracted great attention in respect of biodegradable bone implant applications, while more specific medical functions are still highly demanded to combine with magnesium to widen its application area, especially to treat infection after implant surgery [11].

Silver due to its strong antimicrobial properties has been applied by mankind for thousands of years. Already Alexander the Great used silver vessels to store drinking water [12]. However, the applied formulation of silver kept changing during history, from bulk silver in vessels and coins, to ionic silver supplemented as silver salts (like $AgNO_3$) or adsorbed on carrier materials [13] and now to nanosized [14] or alloyed silver. Silver has outstanding antibacterial reactivity in a variety of chemical states. It is even effective to some extreme microbes, such as Methicillin resistant *Staphylococcus aureus* (MRSA) and Methicillin resistant *Staphylococcus epidermidis* (MRSE), which are famous as "superbugs" and could not be killed by most antibiotics [15, 16]. Some recent studies made use of alloyed silver to provide antibacterial property that shows satisfactory reactivity as well [17, 18].

While a number of magnesium based biodegradable materials were developed, multifunctional magnesium alloys are still rarely reported. To introduce antibacterial properties to biodegradable magnesium, innovative binary Mg–Ag alloys were designed as bone implant material. Combined with its degradability in physiological environments, the antibacterial property could last steadily throughout the whole implant period. Among determination of biocompatibility and antibacterial reactivity [19], it is also necessary to test the corrosion behavior, as it is always a key issue to magnesium alloys [20, 21]. The mini cell system (MCS) employed in this study is based on a transportable mini cell, which has proven already, that it can precisely analyze different metallic biomaterials as applied in patients [22]. Dulbecco's modified eagle medium (DMEM) supplemented with fetal bovine serum (FBS) has been compared to other electrolytes by former studies, and may be a more credible electrolyte for in vitro corrosion tests [23, 24].

In the present work, the mechanical properties of different Mg–Ag alloys were analyzed in order to prove their improvement compared to pure magnesium. The electrochemical behavior of three Mg–Ag alloys was investigated using the MCS system with DMEM and FBS as electrolyte. As a sensitive technology to molecular structure, X-ray photoelectron spectroscopy (XPS) was employed to identify corrosion product species and distribution

D. Tie, F. Feyerabend, N. Hort, D. Hoeche, K. U. Kainer, R. Willumeit
Helmholtz-Zentrum Geesthacht, Institute for Materials Research, Max-Planck-Str. 1, 21502 Geesthacht (Germany)
E-mail: tie-di@hotmail.com

W. D. Mueller
Dental and Biomaterial Research, 'Charité' Universitaetsmedizin Berlin, Assmannshauser Str. 4–6, 14197 Berlin (Germany)

3. Di Tie, et al. Antibacterial Biodegradable Mg-Ag Alloys. European Cells & Materials. (accepted)

Abstract:

The use of magnesium alloys as degradable metals for biomedical applications is a topic of ongoing research and the demand for multifunctional materials is increasing. Hence, binary Mg-Ag alloys were designed as implant materials to combine the favorable properties of magnesium with the well-known antibacterial property of silver. In this study, three Mg-Ag alloys, Mg2Ag, Mg4Ag and Mg6Ag which contain 1.87%, 3.82% and 6.00% silver by weight were cast and processed with solution (T4) and aging (T6) heat treatment.

The metallurgical analysis and phase identification showed that all alloys contained Mg4Ag as the dominant β phase. After heat treatment the mechanical properties of all Mg-Ag alloys were significantly improved, and the corrosion rate was also significantly reduced due to presence of silver. $Mg(OH)_2$ and MgO present the main magnesium corrosion products while AgCl was found the corresponding primary silver corrosion product. Immersion tests under cell culture conditions demonstrated that the silver content did not significantly shift the pH and magnesium ion release. In vitro tests with both primary osteoblasts and cell lines (MG63, RAW 264.7) revealed that Mg-Ag alloys show negligible cytotoxicity and sound biocompatibility. Antibacterial assays performed in a dynamic bioreactor system proved that the alloys reduce the viability of two common pathogenic bacteria, Staphylococcus aureus and Staphylococcus epidermidis. In summary, biodegradable Mg-Ag alloys are biocompatible materials with adjustable mechanical and corrosion properties and show promising antibacterial activity, which warranted their potentials as antibacterial biodegradable implant materials.

4. Invited review: Di Tie, et al. Review: *In vitro* corrosion testing methods for medically used magnesium alloys. Journal of Biomedical Materials Research Part A. (submitted)

Abstract:

Despite the immense potential of biodegradable magnesium alloys, the high corrosion rates of Mg-based biomedical implants in the physiological environment impose severe limitations in many clinical applications. Therefore extensive in vitro studies have been carried out to investigate the materials' performance and fathom the associated mechanisms. The aim of this review was to collect and compare data from different published reports which focused on the description of the influence of different corrosion testing setups for the assessment of magnesium alloy corrosion.

This review includes three sections: (1) in vitro degradation of biomedical magnesium alloys in simulated physiological environments, focusing on comparison and evaluation of different testing setups; (2) selection of suitable test media and test circumstance for in vitro assessment; and (3) a comparison with our own results, effects of protein and cell culture conditions, was made and discussed. Based on the above, advices for in vitro corrosion test on magnesium alloys and future research trends are concluded.